AD NUMBER

AD876197

NEW LIMITATION CHANGE

TO

Approved for public release, distribution unlimited

FROM

Distribution authorized to U.S. Gov't. agencies and their contractors; Administrative/Operational Use; Sep 1970. Other requests shall be referred to Naval Air Systems Command, Washington, DC.

AUTHORITY

Naval Air Systems Command ltr, 2 Apr 1971

20

FINAL REPORT

THE EFFECTS OF HIGH INTENSITY ELECTRICAL CURRENTS ON ADVANCED COMPOSITE MATERIALS

N00019-70-C-0073

15 SEPTEMBER 1970

PHILCO Ford
PHILCO-FORD CORPORATION
Aeronutronic Division
Newport Beach, California

REPORT NO. U-4866

THE EFFECTS OF HIGH INTENSITY ELECTRICAL CURRENTS ON ADVANCED COMPOSITE MATERIALS

FINAL REPORT

15 September 1970

by

A. P. Penton and J. L. Perry of Philco-Ford Corporation

K. J. Lloyd of General Electric Company

Prepared Under Contract
N00019-70-C-0073

for

Naval Air Systems Command
Department of the Navy

PHILCO-FORD CORPORATION
Aeronutronic Division
Newport Beach, Calif. • 92663

ACKNOWLEDGEMENTS

This program was performed under the sponsorship of the Naval Air Systems Command, N00019-70-C-0073, with J. W. Willis as the project engineer. The authors also wish to acknowledge the contributions of Dr. W. M. Fassell and D. W. Bridges, Messrs. T. M. Place. D. R. Doner and C. G. Daniels of Philco-Ford and Messrs. J. A. Plumer and F. A. Fisher of General Electric Company.

CONTENTS

ILLUSTRATIONS

ILLUSTRATIONS (Continued)

ILLUSTRATIONS (Continued)

ILLUSTRATIONS (Continued)

ILLUSTRATIONS (Continued)

ILLUSTRATIONS (Continued)

ILLUSTRATIONS (Continued)

SECTION 1

INTRODUCTION AND SUMMARY

The objective of this program was to perform a research study to investigate high intensity electrical current flow and resulting degradation in advanced composites and to investigate means of providing internal protection from such damage. The approach followed in the the program essentially involved the selection of representative high modulus boron and graphite filaments and composites and the exposure of those filaments and composites to precisely controlled electrical current flow. Necessary electrical, physical, chemical, microstructure, and mechanical analyses and tests were performed to permit modeling of electrical current flow processes and damage mechanisms. The laboratory analyses and tests performed included photomicrographic analysis, electron microprobe, scanning electron microscope, X-ray diffraction, tensile tests, and physical property measurements. The electrical properties measured included resistivity, dielectric strength, and impedance.

In the performance of this program specimen fabrication, physical testing, mechanism testing, specimen inspection and degradation mechanism analyses were performed by Philco-Ford Corporation. Current injection tests, electrical property measurements and current flow process analyses were performed by the General Electric Company High Voltage Laboratory

In this program, filaments and epoxy resin composites of boron and graphite filaments were studied. The boron filaments were of the 0.004 inch diameter variety that are manufactured by the chemical vapor deposition of boron onto a 0.0005 inch diameter tungsten wire. Such filaments typically have a 55 x 10^6 psi modulus of elasticity. Two varieties of graphite filaments were included. One was a 55 x 10^6 psi modulus graphite filament tow as manufactured from a polyacrylonitrile precursor and the other was a

50 x 10^6 psi modulus graphite filament yarn as manufactured from a rayon precursor. The filaments included were manufactured by:

United Aircraft Corp.:	Boron filament
Courtaulds, Ltd.:	HM-S 55 x 10^6 psi modulus graphite tow
Hitco:	HMG-50 50 x 10^6 psi modulus graphite yarn

In the composites evaluated, the epoxy resin matrices were Whittaker Corp. 2387 for the boron composites and DEN 438/MNA for the graphite composites. Each composite was of 50-55% by volume filament content.

In the investigations performed to date by Philco-Ford Corporation and General Electric Company, the approach used was shown in Figure 1-1. This figure shows that a complete understanding of degradation processes and possible methods for improving composite material response requires the investigation of the following interrelated areas:

(1) The resultant degradation mechanisms.

(2) The electric current flow process within the filaments and composites.

To date it has been determined that boron epoxy composites degrade at current levels where the boron filaments themselves begin to crack radially and transversely. For the standard waveform used in the degradation studies, this occurred at crest current injection levels of above 3.7 - 5.7 x 10^4 amps per cm^2 of filament. Above these levels, degradation increases in severity until total loss in filament integrity occurs. The mechanism of the filament degradation has been determined to be due to the fact that the tungsten boride core is much less resistive than boron and, as a result, carries the electric current that is injected into the filaments. The energy dissipated in the core in the form of heat causes the core to expand and stress the boron. This eventually causes the boron to crack.

The graphite filament epoxy composites begin to degrade at crest current levels of 20-25 x 10^4 amps per cm^2 of filament for the standard waveform. Their mechanism of degradation is based on the resin rather than the filaments. Current flows in the filaments and is dissipated partially into heat. At the damaging levels the heat initiates pyrolysis of the epoxy resin matrix. The pyrolysis gases cause a pressure build-up within the laminate until cracking and delamination occurs. At this point the air comes in contact with the hot filaments and gases and the composite bursts into flames.

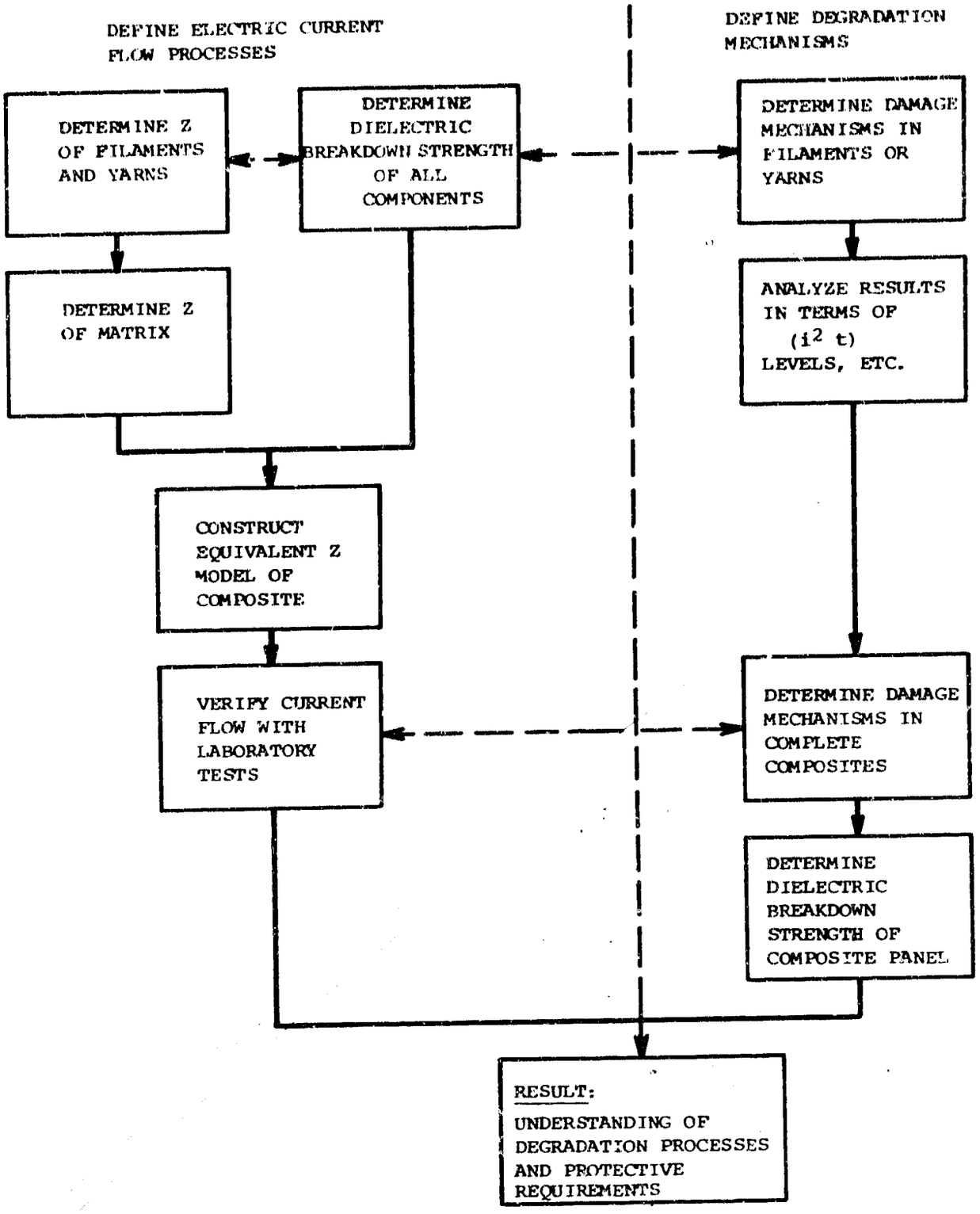

FIGURE 1-1. BLOCK DIAGRAM OF PROGRAM APPROACH

It is believed that the most viable approach for improving the resistance of boron and graphite epoxy composites to degration due to current flow will be improving the conductance of the composites through incorporation of secondary conductive paths. These paths must be less resistive than the filaments and not cause significant reduction of either the strength or modulus of the composite or cause serious weight penalties. The utility of this general approach was demonstrated by incorporating fine tungsten wires in one case, and graphite filaments in another case, within boron-epoxy laminates. Both graphite filaments and tungsten wire are less resistive than the boron filaments. As the result, tests proved that current was diverted away from the boron filaments and the threshold of degradation of the composite increased.

Current flow processes within advanced composites are quite complex and difficult to analyze. Essentially though, a composite acts as a complex array of conductive paths (filaments) imbedded within and separated by films of electrically insulative resin. This model of current flow is complicated by the fact that the dynamic impedances of the composite specimens are constantly changing during current flow. Also, the insulative resin films between filaments and layers or plies of filaments are not continuous and uniform in thickness. Adjacent filaments vary in their spacing and often are in contact with each other. As a result, current flow is not restricted only to the filaments or plies of filaments into which the current was injected and degradation can occur in separate layers or plies of filaments.

All experimental results and analyses are discussed in Section 2.

SECTION 2

INVESTIGATIONS OF CURRENT FLOW PROCESSES, DAMAGE MECHANISMS, AND INTERNAL PROTECTION TECHNIQUES

2.1 APPROACH

The overall objective of this program was to perform research into the effects of high intensity electric currents on advanced filament reinforced plastic composites. Specifically, the work was to be directed toward those current high strength and modulus filament types that have been developed for use in structural composites for advanced aircraft. Also, the electric currents to be used in the study was to be representative of those that might occur as the result of a lightning strike to the surface of an aircraft. Following this overall approach, the program was oriented to study the processes involved in electric flow through filaments and composites and in the determination of the mechanisms of any damage resulting from the current flow. Introductory to this, however, was the materials selections and characterizations that were made preparatory to the current flow and damage mechanisms research. Also, during this program, certain approaches toward minimizing damage due to current flow were conceived and evaluated.

2.1.1 FILAMENTS AND COMPOSITES SELECTED

a. Filaments. In order to select materials for use in this effort a survey was made to determine those types of filaments and resins that are in use for advanced composites so that materials that might be expected to have unique electrical characteristics could be included for investigation.

Two types of graphite filaments and one type of boron filament were selected as representative of commercially available advanced high modulus reinforcements. One type is Hitco's HMG-50, a continuous filament high modulus

graphite yarn with a proprietary surface finish (E-8095) for the achievement of optimum composite properties. Yarn construction for HMG-50 utilizes two plies of yarn with 720 filaments per ply with a filament diameter of 2.7×10^{-4} inches, a twist of four turns per inch and a calculated yarn cross sectional area of 82.8×10^{-6} square inches. Typical yarn properties are 50×10^{6} psi tensile modulus and 287×10^{3} psi ultimate tensile strength.

The second type of graphite filament selected is manufactured by Courtaulds (Type HM-S) and is a continuous twist-free high modulus roving tow with a proprietary surface treatment for the improvement of interlaminar shear strength in the composite. The tow strand of the HM-S contains 10,000 filaments, each typically 3×10^{-4} inches in diameter. The calculated cross-sectional area of the tow is 785×10^{-6} square inches. Typical filament properties are 55×10^{6} psi tensile modulus and 275×10^{3} psi ultimate tensile strength.

Boron filaments were obtained from the Hamilton Standard Division of United Aircraft Corporation. At the present time only one type of boron filament is in current use (a pyrolytic boron coating deposited over a 0.0005 inch diameter tungsten wire substrate). During the process of deposition of boron on the substrate, a chemical reaction occurs and portions of the substrate change from tungsten to tungsten boride.

A typical boron filament is 4×10^{-3} inches in diameter, with a 5×10^{-4} inch diameter tungsten or tungsten boride core. The filament typically has one twist per ten feet of length and has a calculated cross sectional area of 12.57×10^{-6} square inches.

b. Resin Matrices. Two epoxy resin systems were chosen as typical of those presently in use for high modulus composites. Dow Chemical's DEN 438/MNA resin system is typical of the unfilled epoxy resins used in graphite composites for environments up to 350°F.

Whittaker Corporation's 2387 resin system is typical of those modified epoxy resins used with boron reinforcement for potential usage up to 350°F.

c. Composite Preparation. The filaments and resins to be used in the program were fabricated into composite test specimens. For this program, the most simple filament orientation pattern was used; one in which all filaments are unidirectionally oriented parallel to one another. The composite laminates of each filament type were fabricated of precollimated and preimpregnated filament layers using conventional 100 psi vacuum bag autoclave curing techniques with 350°F maximum cure temperatures. The compositions of the unidirectional test laminate are summarized in Table 2-1.

TABLE 2-1

COMPOSITE LAMINATE COMPOSITION

Filament	Hitco HMG-50 Graphite	Courtaulds HMS Graphite	Hamilton Standard Boron
Number of plies	2	2	5
Filament Volume Content, %	50-55	50-55	48-54
Resin Matrix	DEN438/MNA	DEN438/MNA	Whittaker 2387
Resin Content, % by weight	30-37	30-37	27-32

2.1.2 PHYSICAL, CHEMICAL AND MECHANICAL TESTS

Four basic types of tests were performed on exposed as well as non-exposed specimens in order to investigate the degree as well as mechanisms of damage in the filaments and composites through which current had been passed. These were:

(1) Breaking strength of filaments and tensile strength of composites.

(2) Visual and photomicrographic inspection of filaments and composites.

(3) Electron microprobes of selected filaments.

(4) Scanning electron microscope inspection of selected filaments.

As shown in Figure 2-1, individual specimens of graphite yarn and tow as well as boron filaments were positioned on 1" x 15" pieces of artboard and adhesively bonded at points 1½ inches from each end. These filament mounts were utilized to prevent filament damage to and from the electrical exposures and for purposes of breaking strength testing. For the breaking strength tests, aluminum tabs were bonded to the filament ends. After each specimen was mounted in the test machine, the artboard strip was cut with a razor blade. The specimen was tested to failure at 0.05 in/min of machine head travel.

Each of the composite laminates fabricated were of 0.020-0.025 in. in thickness. For the electrical exposure tests, as well as the tensile strength tests, a specimen size of 0.5" x 7.0" (filaments in 7.0" direction) was selected. Prior to the tensile tests, glass reinforced plastic tabs were bonded to the ends of each specimen. The tabbed specimen ends were then clamped in the test machine and loaded to failure at 0.05 in/min. of hand travel.

2.1.3 ELECTRICAL CURRENT INJECTION TEST PROCEDURE FOR MATERIAL DEGRADATION STUDIES

Electrical testing was conducted at the General Electric High Voltage Test Laboratory. The impulse generator and peripheral measuring equipment utilized are presented in Figure 2-2. Figure 2-3 illustrates an actual specimen during testing and Figure 2-4 is a photograph of the different types of current probes which were used.

End contacts for the graphite yarns and tow were achieved by painting the ends of the filaments with a silver paint which penetrated and wet each fiber thus allowing good electrical contact. The boron filament ends were

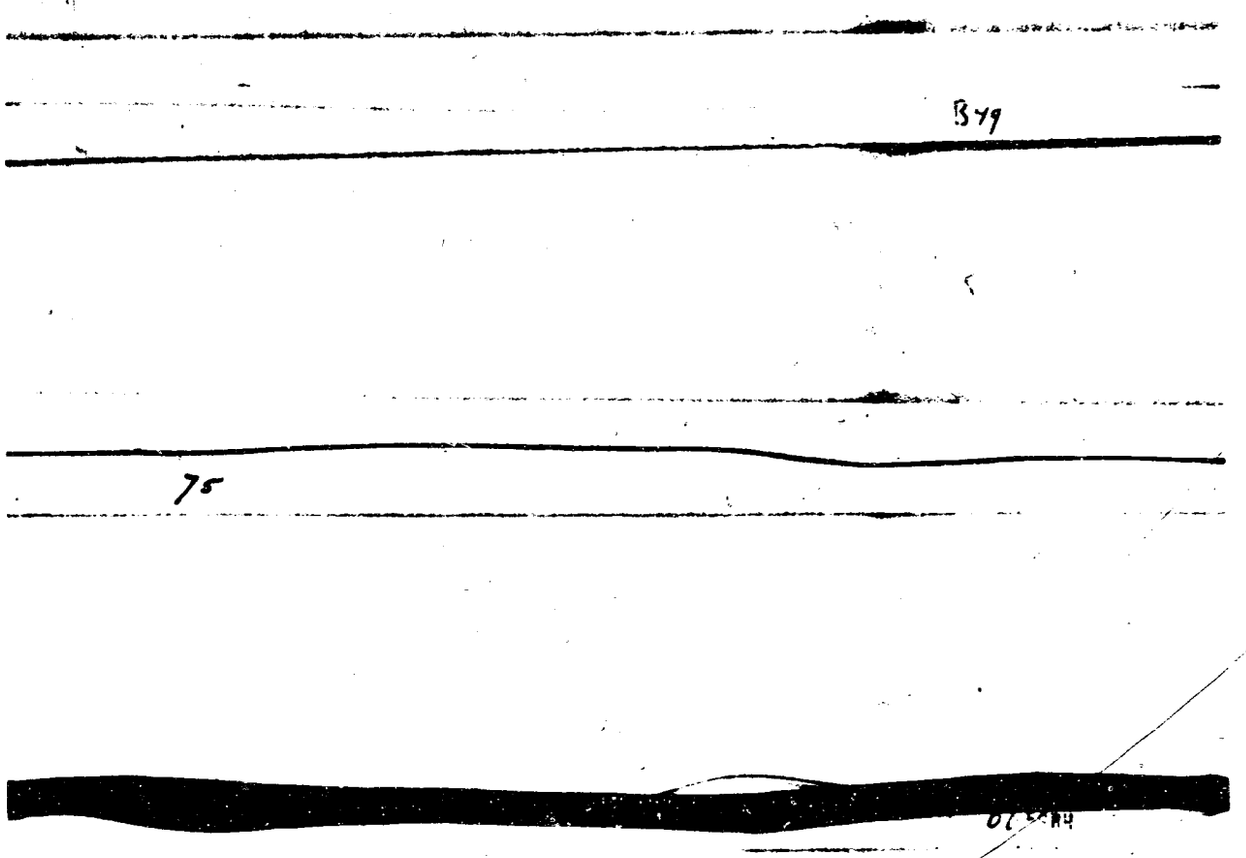

FIGURE 2-1. BORON FILAMENT, GRAPHITE YARN AND GRAPHITE TOW ELECTRICAL AND BREAKING STRENGTH TEST SPECIMEN.

FIGURE 2-2. IMPULSE GENERATOR AND PERIPHERAL MEASURING EQUIPMENT.

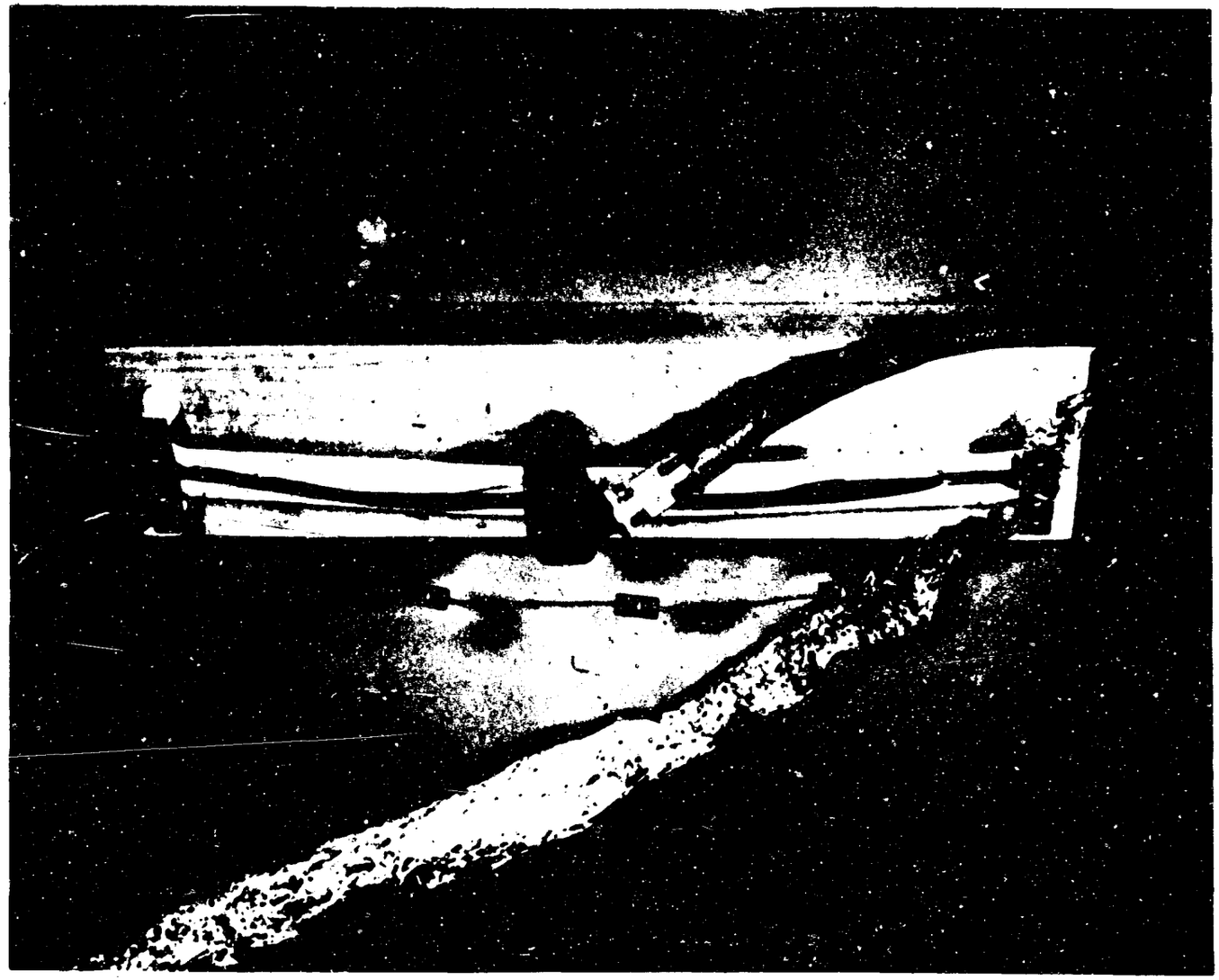

FIGURE 2-3. ELECTRICAL CURRENT INJECTION TEST SET-UP

FIGURE 2-4. DIFFERENT TYPES OF CURRENT PROBES EVALUATED FOR FIBER ELECTRICAL CURRENT INJECTION TESTS

placed between two aluminum foil pads and wetted with silver paint. Each end of the filament along with its pool of conducting paint was then compressed between these two pads. Oscillograms were taken during the tests and included a voltage measurement across the test sample in addition to a measurement of the current through the sample. Typical oscillograms of a boron filament, graphite yarn and graphite tow are represented by Figure 2-5. The top line represents voltage across the sample and the bottom line represents injected current. The sweep was 5 microseconds per division.

For these initial tests a standard waveform shape was established, as shown in Figure 2-6. Natural lightning comes in many different configurations; therefore, when conducting electrical exposures that are intended to simulate current flow as might result from lightning, it is necessary to define and control waveform shape. One IEEE recognized standard[1] for lightning simulation recognizes the following impulse waves: an 8 x 20 microsecond wave for lightning discharge currents and a 1.2 x 50 microsecond voltage waveform. The meaning of this can be seen in Figure 2-6. The virtual value for the duration of the wavefront is as follows: for current waves, 1.25 times the time taken by the current to increase from 10% to 90% of the crest value; for voltage waves, 1.67 times the time taken by the voltage to increase from 30% to 90% of its crest value. The standard current wave applied in the exposure was somewhat of a compromise between the standard voltage wave and the standard current wave as just defined.

The schematic set-up for the current injection tests at high current levels is shown in Figure 2-7. The impulse or lightning current generator depicted is larger, in all respects, than the one shown in Figure 2-2. It not only possesses larger dimensions, but also higher voltage and energy capabilities. Since it is desirable to maintain a large resistance in series with the test specimen in order to prevent fluctuations in the current flowing through the specimens, it became necessary to go to this unit for the higher energy tests.

The primary difference to be noted in the set-up pictured in Figure 2-2 and 2-7 is the technique used for measuring the injected current. Previously these measurements were made by using a current pulse transformer. During testing these transformers were found to fall off slightly at low frequencies which required a small correction factor to be introduced when reading values out on the tail of the wave (a necessity when determining the dynamic impedance of the specimen). The technique employed in measuring the current is to measure the voltage across a linear (non-inductive) resistance shunt in series with the test specimen. By using a shunt resistance value which is much smaller than the test specimen resistance, there is an insignificant amount of error in the voltage signal

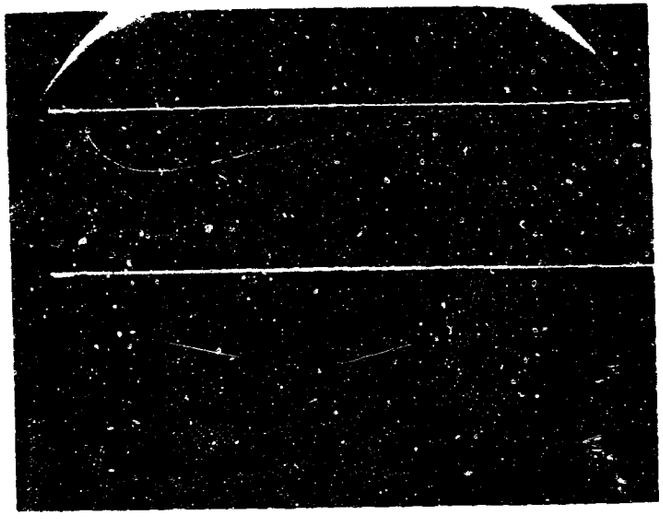

BORON

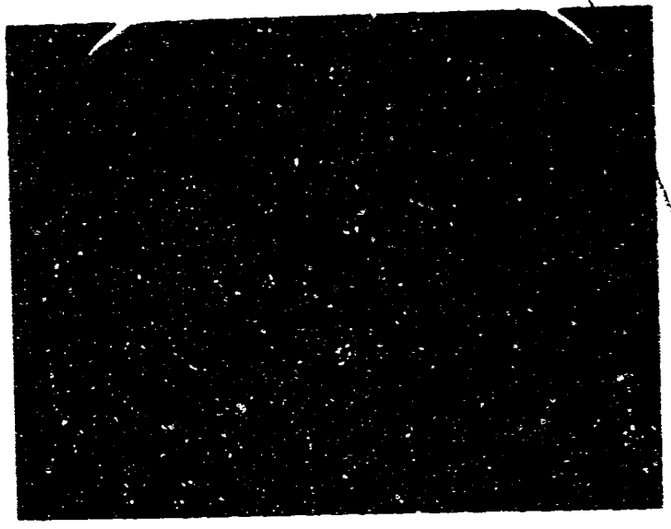

GRAPHITE TOW, HM-S

GRAPHITE YARN, HMG-50

FIGURE 2-5. TYPICAL OSCILLOGRAMS

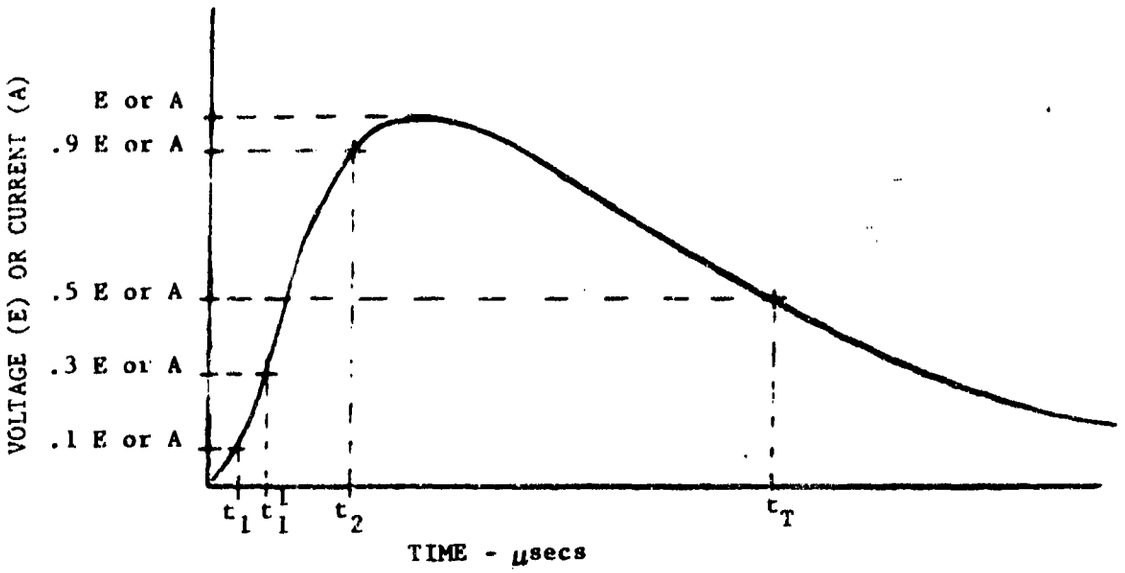

T $t_f = 1.25\ (t_2 - t_1)$ for current

$t_f = 1.67\ (t_2 - t_1')$ for voltage

FIGURE 2-6. WAVESHAPE DEFINITIONS

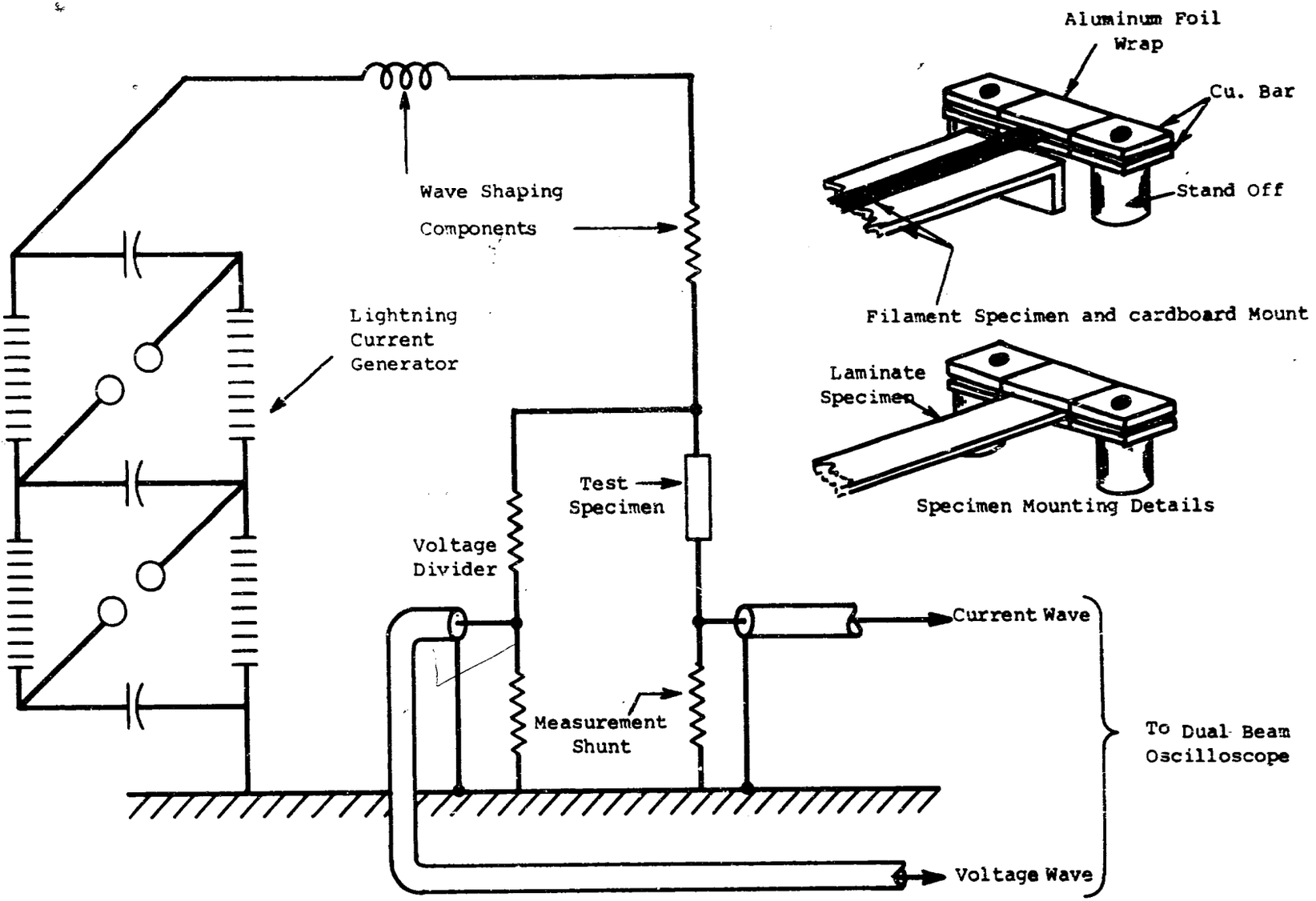

FIGURE 2-7 Test Set-Up for Higher Energy Current Injection Tests

measured by the divider circuit. As the shunt resistance is a known value, this error can, if desired, be eliminated entirely.

The unidirectional composite specimen electric current injections were performed in the same manner as were the injections of the filaments with the exception of the electric contact. For the composites, each specimen was beveled on each end to 45°. The specimen ends were then vapor honed to insure exposure of the filament ends. One-half inch on each specimen end was then plated with a 0.001-0.0015 inch thick nickel coating. In the case of the filaments, as previously noted, silver filled epoxy paint was used on the specimen ends. Both the filament and composite specimens were clasped into the test fixture for current injection as shown in Figure 2-7.

The resistivity of each filament and composite specimen was measured prior and subsequent to electric current injection. Also, "Thermopapers" were used to provide a gross indication of the peak temperature of the composite specimens as the result of current injection.

Other special electric injection test procedures, such as dielectric breakdown strength, were provided in the discussions of those results.

2.2 CURRENT FLOW PROCESSES

In studying the effects of high intensity electric current flow on advanced composite materials it is essential that more than just damage studies be performed. In other words, the quantity of current flowing through a damaged element of a composite must be established. To do this, it is then imperative that the processes whereby current flows into and through the composite be understood. This then results, hopefully, in an approach toward mathematically modeling of and analytical techniques for predicting current flow. Since a composite is composed of an array of conductive filaments within a dielectric matrix of epoxy resin, certain electrical properties such as dielectric strength and dynamic impedance must be measured as related to the current flow processes involved. Therefore, the following is a summary of the electrical property characterization results and the understanding of the electric current flow processes that has to date been developed.

2.2.1 DIELECTRIC STRENGTH TEST RESULTS--EPOXY RESIN MATRICES

Since epoxy resins are known to be non-conductive, it is essential that their dielectric breakdown strength be determined on films of resin that are typical of the thickness of the resin film layers that exist between layers or plies of filaments in composites. Such resin films act as electrical insulation and tend to confine the current flow to the filaments

into which the current was injected. At a sufficient energy level the resin would breakdown thereby permitting current flow from one filament to another.

The resin films tested for dielectric strength were as follows:

Four sets of specimens were tested.

1. Pure DEN 438 film (2-6 mil thickness range)
2. DEN 438/104 glass cloth (3-3.5 mil thickness range)
3. DEN 438/104 glass cloth (2-2.5 mil thickness range)
4. Whittaker 2387/104 glass cloth (1-2.5 mil thickness range)

The resin films of interest were tested with 104 glass scrim cloth included because it is standard practice in industry that filaments be collimated onto the very thin (<0.0012 inch) glass scrim cloth. The scrim then becomes an integral part of the interply resin film and occupies a small fraction of the total volume of the composite.

The volt-time curves of Figure 2-8 through 2-11 were determined by exposing samples of each material to three different voltage waveforms, one with a fast rise time, a moderate rise time, and a slow rise time. The volt-time curves then were constructed by plotting the voltage and times where breakdown occurred with each waveform shape.

2.2.2 DIELECTRIC STRENGTH TEST RESULTS--BORON SURROUNDING SUBSTRATE CORE

It had originally been suggested that the boron sheath which surrounds the tungsten core might act as a dielectric material because of its high resistivity. Testing (conducted as shown in Figure 2-12) resulted in data which indicates that measurable conduction occurs as low as 1.0 volt and that the material behaves as a conductor and not as a dielectric as originally suggested. From other data sources, it appears that the boron is a poor conductor.

During these tests, voltages were held for fixed periods of time and current flow recorded. The resulting data did show considerable variation, and for this reason additional tests were conducted under more controlled conditions. The results of these tests made on the boron, show it to have a high value of resistance as would be expected from calculations. Of interest, however, is the fact that with a voltage (V) of 35 to 50 volts an avalanche phenomenon occurs and the boron does, in fact, breakdown.

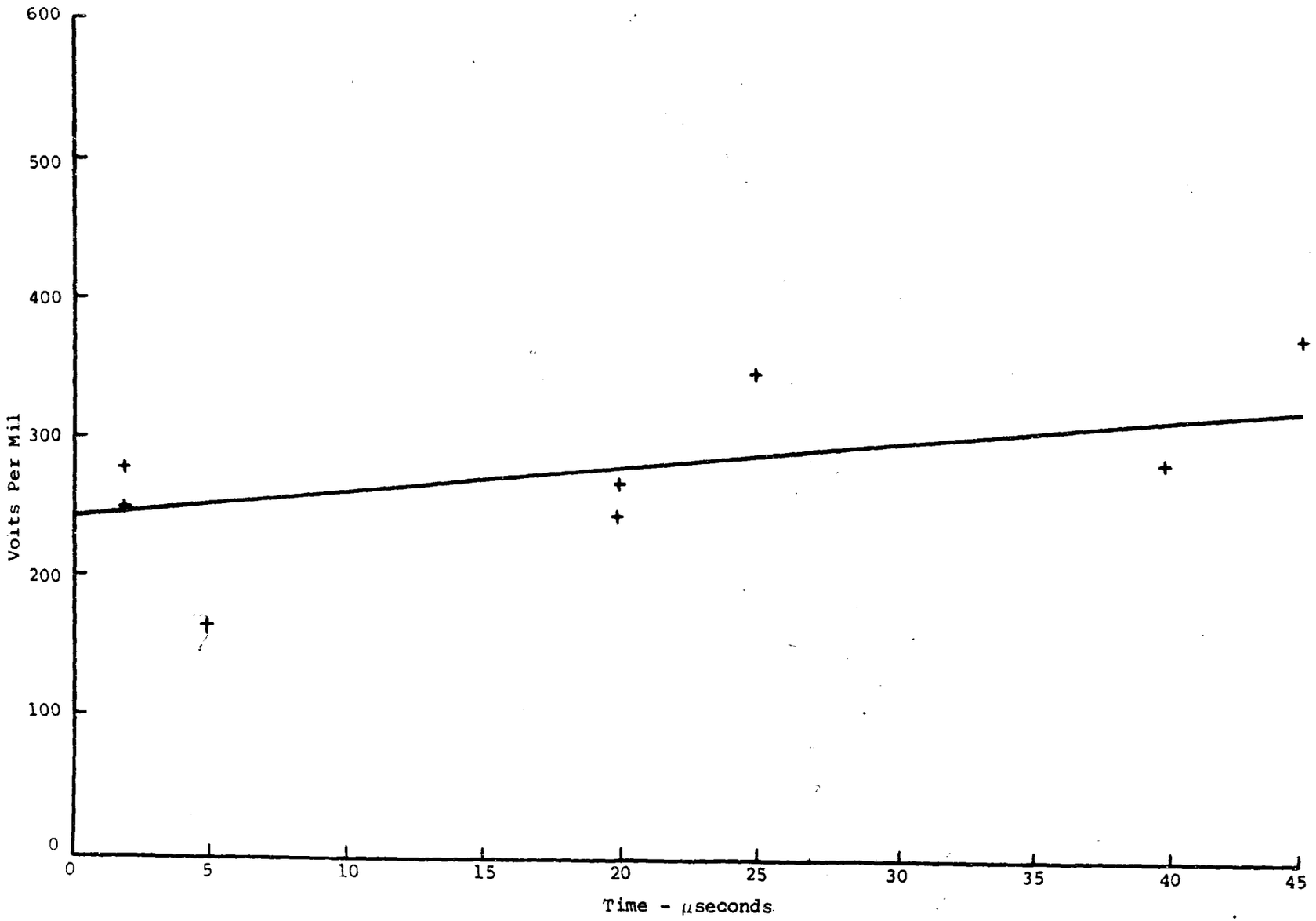

FIGURE 2-8. Dielectric Strength of DEN 438 (2-6 mil thickness)

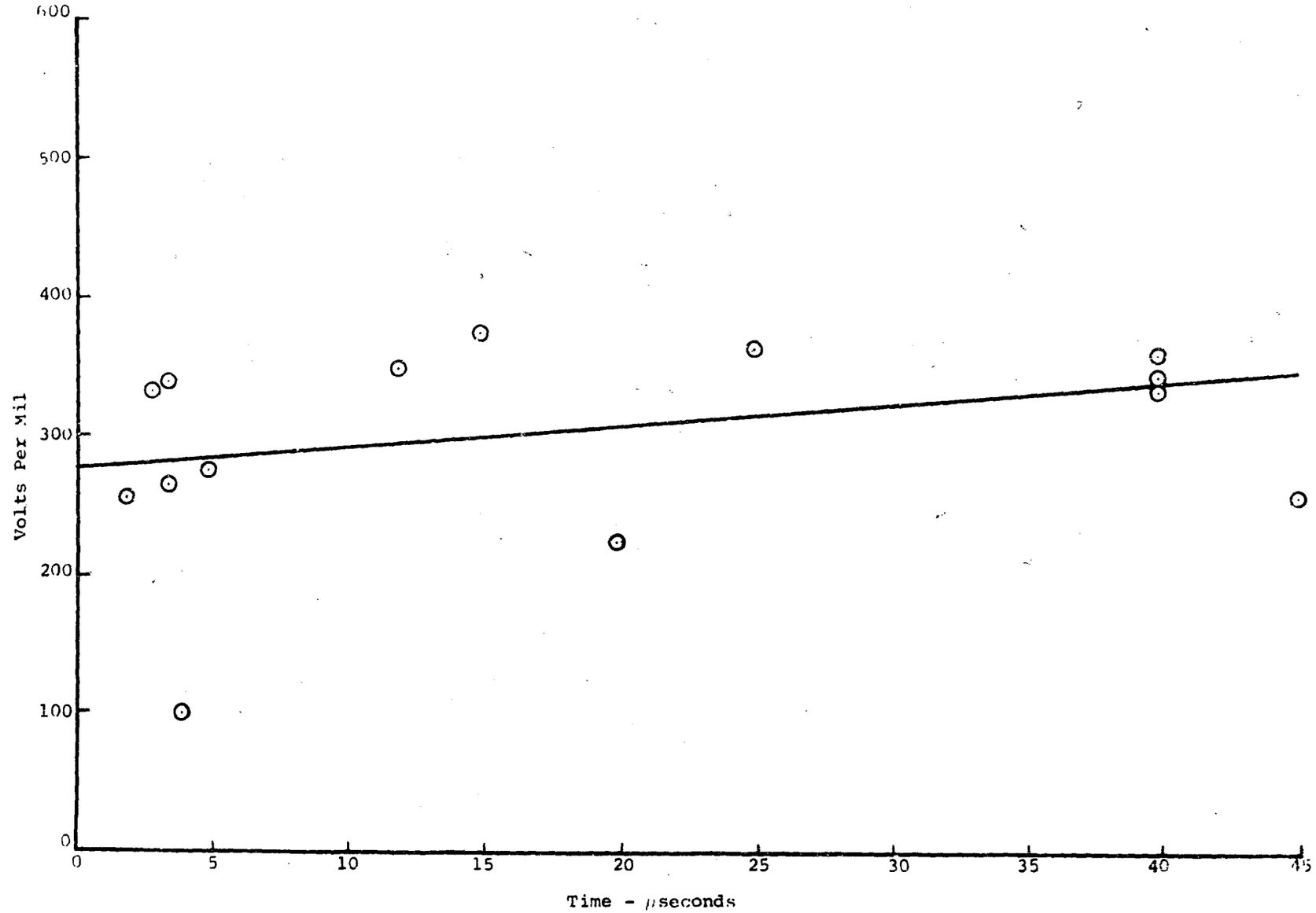

FIGURE 2-9. Dielectric Strength of DEN 438/104 Glass Cloth (3-3.5 mil thickness)

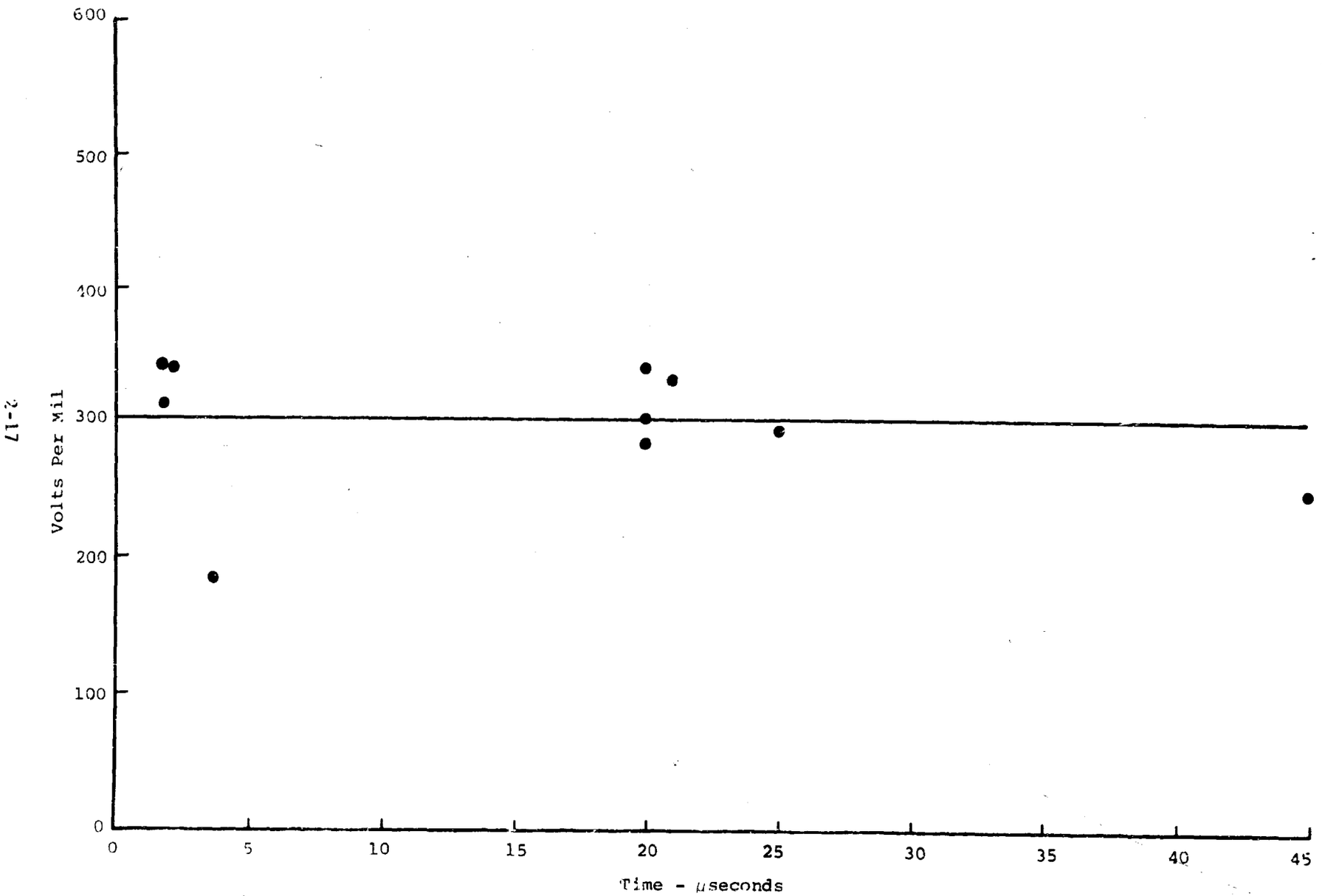

FIGURE 2-10. Dielectric Strength of DEN 438/104 Glass Cloth (2-2.5 mil thickness)

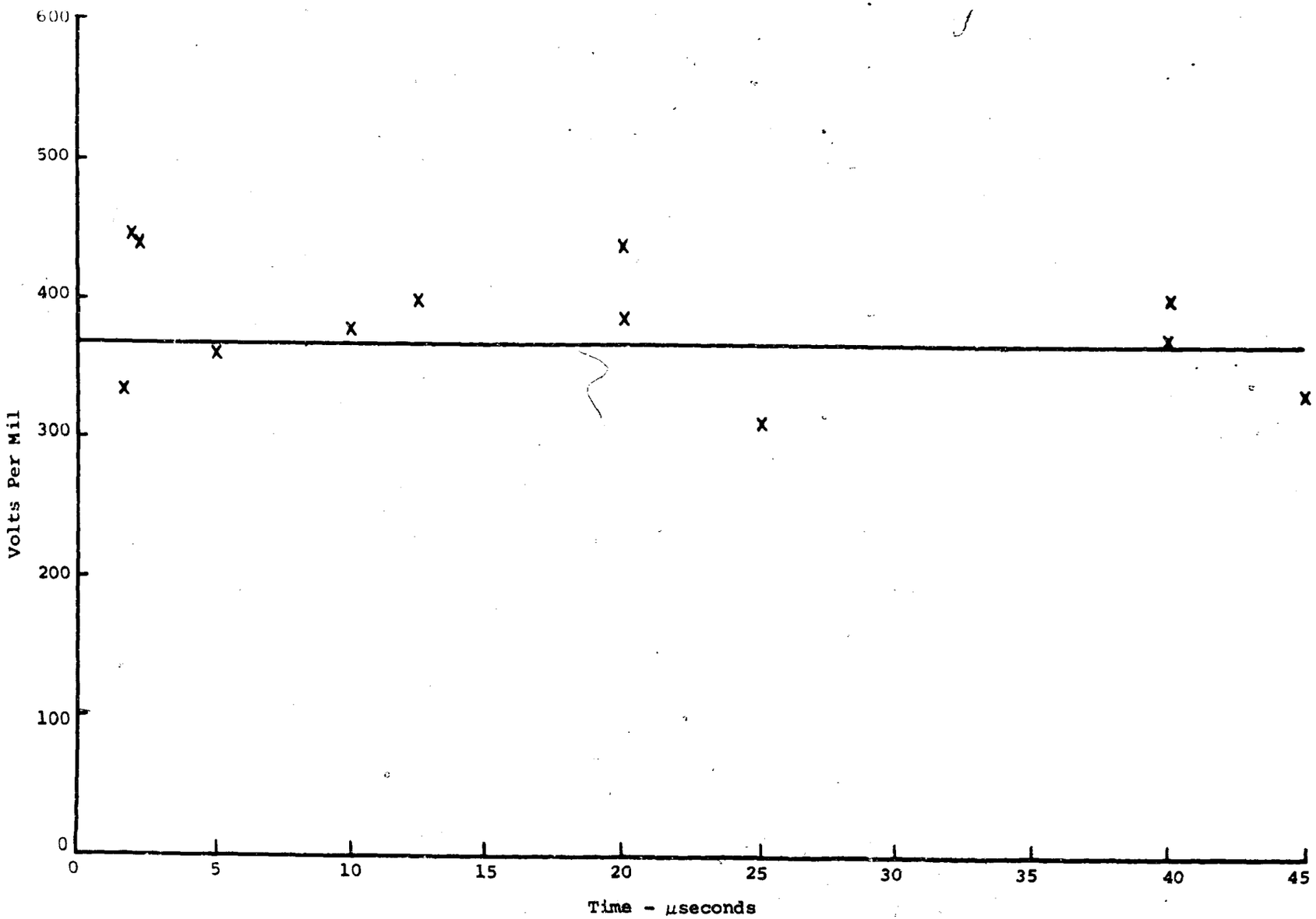

FIGURE 2-11. Dielectric Strength of Whittaker 2387/104 Glass Cloth

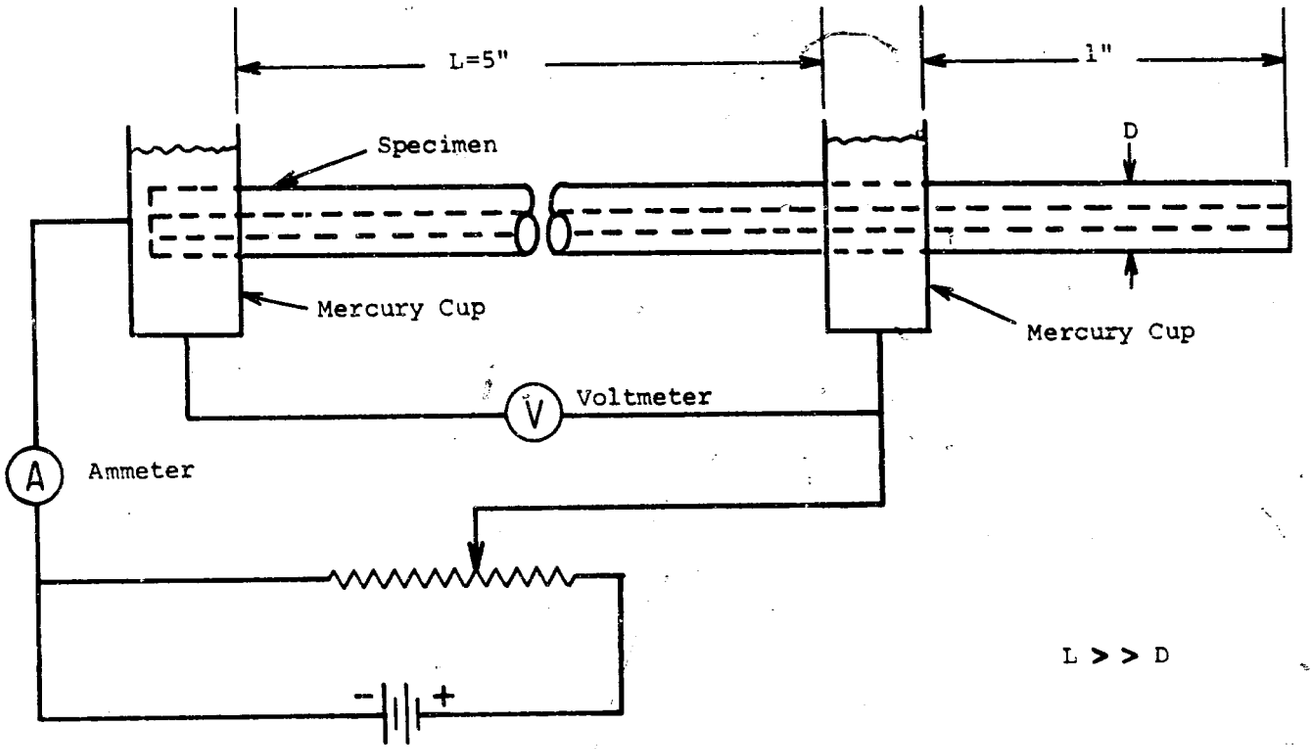

FIGURE 2-12

Set Up to Test Dielectric Strength of Boron Sheath.

Initially, at low voltages, the resistance of the approximately 5-inch long filament is measured at 1 megohm (as determined from voltage and current measurements). If the voltage is increased, however, a value is reached (somewhere between 35 to 50 volts) where the resistance drops instantaneously to approximately 500 ohms (again determined from the voltage and current measurements).

Consider now what one would expect, as determined by calculations. From earlier current injection tests it was found that mercury (because of surface tension) made poor contact with the substrates of the filaments. It may, therefore, be assumed that the test piece under consideration here is depicted by Figure 2-13. That is to say, electrical contact is not made by the mercury, with the substrate, at either end.

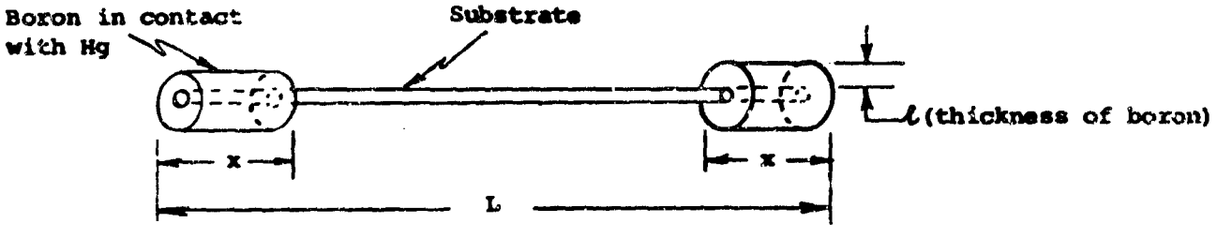

FIGURE 2-13. EQUIVALENT MODEL OF DIELECTRIC TEST SPECIMEN

For boron surrounding substrate (one end only):

mean radius of boron $= 1.125 \times 10^{-3}$ inch

$A = 2\pi\,(1.125 \times 10^{-3})(2.54)(0.635) = 11.4 \times 10^{-3}\ cm^2$

$x = 0.25\,(2.54) = 0.635$ cm

$\ell = (2 - 0.25)(10^{-3})(2.54) = 4.45 \times 10^{3}$ cm

$\rho_B = 1.2 \times 10^{6}\,\Omega$ - cm

$$R_B = \rho_B \frac{\ell}{A} = \frac{(1.2 \times 10^{6})(4.45 \times 10^{-3})}{11.4 \times 10^{-3}} = 0.515 \times 10^{6}\,\Omega$$

or for both ends

$$R_B = 1.03 \text{ megohms}$$

Thus, agreement is obtained between the calculated and measured.

If the boron does, in fact, breakdown completely, then the final value of resistance should be that of the substrate.

For an approximately 5 inch length of specimen (pure tungsten substrate):

$$\rho_w = 5.5 \times 10^{-6} \Omega \text{ - cm}$$

$$A = 1.265 \times 10^{-6} \text{ cm}^2$$

$$\ell = 5\ (2.54) = 12.7 \text{ cm}$$

$$R_W = \rho_W \frac{\ell}{A} = \frac{(5.5 \times 10^{-6})(12.7)}{1.265 \times 10^{-6}} = 55.2\ \Omega$$

It is known that the substrates are not pure tungsten, but are borides of tungsten. Measurements at test and dynamic impedance plots have shown these substrates to have an impedance value approximately 10 times that of pure tungsten. Therefore, this 5 inch length of substrate should measure about 550 ohms. Since the measured values were in the order of 500 ohms, close agreement between measured, and anticipated, is observed.

2.2.3 DYNAMIC IMPEDANCE OF FILAMENTS

The dynamic impedance of boron filaments subjected to 2 amp, 5 amp and 7 amp current levels (4.3 x 22μs wave) have been obtained from the oscillograms taken during current injection for the degradation studies. The median values are plotted in Figure 2-14. Also shown are the maximum and minimum value measured at each time increment. It will be noted that if each of the curves obtained is extended back to t = 0, they all converge at 1300 - 1350 ohms, indicating that the median value of this specimen type before test is in order of 1300 ohms. The lowest value measured at the time of test was 1396 ohms, but it has been established that good electrical contacts have not been achieved. A first look at these curves raises the question that perhaps the negative temperature coefficient of resistivity for boron is more significant than first thought. Also, preliminary analysis indicates that the substrate is not pure tungsten, as previously known, so the magnitude of the spread between resistivities of the boron and substrate core becomes a question of prime importance.

A similar set of dynamic impedance curves for the HMG-50 graphite yarn for exposures of 13 amp, 132 amp, and 163 amp (3.12 x 22μsec); and 300 amp (3.5 -33μsec); and of 500amp (2.4-25μsec) are given in Figure 2-15. The

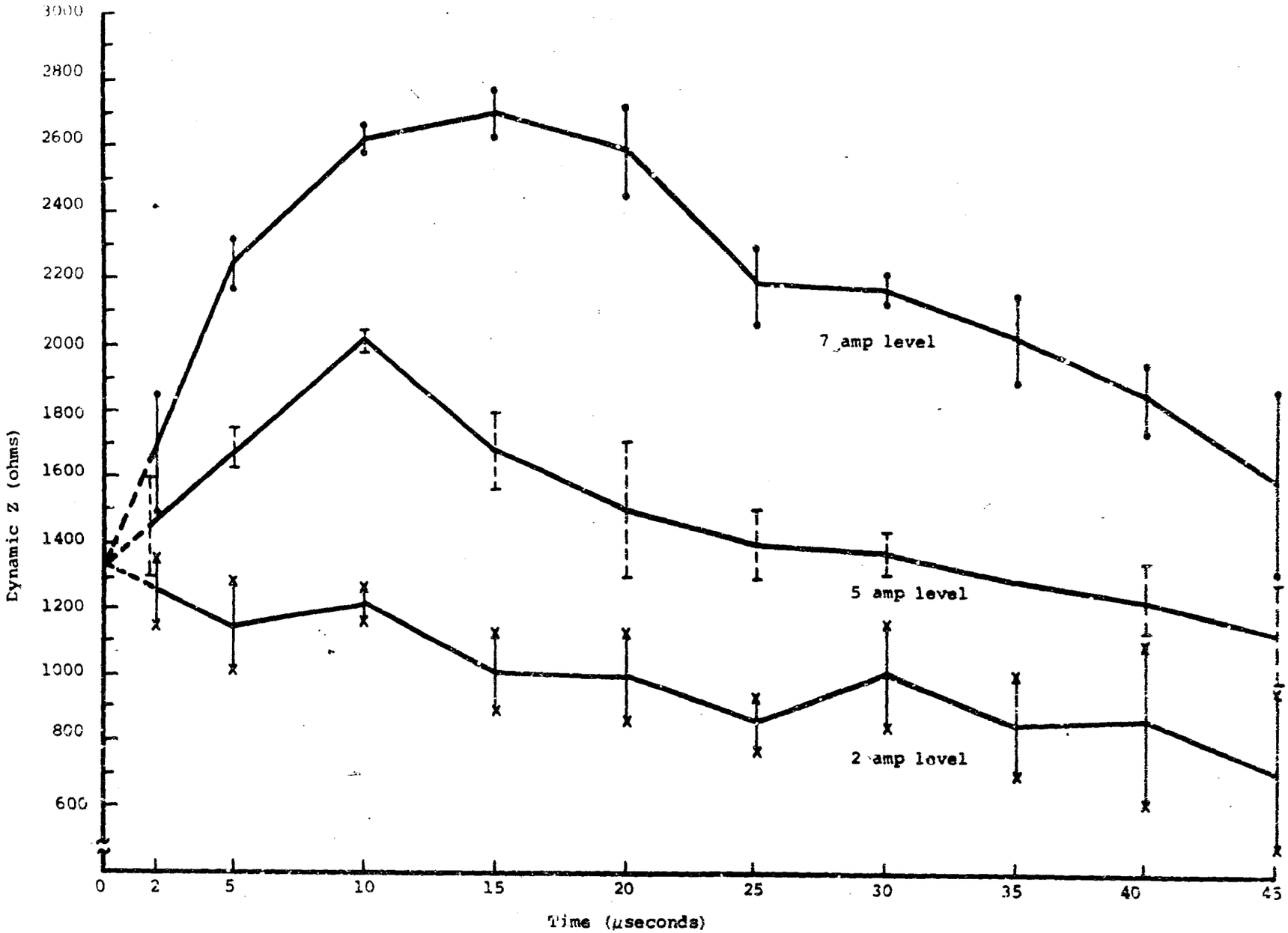

Figure 2-14 Dynamic Impedance of Boron Filament Specimen

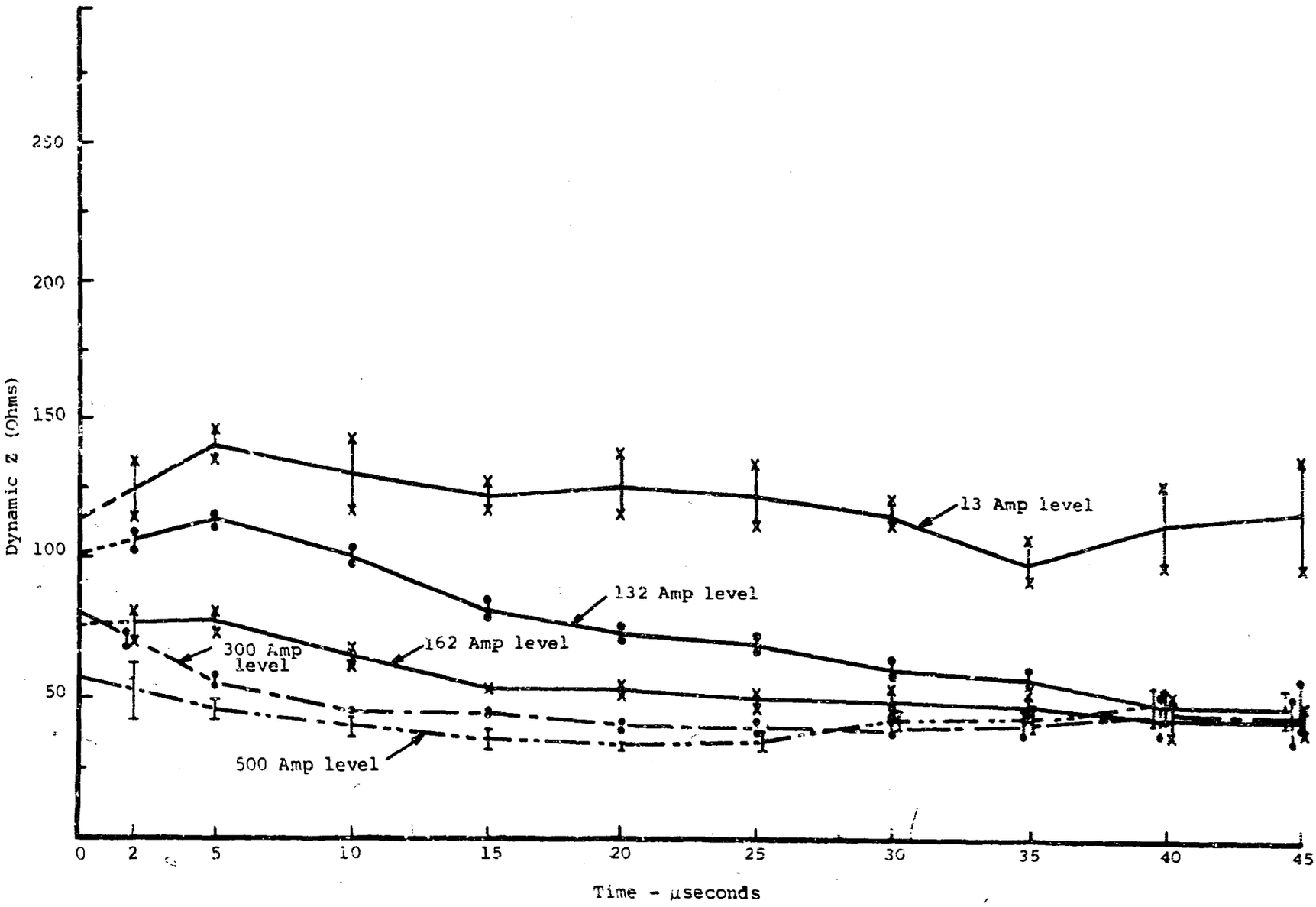

FIGURE 2-15. Dynamic Impedance of HMG 50 Graphite Yarn

median values are plotted, but also shown are the maximum and minimum values measured at each time increment.

The dynamic impedance curves for graphite tows subjected to 625 amp, 3000 amp, and 5000 amp current levels is given on Figure 2-16. Dynamic impedances for boron unidirectional laminates subjected to 2600 amp, 3900 amp, and 5200 amp current levels are plotted on Figure 2-17. At the 3900 amp level half of the samples exhibited a partial breakdown in impedance. Therefore, Figure 2-17 shows three plots at the 3900 amp current level: the upper plot is of those specimens showing no breakdown effect, the lower plot is of those specimens showing breakdown effects, while the center plot is a median of all specimens at this level.

2.2.4 CURRENT FLOW TRANSVERSE TO BORON FILAMENT DIRECTION

Some testing has been done on boron unidirectional transverse specimens (fiber direction 90° to that of specimen length). The specimens were supported in a test jig in the same manner as all previously tested specimens.

The 90° boron filament orientation will not provide a conductive path until a resin breakdown or a flashover occurs. This breakdown voltage, therefore, becomes a determining factor.

The test circuit used is shown in Figure 2-18. This circuit allows a controlled voltage wave to be applied to the specimen. In order to establish a conductive path through one of these 6-inch long specimen in this configuration, it is estimated that approximately 1.5 inches of resin must be broken down.

From the dielectric strength curves just presented, it can be seen that 300V/mil would be a reasonable figure to work with for resin dielectric strength.

The required voltage for breakdown would, therefore, be (1500 mils) x (300V/mil) = 450 kV. A voltage of this magnitude could be expected to breakdown a 6-inch air gap. Therefore, with the specimen present in the gap, flashover could be expected at voltages considerably below this 450 kV value. This expectation became reality when flashover of the test piece occurred at 100 kV.

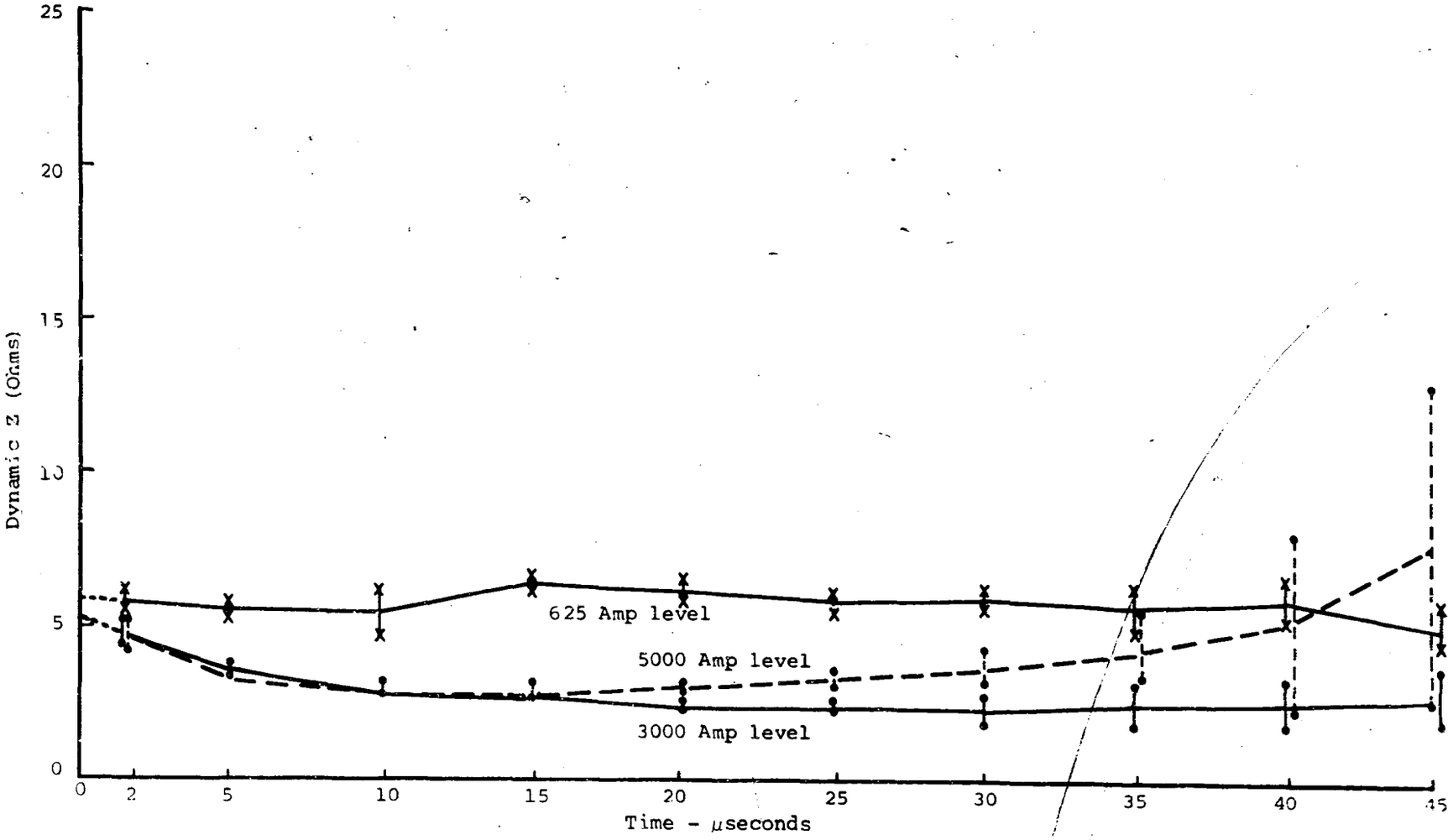

FIGURE 2-16. Dynamic Impedance of HM-S Graphite Tow

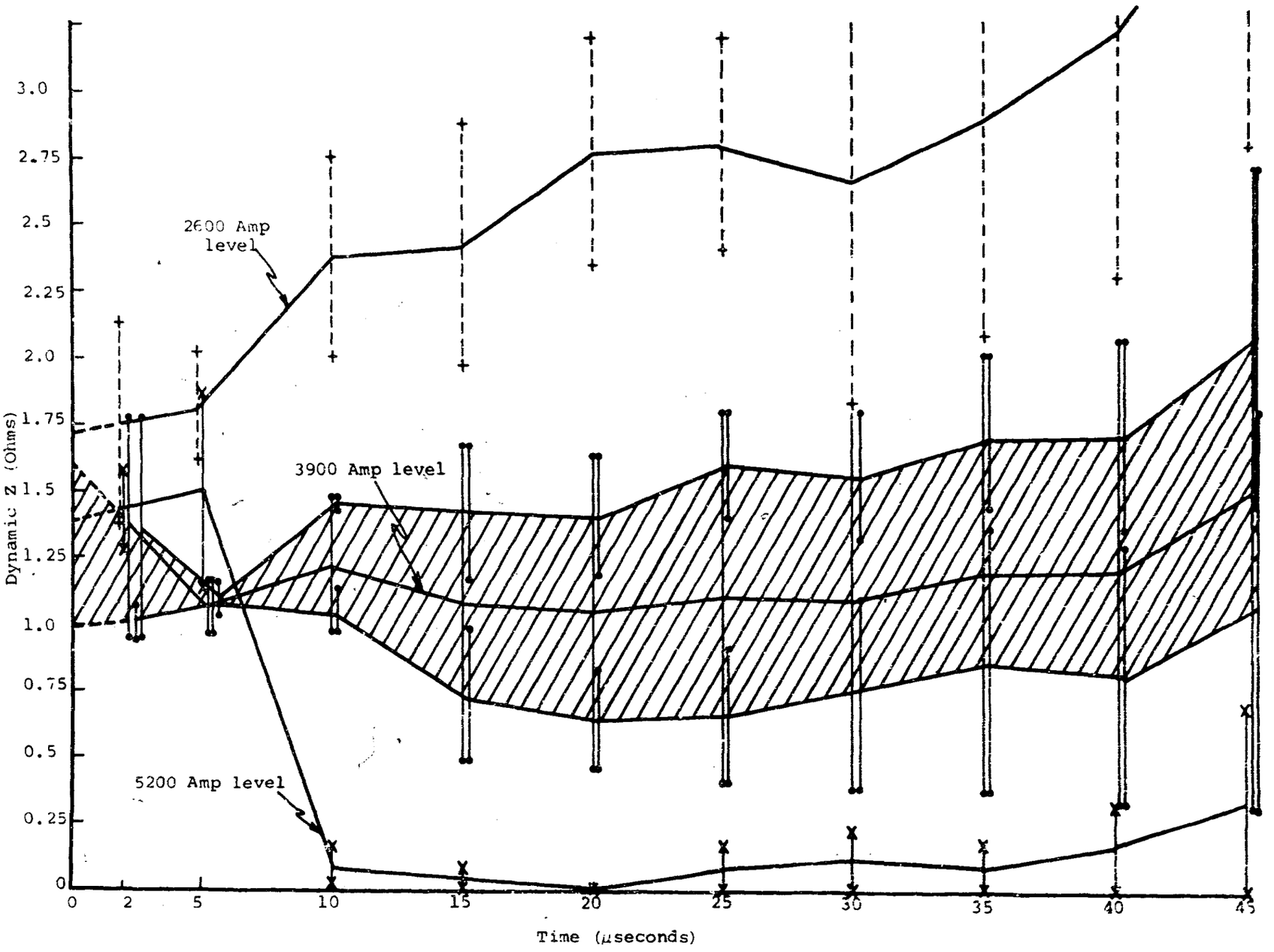

FIGURE 2-17. Dynamic Impedance of Boron Unidirectional Laminates

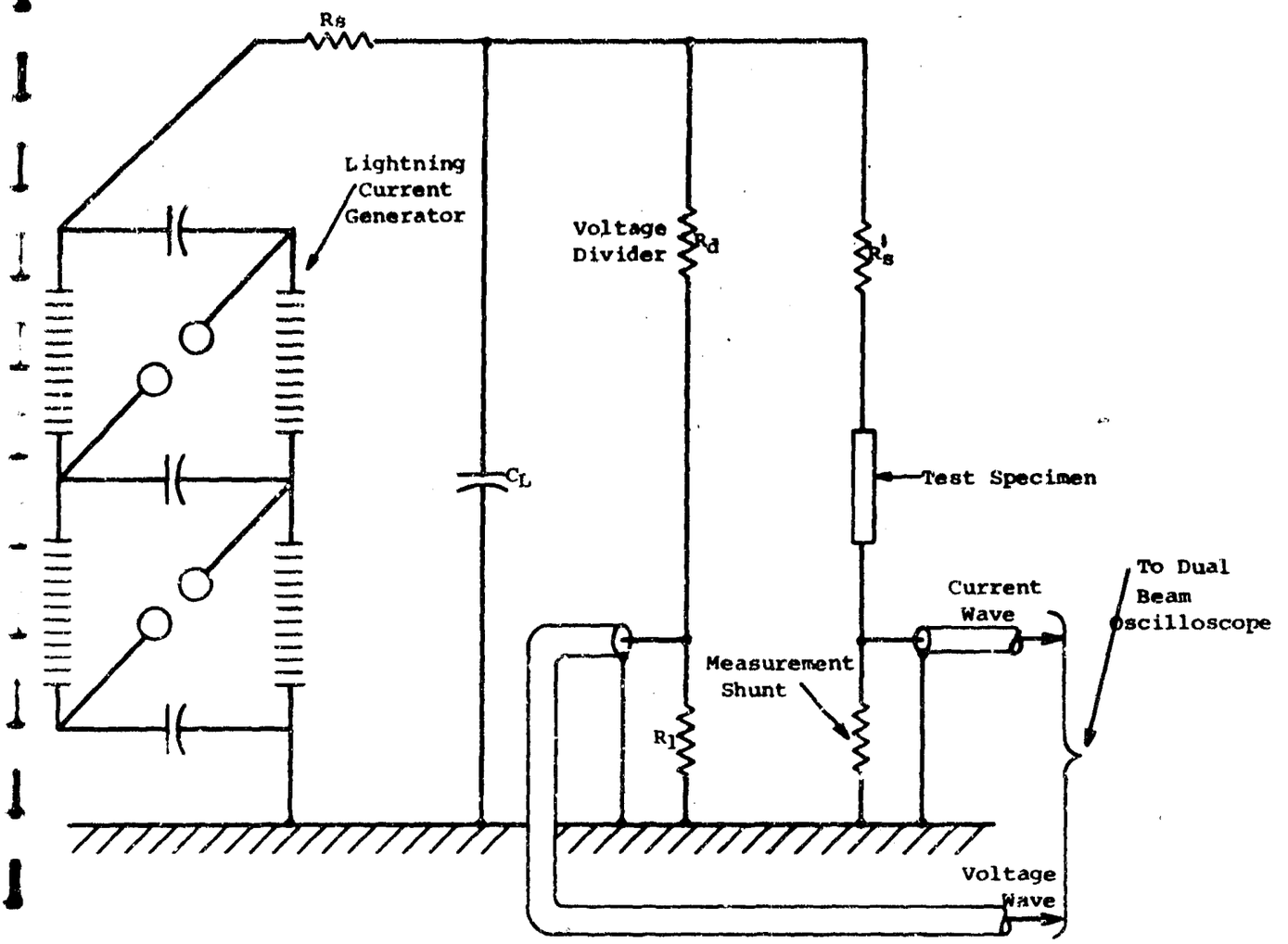

FIGURE 2-16. TEST SET-UP FOR CURRENT FLOW TRANSVERSE TO BORON FILAMENTS.

2.2.5 BASIC ELECTRICAL CURRENT FLOW MODELS

As reported in Reference 2 by Philco-Ford and General Electric, a model was envisioned for the case of an electrical current impulse introduced into one side of a composite, or into one ply. This model is reported below:

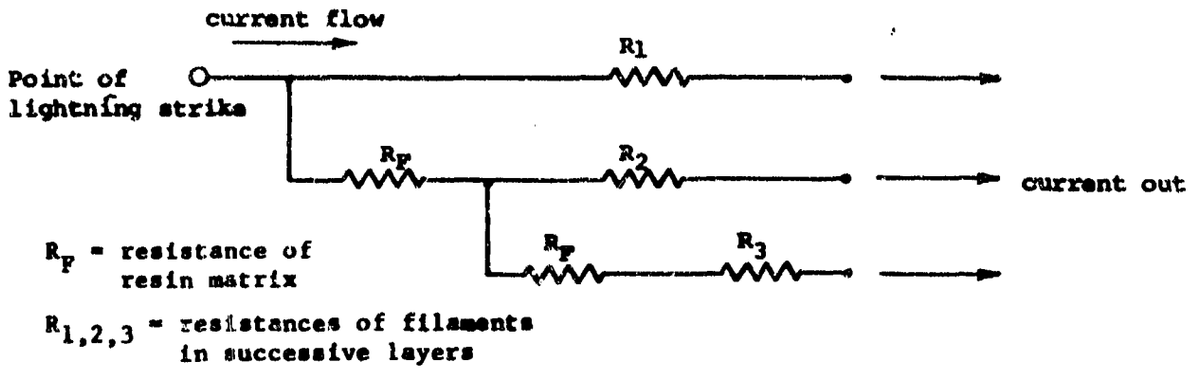

FIGURE 2-19. INITIAL MODEL OF CURRENT FLOW IN A UNIDIRECTIONAL COMPOSITE.

Results of this program to date now allow for modifications to this model and for the introduction of others.

Observation of current flow during impulse tests have shown that the filaments do not fail at the current crest. That is to say, the current waveform is continuous.

As discussed in Section 2.3, boron filament failure probably results from the differences in thermal expansion between the substrate and the surrounding boron. Furthermore, the severe transverse and axial cracking of boron filaments has been observed to occur sometime after the current impulse has ceased.

It has also been observed during this program that the resin matrices exhibit a definite voltage breakdown level. With this much information the initial model may be modified as Figure 2-20.

The zener diodes represent the breakdown strength of the resin matrix and R1, R2, and R3 are again the filament substrate resistances. This model, however, only applies to the case of an electrical current impulse introduced into one side of the outermost ply of a boron/epoxy unidirectional

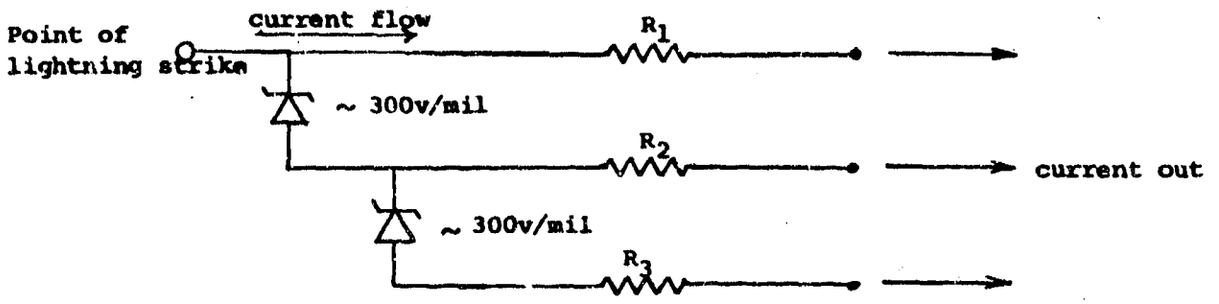

FIGURE 2-20. FIRST MODIFICATION OF INITIAL CURRENT FLOW MODEL OF FIGURE 2-19.

laminate. It assumes that the first stroke or pulse of current is carried by the outer ply of filaments. When the threshold current of degradation of that ply has been exceeded, the filaments fail by transverse or axial cracking, which interrupts the current flow path by increasing the resistance of that ply. As the resistance increases so does the voltage drop along the ply until the breakdown level of the resin film between plies of filaments is reached. After this interply resin punctures, the current goes to the next, or deeper, filament or layer of filaments. This process is assumed to be progressive if multiple strokes are applied.

More basic than this composite current flow model is that of a single boron filament. Shown in Figure 2-21 is a unit length model of such a filament.

If contact is made directly with the filament substrate, then predominately all of the current flows in the substrate (R_s). This results from the fact that the conductivity of the substrate is much greater than that of the boron ($R_s \ll R_B$). If contact is made with the boron only, then current flows in the boron (R_B) until a sufficient voltage appears at some point to cause the avalanche effect noted and reported in Section 2.2.2. This avalanche breakdown effect is represented, in the model, by the zener diode and shunt resistor. This model is incorporated in the initial model presented, but is reduced simply to R_s. The reduction is valid since the 20-25 volts required to breakdown the boron would surely be present once the interply resin punctured.

If this simplified model of the filament is again employed, a general model of a boron/epoxy unidirectional laminate can now be developed. This model considers the laminate on a per unit length basis, and allows current entry from any point. (Figure 2-22).

In this general model all filaments are represented simply by k_s, for reasons just explained; all interply resin layers are represented as zener diodes, which effectively model their breakdown strength; and all

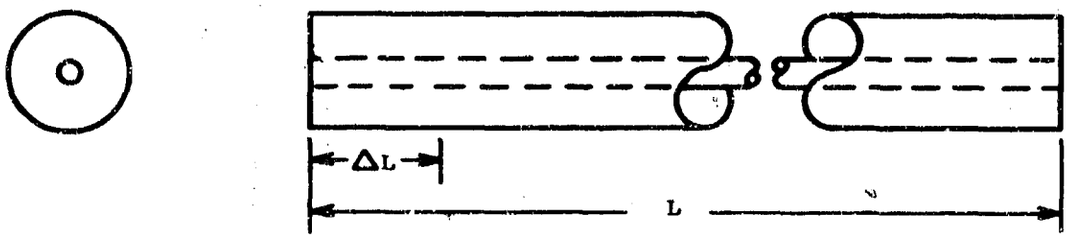

Boron Filament

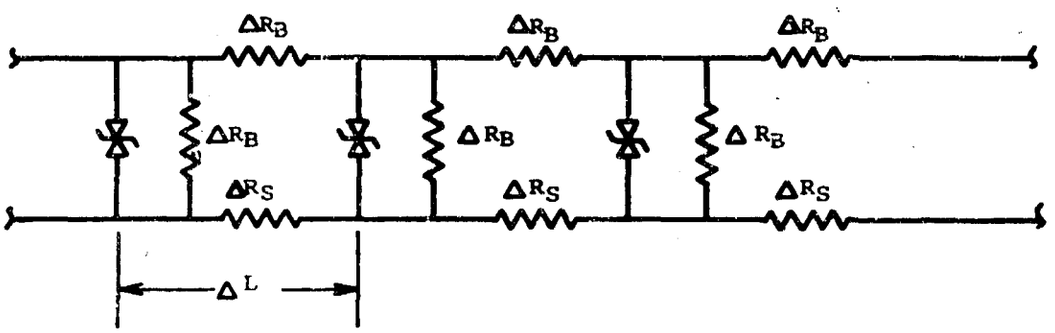

Equivalent Model Of Boron Filament

FIGURE 2-21. UNIT LENGTH CURRENT FLOW MODEL FOR A BORON FILAMENT.

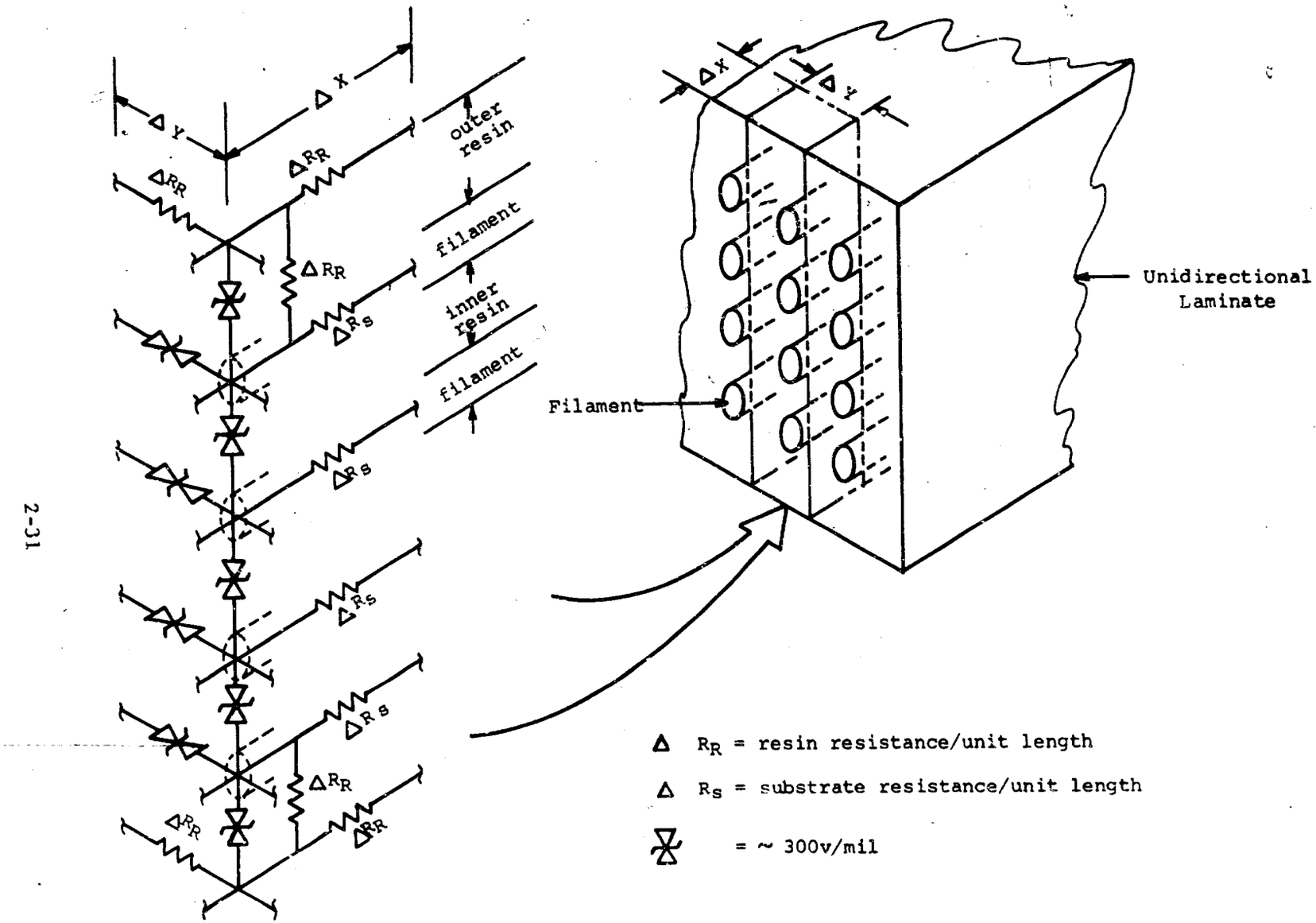

FIGURE 2-22. CURRENT FLOW MODEL OF BORON/EPOXY UNIDIRECTIONAL LAMINATE.

outer resin layers are modeled completely in order to allow current entry from any point on the surface. A current flowing at the specimen surface would cause a voltage rise across ΔR_r (resin resistance), in parallel with the zener diode. Once the resin breakdown voltage is reached, as represented by the diode, a direct low resistance current path to the filament is formed.

It should be noted that the model delineated here is that of a finite portion of the whole specimen. Although construction of a model of the entire specimen is possible, it would be extremely complex.

2.2.6 INITIAL CONSIDERATION OF CURRENT FLOW PARAMETERS THAT AFFECT BORON FILAMENT DEGRADATION

For further discussion it will be assumed that current is injected directly into the filament substrate core and that the current is carried uniformly by all filaments within the specimen. Consider now any two filaments within a laminate (based on the general model presented in Figure 2-22), as shown in Figure 2-23.

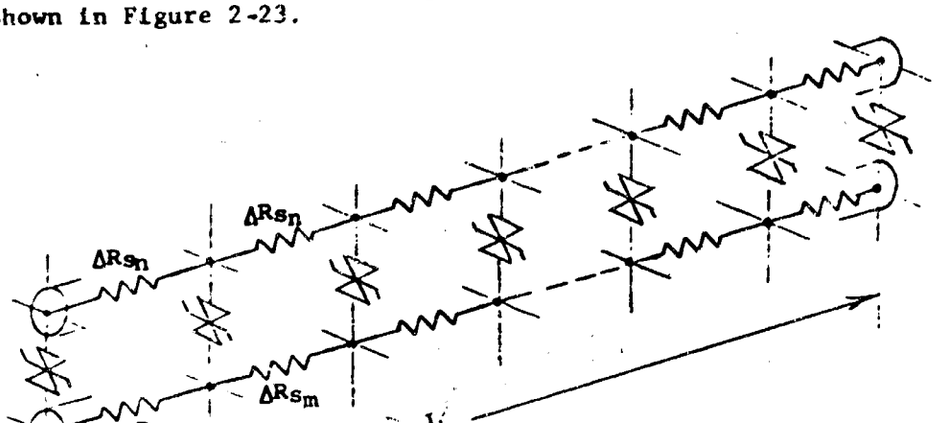

FIGURE 2-23. SCHEMATIC OF TWO FILAMENTS WITHIN LAMINATE.

It will be noted that the filament is made up of incremental sections. That is the total filament resistances are:

$$R_{s_n} = \Sigma \Delta R_{s_n}$$

$$R_{s_m} = \Sigma \Delta R_{s_m}$$

(The subscripts m and n are used only to facilitate the discussion, by generating a means of differentiating between the two substrates.) Recall also that the zener diodes represent the breakdown strength of the epoxy resin separating the filaments.

The current flow process for the particular case when current was injected into the outer ply has already been presented. In addition to that singular condition, it now becomes desirable to explain the current flow processes in general. An explanation of the reduction in impedance seen when higher level current pulses are injected is also desired.

Until now all discussions have considered the substrates of boron filaments to be homogeneous, and thus behaving as uniformly distributed resistors as shown in Figure 2-24. Most investigations, however, have shown that the substrates are not pure tungsten, but borides of tungsten. In fact in nearly all cases there is no free tungsten at all within the substrate. It may, therefore, be assumed that the resistance per unit length of each filament will be inconsistent resulting in a non-uniform resistor, and the overall effect will vary from filament to filament.

Return now to filaments m and n of Figure 2-23. Since these are two typical filaments, it is entirely possible and probable that their makeups are different with respect to substrate composition and that neither one is uniform. This situation is shown in Figure 2-25.

There are two distinct possibilities as to how the specimen initially fails. The first of which is depicted in Figure 2-26. Here it can be seen that between points A and B of the curves for filament n, 25% of the total voltage is supported by approximately 7% of the specimen length. This amount of stress could possibly cause a breakdown (flashover) within the filament and thus initiate a "snowball" effect. Just what results after this initial failure is unclear, mainly because of the complexity of the situation. The breakdown would result in a 25% reduction in resistance, with a simultaneous increase in current through the filament and voltage rise across it. At the same time, only 93% of the initial specimen length is supporting the voltage.

It must be pointed out that the failure need not occur at the filament end, the stressed region of other filaments might be internal from the ends. Thus, simultaneously and continuously the current magnitudes and voltage stresses are changing within a laminate, resulting in an extremely complicated situation.

The second possibility for initiation of failure is depicted in Figure 2-27. Here it is seen that the two filaments under consideration have a difference in potential between them, at one point, which is equal to 45% of the voltage across the entire specimen. Once this potential difference exceeds the breakdown strength of the epoxy resin (approximately 300V/mil) the resin will puncture.

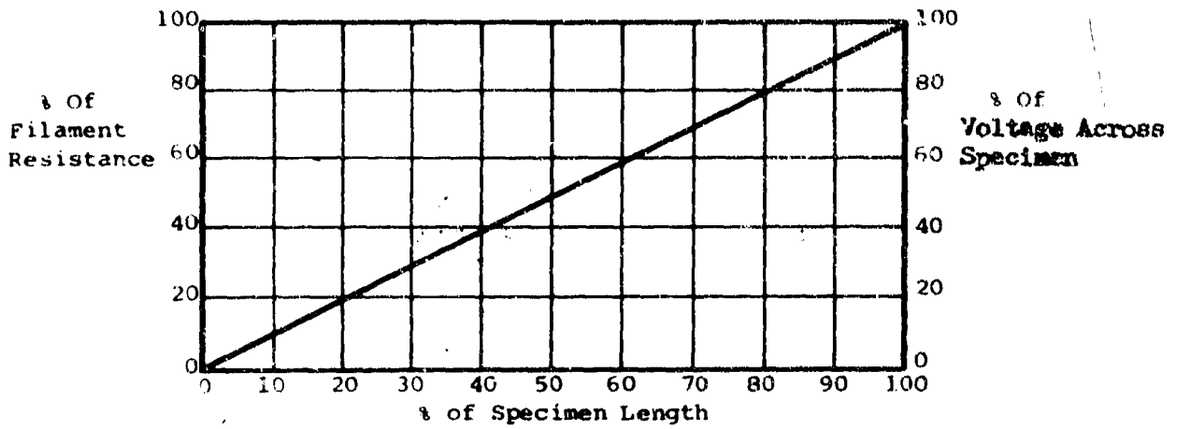

FIGURE 2-24

Resistance and Voltage vs. Length of Specimen

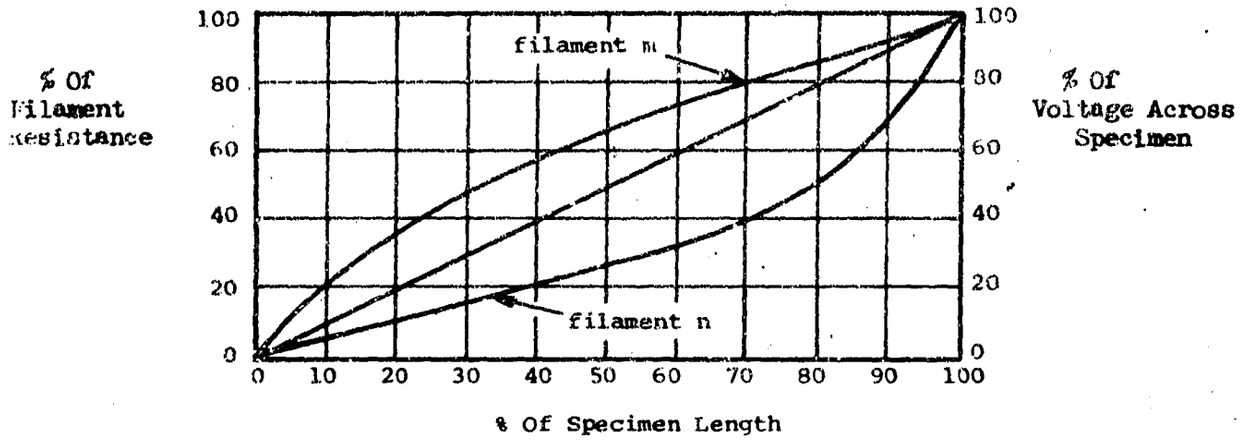

FIGURE 2-25

Resistance and Voltage vs. Length of Specimen

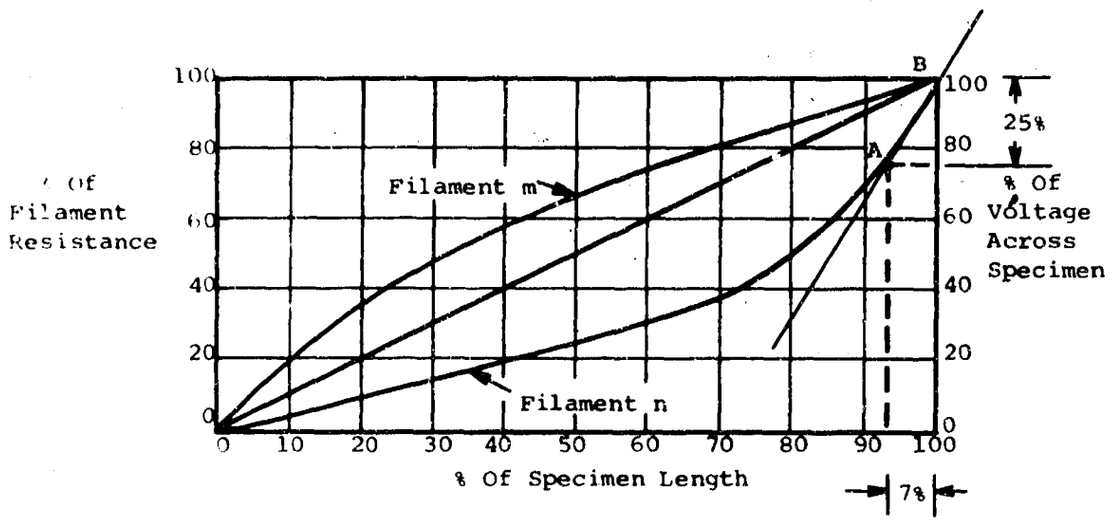

FIGURE 2-26

Resistance and Voltage vs. Length of Specimen

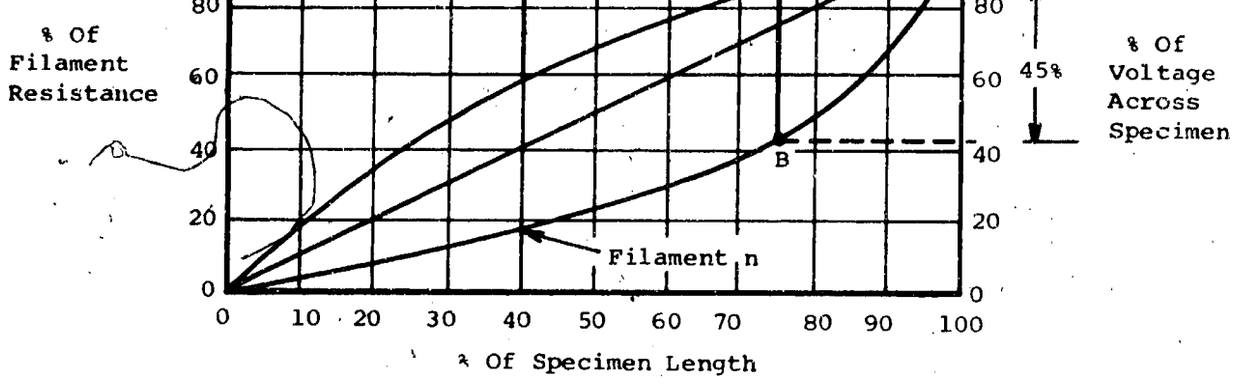

FIGURE 2-27

Resistance and Voltage vs. Length of Specimen

Once again, the sequence of events after initial failure are complex and unclear. The two filaments at the point of puncture seek the same potential which is determined by the parallel resistance combinations of their two halves, and again the currents through the filaments and the voltage stresses across them change.

It also becomes evident that combinations of these two mechanisms can occur simultaneously, and to varying degrees, adding further complications after failure initiation. Clearly these initiation factors are of prime importance for this study.

2.2.7 FORCES ON SPECIMENS CAUSED BY INJECTED CURRENTS

High currents, injected into some graphite fiber composite specimens during this investigation have caused a separation of fibers. This has been witnessed as varying degrees of "ballooning" and exfoliation of fibers. A question which now arises is how the "ballooning" relates to the current.

Inside of a conductor itself is a mechanical force exerted between the magnetic flux and the current-carrying conductor. The force between the 0.0003 inch diameter graphite filaments of the conductor is an attraction, so that current in a conductor tends to contract or "pinch" the conductor. This being the case, the resulting "ballooning" which is observed would not result directly from the current flow, but is due perhaps to a secondary effect such as gas vapors escaping from the pyrolyzing resin materials at an extremely rapid rate, as discussed in Section 2.3.

2.3 DEGRADATION OF FILAMENTS AND COMPOSITES

In accordance with the test procedures discussed in Section 2.1, several series of tests were performed whereby electric current of varying crest amplitudes and waveforms was injected into filament and composite specimens. The filament specimens included boron monofilaments, HMG-50 graphite yarn and HM-S graphite tow. Also, as previously discussed, unidirectional epoxy resin matrix specimens of each filament type were similarly exposed. Crest amplitude and waveform as well as resistivity before and after test were recorded. Visual observations during and after current injection were noted. Also, current applied per unit cross-sectional area of the specimen as well as per unit cross-sectional area of filament in the composites were calculated. From each set of typically six specimens, two were used for photomicrographic inspection and four were tested for strength subsequent to the current injections. All such data is tabulated in the appendix of this document. Following is a discussion of the degradation observed and interpretation of the degradation mechanisms involved.

2.3.1 BORON FILAMENT AND COMPOSITE DEGRADATION

In order to determine the limiting factors relative to boron-epoxy composite degradation, both the composites and filaments were subjected to electric current injection. The tests and inspections to determine degree of degradation, causes of degradation, and mechanics of degradation as well as degradation models developed are summarized as follows:

a. Strength Degradation of Boron Filaments and Composites. The tensile strength of exposed boron filaments was determined subsequent to electric current injection. The results were compared to the tensile strength of non-exposed filaments from the same lot and roll of filament. The typical results for the standard waveform are illustrated in Figure 2-28. Typically the tensile strength of the filaments was unaffected until a current crest amplitude in excess of approximately 3.7×10^4 amperes per cm^2 of filament cross-section was injected. The strength degradation then was rapid with total disintegration occurring when crest currents of 7.5 - 8.0×10^4 amperes per cm^2 were injected. These filaments disintegrated into varying lengths of segments that were often split axially.

Similarly, the typical degradation of boron-epoxy composites as the result of current flow per the standard waveform is illustrated in Figure 2-29. The threshold for degradation of the composites appears to be in excess of a crest current injection level of 5.7×10^4 amperes per cm^2 of filament cross-section. The current densities were computed by dividing the crest current level by the total cross-sectional area of the filaments within the composite. As noted, the strengths dropped rapidly until a crest current density of 7.85×10^4 amperes per cm^2 was achieved. Attempts to test at current injection levels of greater than 12.3×10^4 amperes per cm^2 (where the composite was degraded to 39% of its original strength) resulted in flash-over

across the specimen. It is noted, however, that the composites did not degrade as severly at the same average current densities as was noted in the results of the single filament tests. This can be explained by consideration of two points. First, even though the filaments within the composite may be split and cracked, they still will reinforce the epoxy resin to a degree and the composite will have some (but reduced) structural integrity. Secondly, the current is not distributed equally among each of the boron filaments within the composite. The filaments do carry the current because of the highly non-conductive dielectric nature of the epoxy resin matrix. The boron filaments typically have a resistivity of 4 - 8 x 10^{-3} ohm-cm. As will be noted later, degraded boron-epoxy composites show evidence that only a portion of the filaments were degraded. It is presently thought that the degraded fraction carries the majority of the current and that some of the filaments carry little or no current. The degraded filaments over the 0.025 inch x 0.50 inch cross-section of the composite specimens occurred at random. This occurred even though the composite ends were scarfed, vapor honed to expose all filament ends and over plated with nickel for electrical contact.

In addition to the fact that the electric current is not uniformly dispersed throughout all filaments within a composite, it also appears that the waveform may be a more important factor in degree of damage than is the crest amplitude of current injected. In the majority of the tests performed, a typical injected current waveform shape was utilized and the exposure levels were changed by varying the crest amplitude of the current. This can be a misleading approach. The degree of degradation is not solely dependent on the crest amplitude. Instead, it is dependent on the total energy dissipated within the specimen, which in turn is proportional to the total energy injected and the particular wave shape or wave form. The total energy injected is varied by lengthening or shortening the current waveform in addition to varying the crest amplitude. To demonstrate this, current injections of boron filaments were accomplished at the same crest but with different waveshapes. To accomplish this, the front time and tail times of the waveshapes were varied. When the waveform was varied from the standard t_f = 2.5 - 4.3μsec and t_t = 22 - 25μsec, the degree of degradation varied from the typical values of Figures 2-28 and 2-29. Typical examples of the influence of waveform on degree of degradation are as follows:

	Current Crest, Amperes per cm^2	Front Time/Tail Time	Percent Strength Degradation
(1)	8.88 x 10^4	1.2/13.5	71
(2)	7.40 x 10^4	4.0/24.0	100
(3)	7.40 x 10^4	4.0/12.0	13

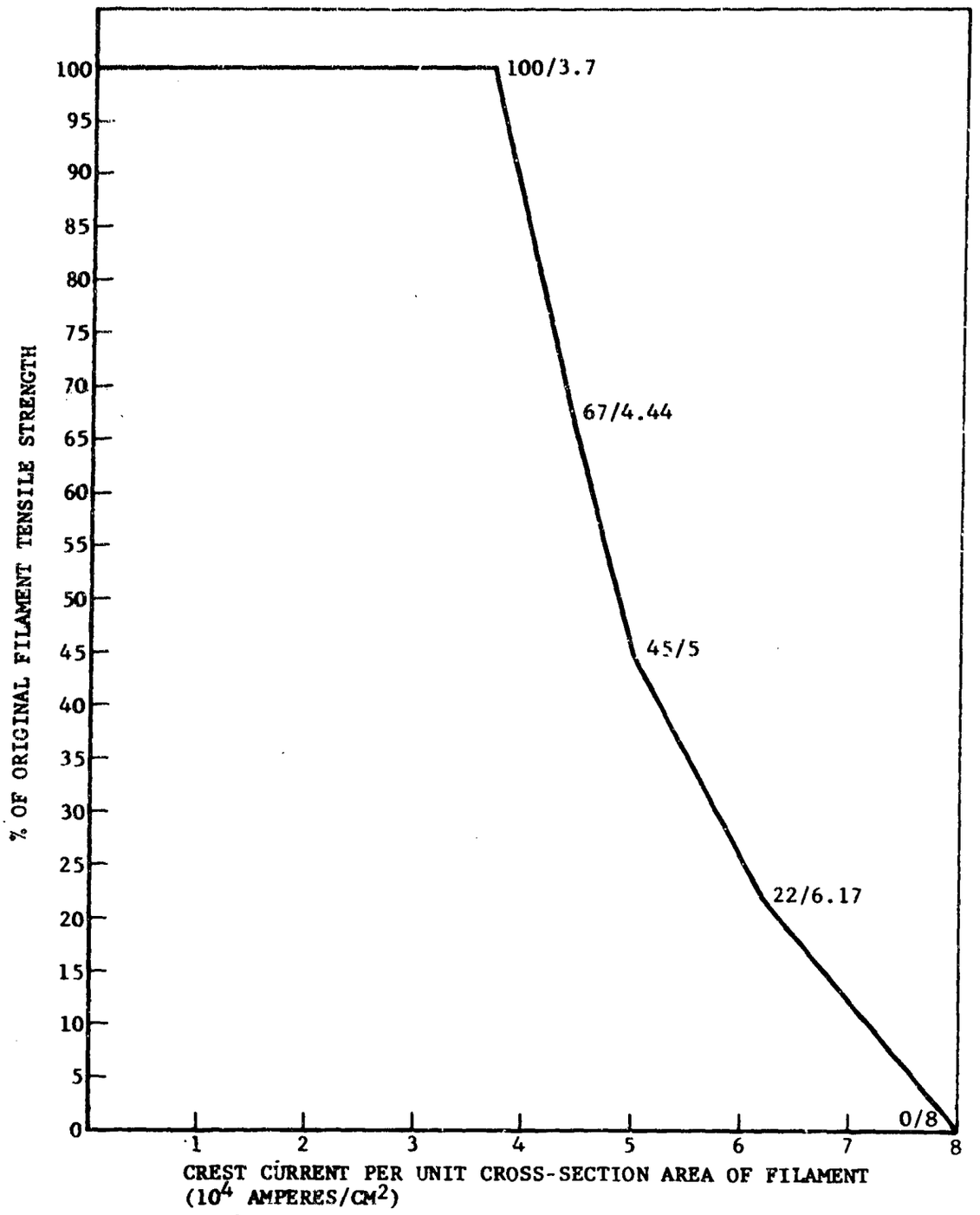

FIGURE 2-28. BORON FILAMENT TYPICAL STRENGTH DEGRADATION VERSUS CREST CURRENT DENSITY (FOR STANDARD WAVEFORM)

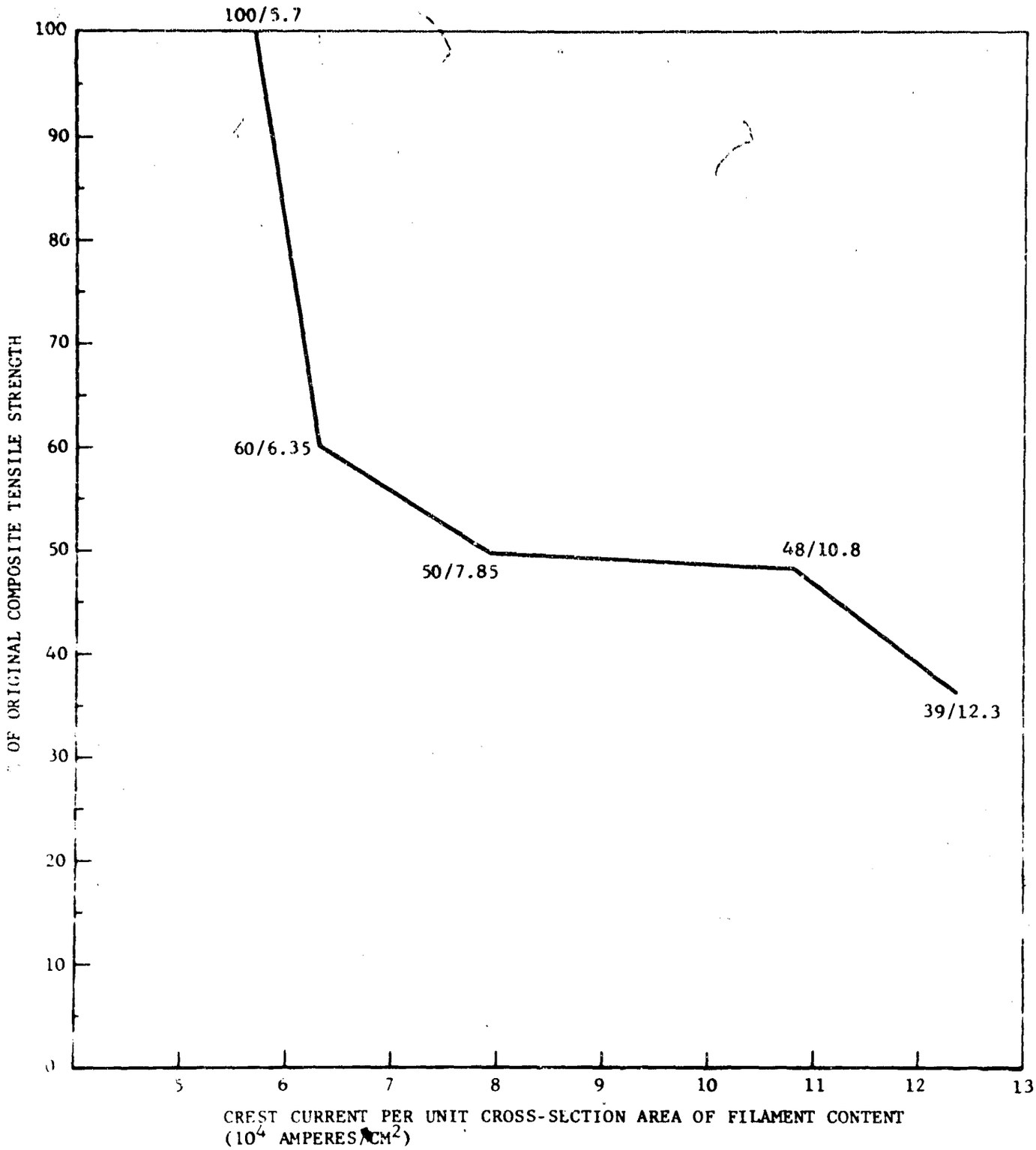

FIGURE 2-29. BORON/EPOXY TYPICAL STRENGTH DEGRADATION VERSUS CREST CURRENT DENSITY (FOR STANDARD WAVEFORM)

As can be seen in (1) and (2), a crest current density of 7.4×10^4 amperes per cm^2 produced total disintegration (100% degradation) while a higher crest current density (8.88×10^4 amperes per cm^2) produced only 71% loss in strength because a shorter waveshape was used, which represented a lower energy input. Also, as can be seen in (3), the same current density of 7.4×10^4 amperes per cm^2 produced only a 13% loss in strength with a shorter waveform. Because of these and similar experimental results, it appears that the most meaningful relationship between electric current flow and boron degradation is one which is based on energy input and resulting energy dissipation, and not solely on crest current amplitude. Furthermore, it was noted during the current injection of boron filaments that distintegration did not occur at crest but an interval of time later.

To further illustrate the dependance of degree of degradation of boron filaments and composites on total energy, Figures 2-30 and 2-31 were drawn. In these, percent degradation versus energy dissipation per unit resistance was plotted for all waveforms and current amplitudes. On this energy basis, all data points fall within bounded regions regardless of waveshape.

b. Photomicrographic Inspection of Degraded Boron Filaments and Composites. A series of photomicrographs were taken of boron filaments and composites that showed a marked decrease in strength. The photomicrographs were taken in order to better understand the changes and/or damage that occurred within the filaments as the result of electric current injection. Standard techniques were used in taking these photomicrographs.

For reference purposes in examining the photomicrographs of damaged filaments, Figures 2-32 and 2-33 are cross-sections of filaments that have not been exposed to current injection. In both of these pictures the 0.0005 inch diameter substrate core is readily distinguishable within the 0.004 inch diameter boron filament.

Figure 2-34 (Specimen B-20) is a longitudinal view of an actual boron filament which represents a six specimen set of boron filaments which lost 54% of their tensile strength, after exposure to 4 amperes current injection. Note the longitudinal and axial cracks and compare with the undegraded control specimen in Figure 2-33. Figure 2-35 and 2-36 show a burned spot or hole between the core and boron sheath, corresponding to the line in Figure 2-34. Also note the irregular cross-section in Figure 2-35.

Figures 2-37, 2-38 and 2-39 illustrate three types of damage occurring in boron filament #50, which had a current injection level of 7.2 amperes. The specimen from which the piece was taken was mechanically tested and yielded a breaking strength 70% lower than unexposed filaments. Surface spallation from the filament is indicated because of its irregular outer

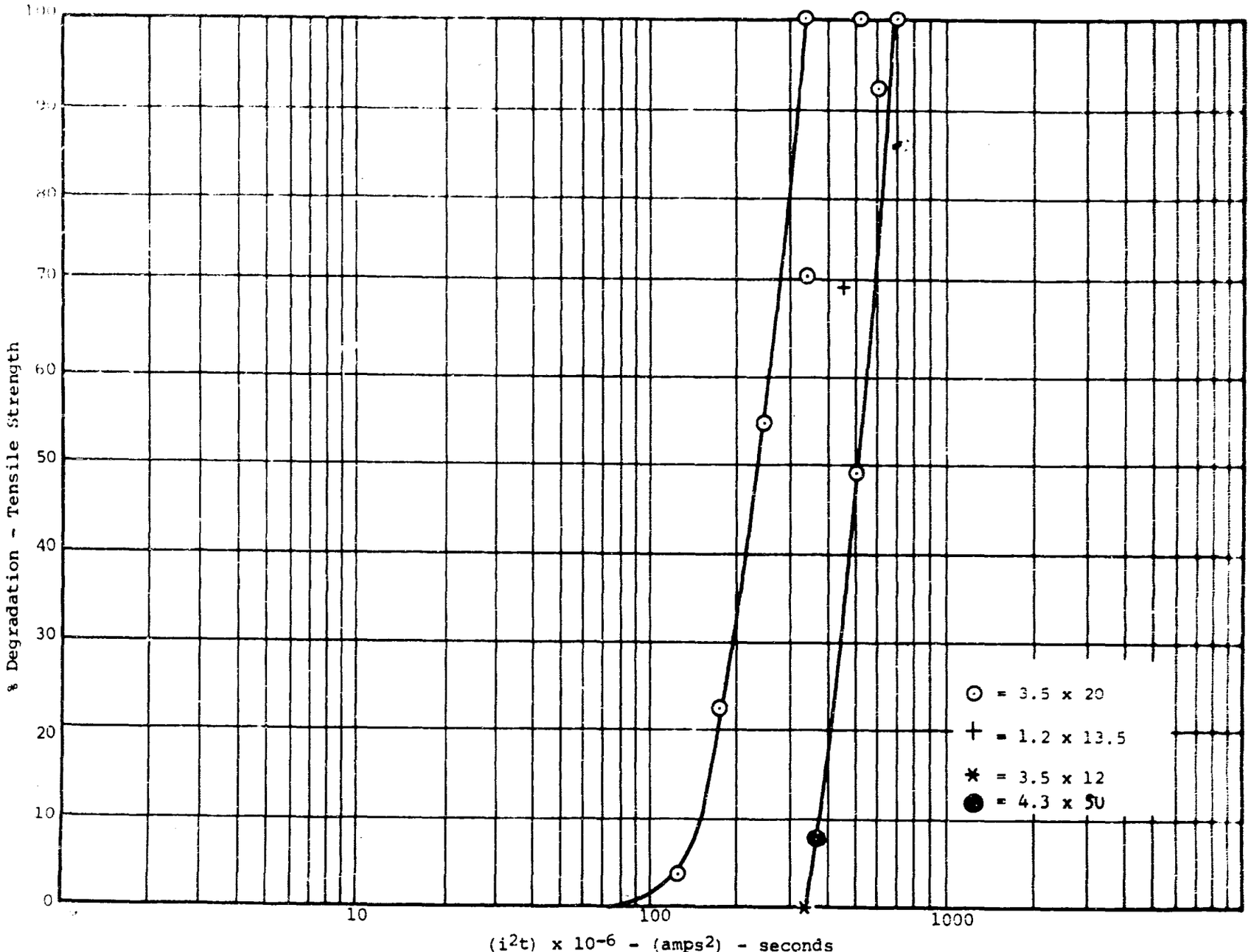

FIGURE 2-30. Degradation vs. Energy per Unit Resistance. (Boron Filaments)

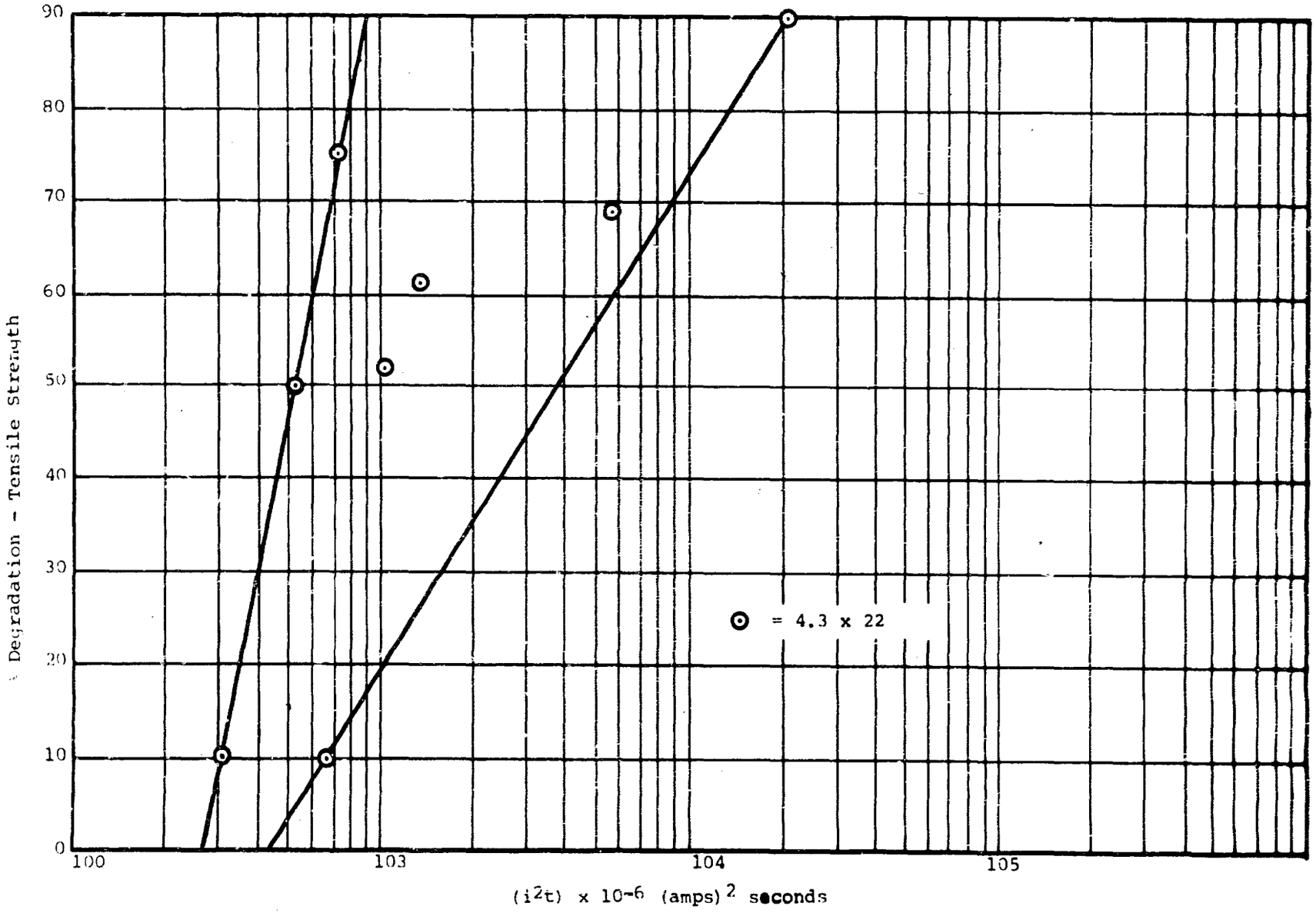

FIGURE 2-31. Degradation vs. Energy per unit Resistance (Boron Unidirectional Laminates-on a per filament ba

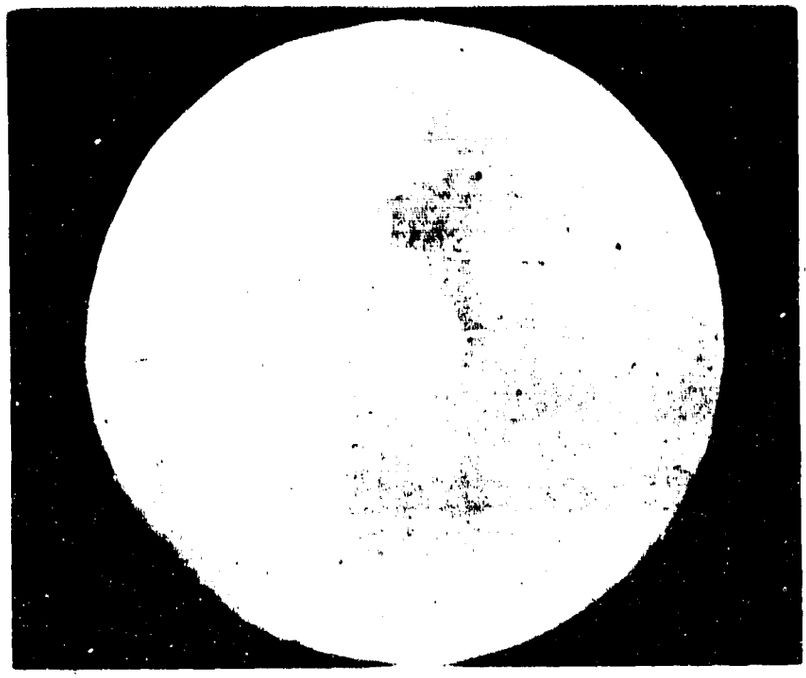

FIGURE 2-32. (800X) VIEW OF UNEXPOSED BORON FILAMENT CROSS SECTION.

FIGURE 2-33. (250X) VIEW OF UNEXPOSED BORON FILAMENT LONGITUDINAL CROSS SECTION.

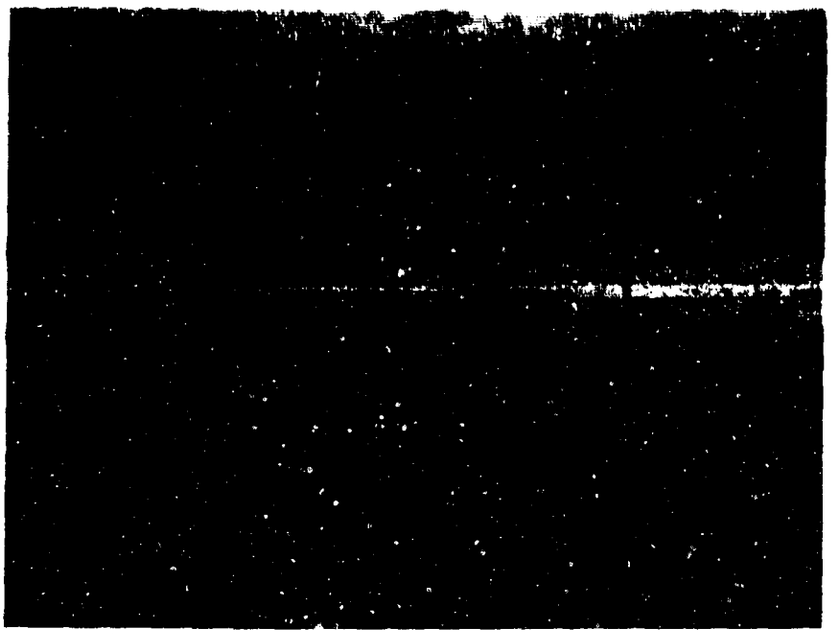

FIGURE 2-34. (125X) VIEW OF LONGITUDINAL CROSS SECTION OF BORON FILAMENT #20 (4.93×10^4 Crest Amps per cm^2 of Filament.)

FIGURE 2-35. (1000X) VIEW OF CROSS SECTION OF BORON FILAMENT #20 (4.93×10^4 Crest Amps per cm^2 of Filament.)

FIGURE 2-36. (2000X) VIEW OF CROSS SECTION OF BORON FILAMENT #20 (Core Region)

FIGURE 2-37. (800X) VIEW OF BORON FILAMENT #50 CROSS SECTION (8.88×10^4 Crest Amps per cm^2 of Filament)

FIGURE 2-38. (800X) VIEW OF BORON FILAMENT #50 CROSS SECTION (8.88×10^4 Crest Amps per cm^2 of Filament)

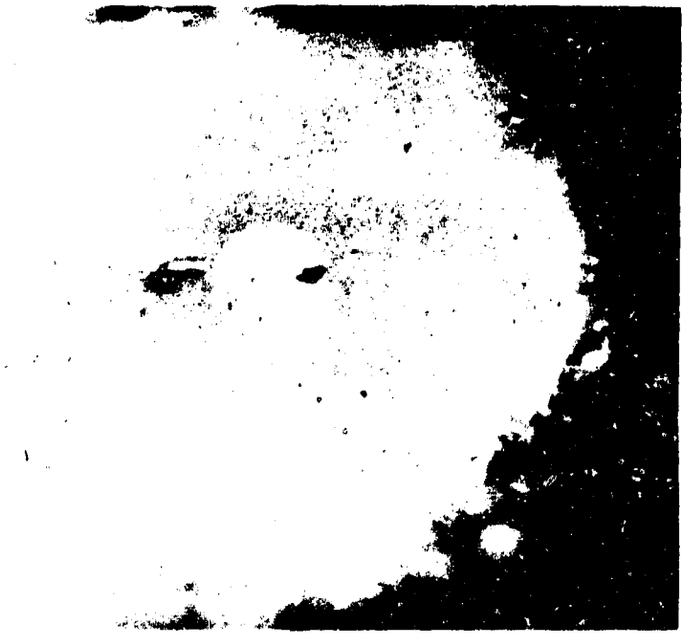

FIGURE 2-39. (800X) VIEW OF BORON FILAMENT #50 CROSS SECTION

surface. The internal damage ranges from burned holes to cracks, as can be seen.

Figure 2-40 is a photomicrograph of the surface condition of an unexposed filament using the replica technique. Figure 2-41 and 2-42 are, respectively, replicas of the surface condition of two exposed boron filaments, B-55 and B-50. As noted above, B-50 had been exposed to a crest current injection of 7.2 amperes. Both show evidence of surface cracks. The B-55 filament shattered into many >0.08 inch long pieces as a result of a 6.5 ampere current injection. The replica is of one of the pieces.

Figure 2-43 is a 100X picture of the surface of an unexposed unidirectional boron filament composite. Please note that only a portion of each boron filament is visible because of the surrounding epoxy resin. Figure 2-44 is a 100X view of a boron epoxy composite that has been exposed to a damaging level of current injection. As can be seen, considerable transverse and longitudinal cracking is present in the surface boron filaments. Based on the total number of filaments, the current injection level averaged approximately 7 amperes per filament, a level previously determined to cause damage in single filament tests.

Figures 2-45 and 2-46 are cross sections, respectively of one unexposed and one exposed boron filament composite. The complete 1/2 inch cross-sectional width of three exposed composite specimens is shown in Figure 2-47. Examination of these figures yields the observation that specimen BU #26 has the greatest number of damaged filaments and BU #17 has the least. This is in proportion to their strength degradation as reported in Table A-5 of the appendix. The tensile strengths of BU #26, #13, and #17 after current injection were degraded by 75%, 67%, and 10%, respectively. Since the number of filaments degraded in each specimen varies, and caused a variation in strength retention, it is probably safe to assume that fewer numbers of filaments carried more current in the core of the specimens showing less degradation. This phenomena is no doubt caused by the electrical contact to the specimen ends, wherein the nickel coating is probably not in uniform contact with all filament ends.

Figure 2-48 shows a cracked boron filament just under the nickel plated contact on boron epoxy specimen #26. Figures 2-49 and 2-50 of damaged boron filaments in the same composite show the typical radial cracking as a result of current injection, as previously reported by Philco-Ford and General Electric (Ref. 2). Again within damaged composite BU #26, Figure 2-51 shows a damaged boron filament that was etched with Murikamis reagent to indicate that the core was melted and resolidified. Figure 2-52 shows another damaged filament that was etched in the same manner but does not show evidence of having been melted due to current flow. Figure 2-53 is a view of the core of a boron filament in BU #26. The core has been lost either due to melting or vaporization as a result of the current injection.

FIGURE 2-40. (400X) VIEW OF UNEXPOSED BORON FILAMENT SURFACE REPLICA.

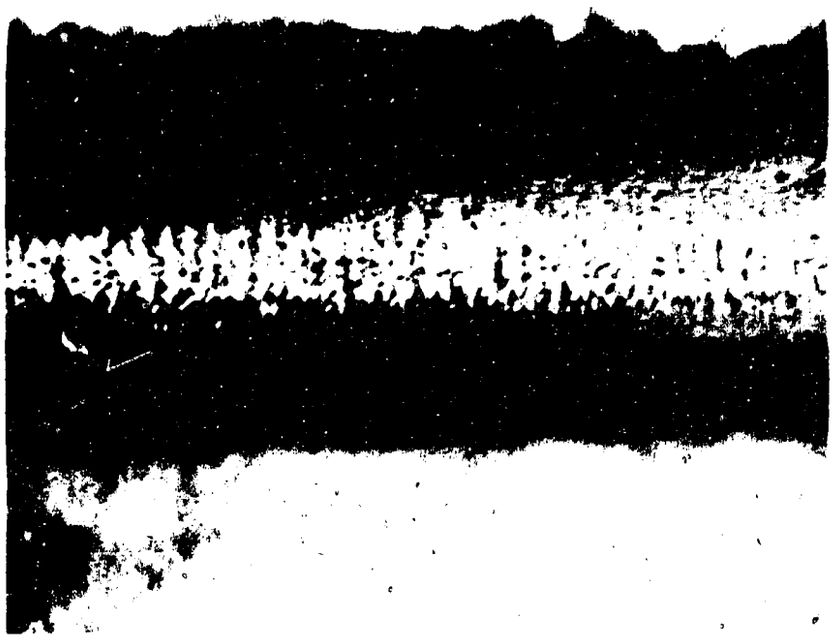

FIGURE 2-41. (500X) VIEW OF BORON FILAMENT #55 SURFACE REPLICA (8.01×10^4 Crest Amps per cm^2 of Filament)

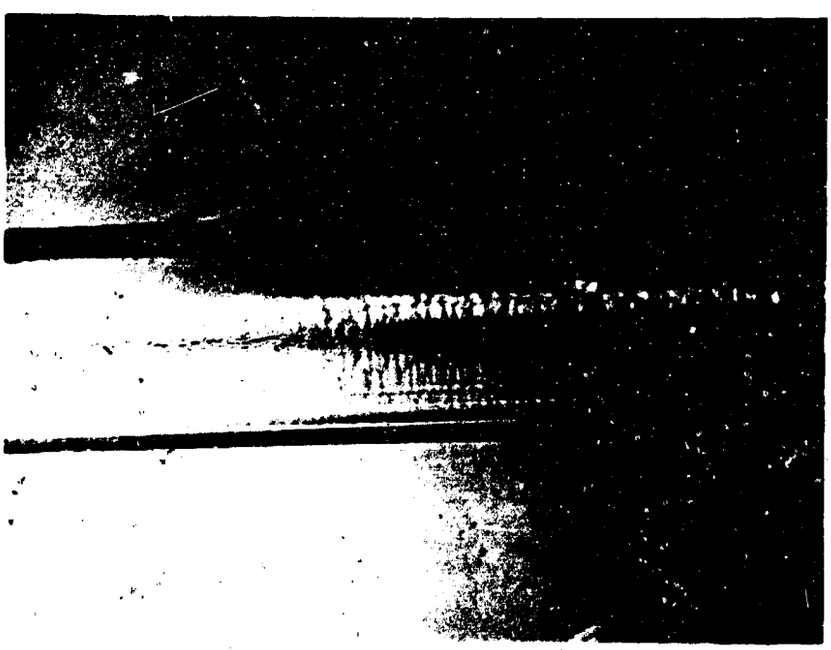

FIGURE 2-42. (250X) VIEW OF BORON FILAMENT #50 SURFACE REPLICA (8.88×10^4 Crest Amps per cm^2 of Filament)

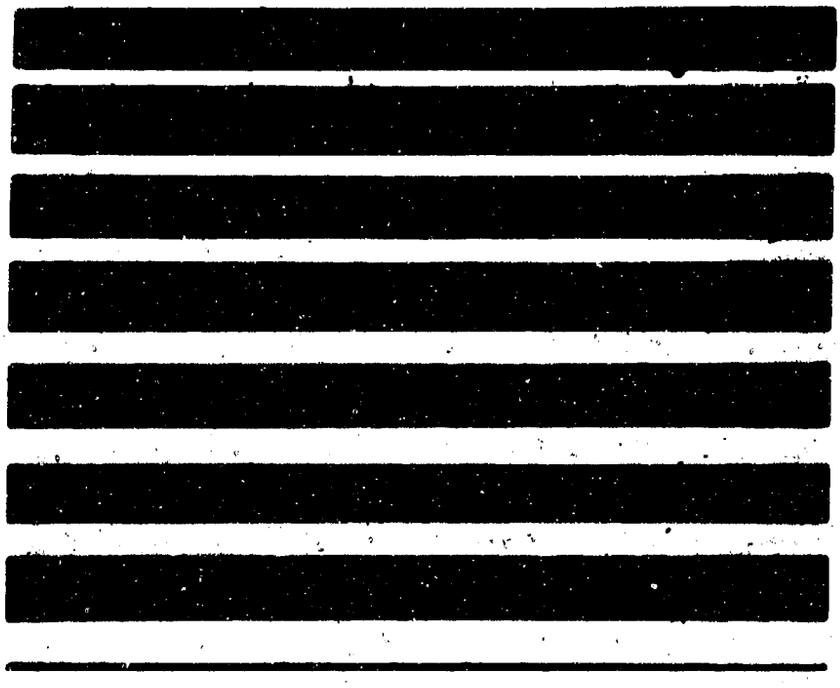

FIGURE 2-43. (100X) VIEW OF UNEXPOSED BORON EPOXY COMPOSITE SURFACE

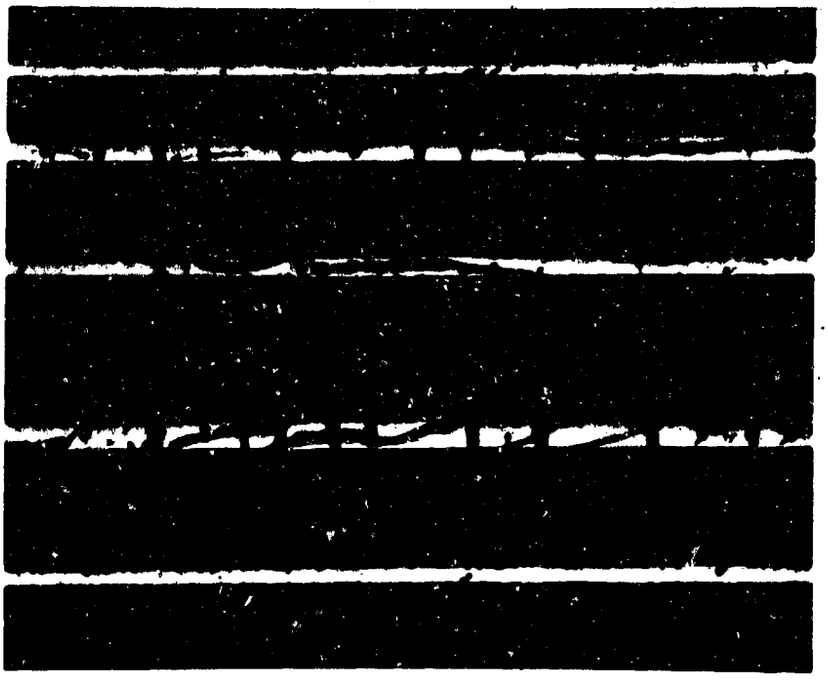

FIGURE 2-44. (100X) VIEW OF EXPOSED BORON EPOXY COMPOSITE SPECIMEN #13 ($\sim 9 \times 10^4$ Crest Amps per cm^2 of Filaments)

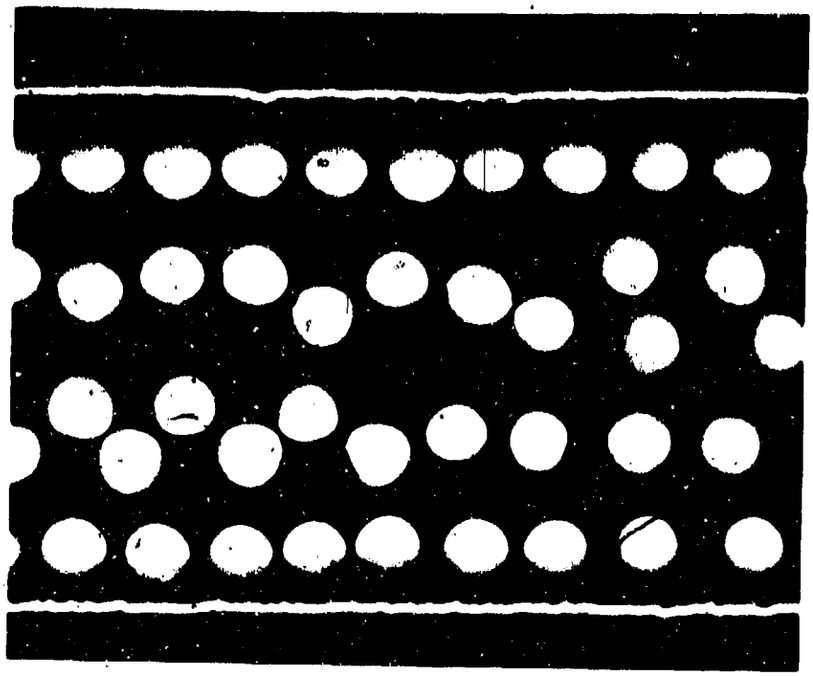

FIGURE 2-45. (100X) CROSS SECTION VIEW OF UNEXPOSED BORON EPOXY COMPOSITE.

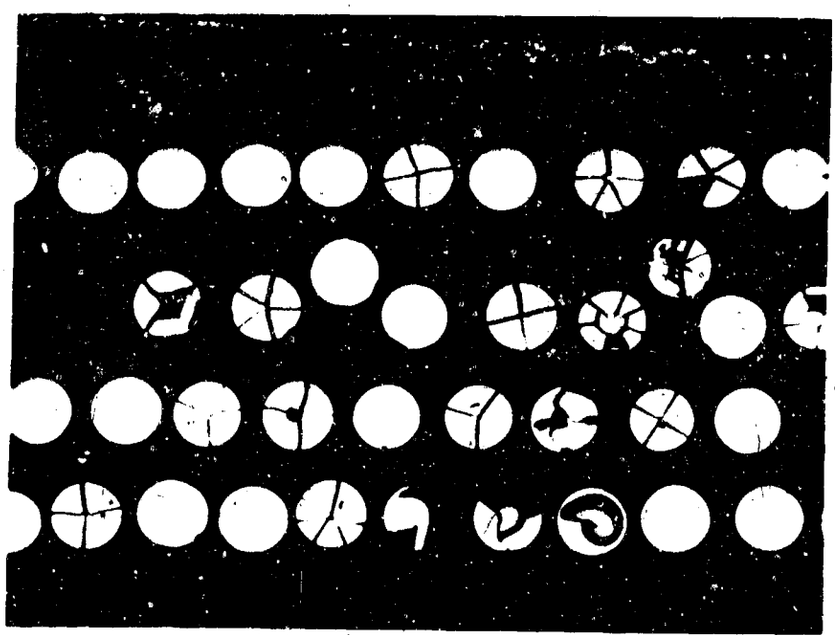

FIGURE 2-46 . (100X) CROSS SECTION VIEW OF EXPOSED BORON EPOXY SPECIMEN #26 (9.18×10^4 Crest Amps per cm^2 of Filaments)

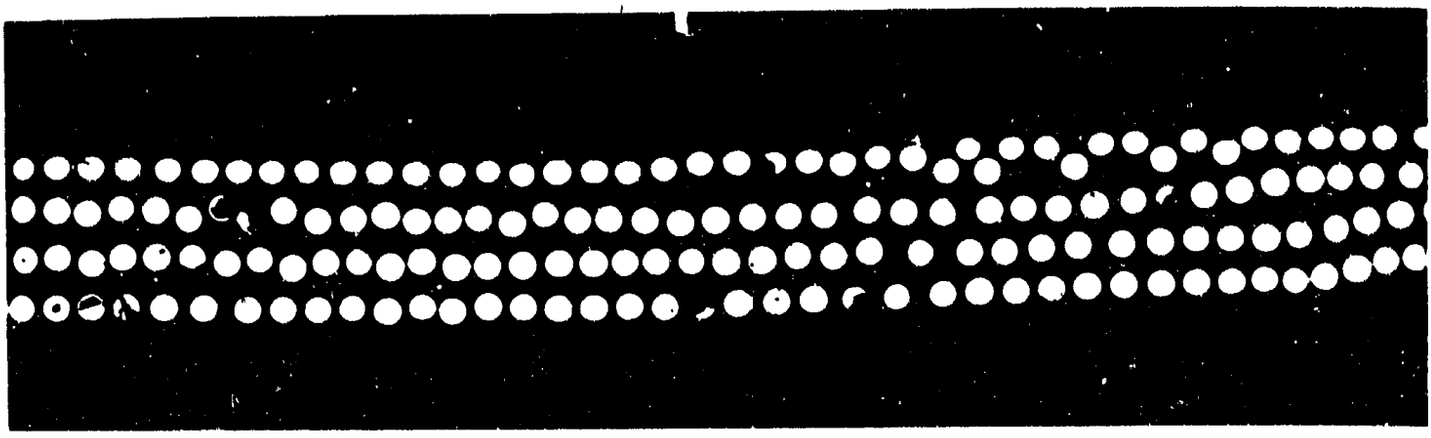

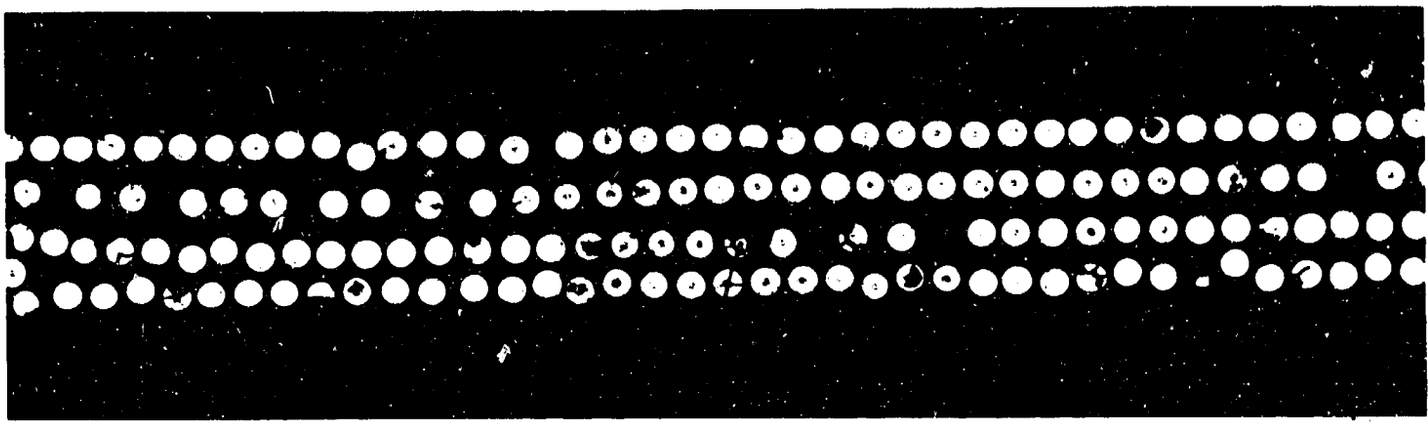

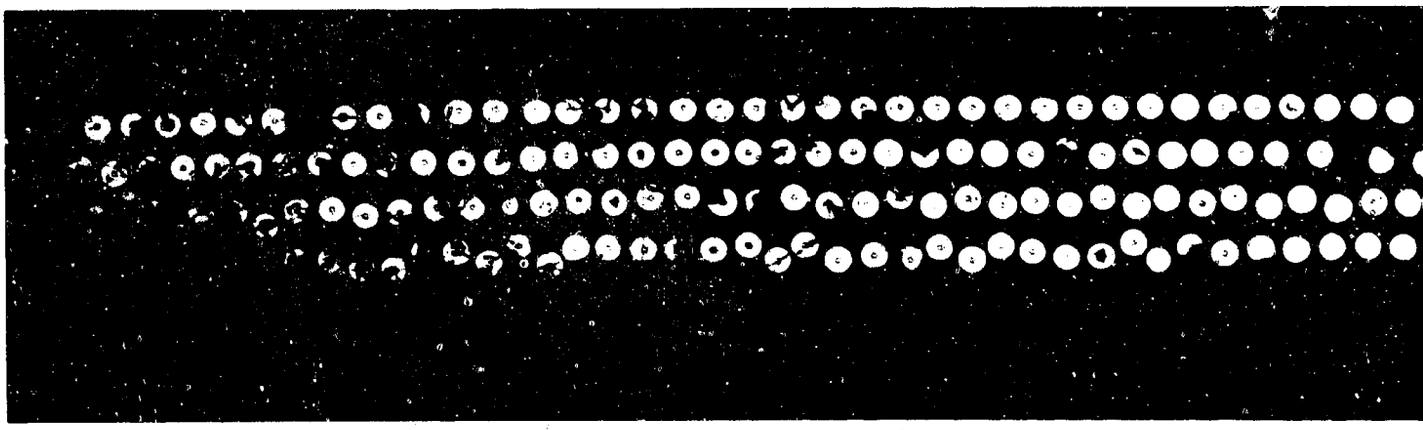

A

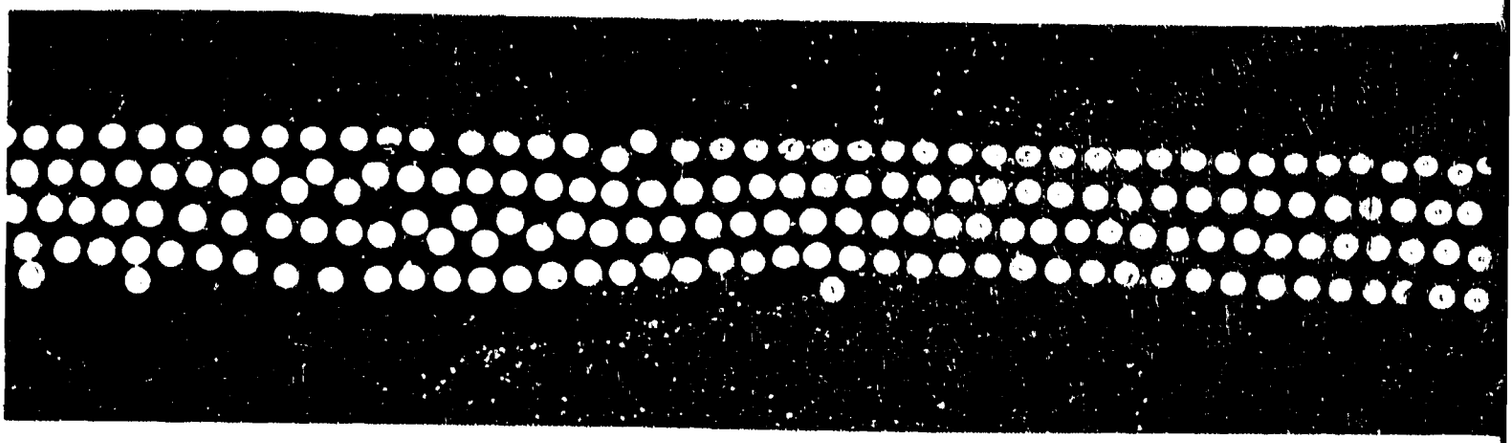

BORON UNIDIRECTIONAL LAMINATE SPECIMEN #BU-17
(8.64×10^4 CREST AMPS PER CM^2 OF FILAMENTS)

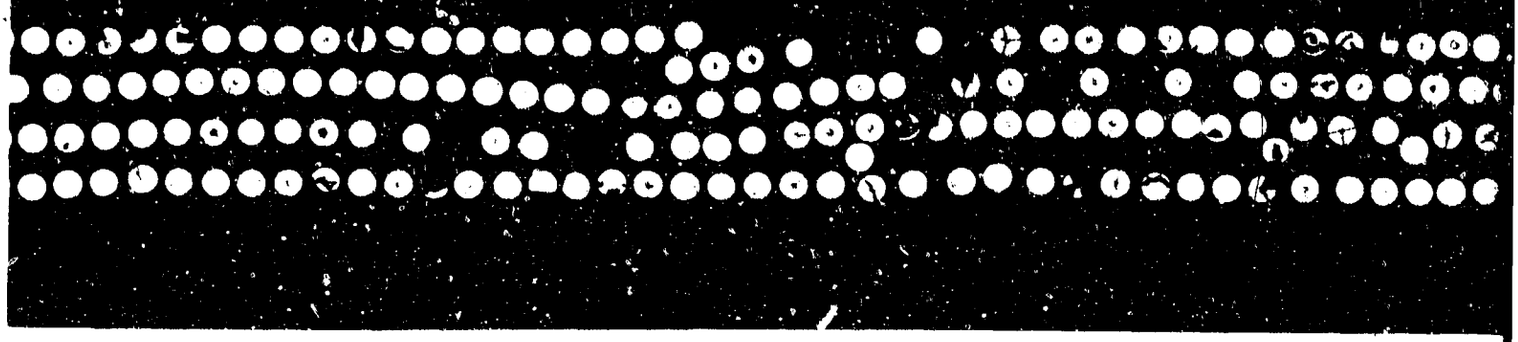

BORON UNIDIRECTIONAL LAMINATE SPECIMEN #BU-26
(9.18×10^4 CREST AMPS PER CM^2 OF FILAMENTS)

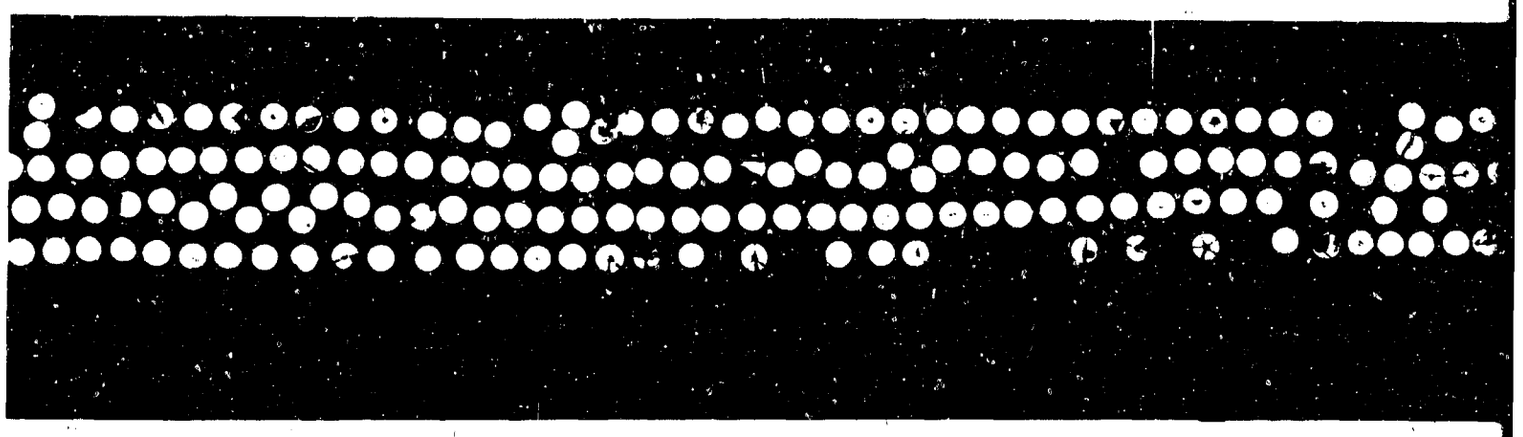

BORON UNIDIRECTIONAL LAMINATE SPECIMEN # BU-13
($\sim 9 \times 10^4$ CREST AMPS PER CM^2 OF FILAMENTS)

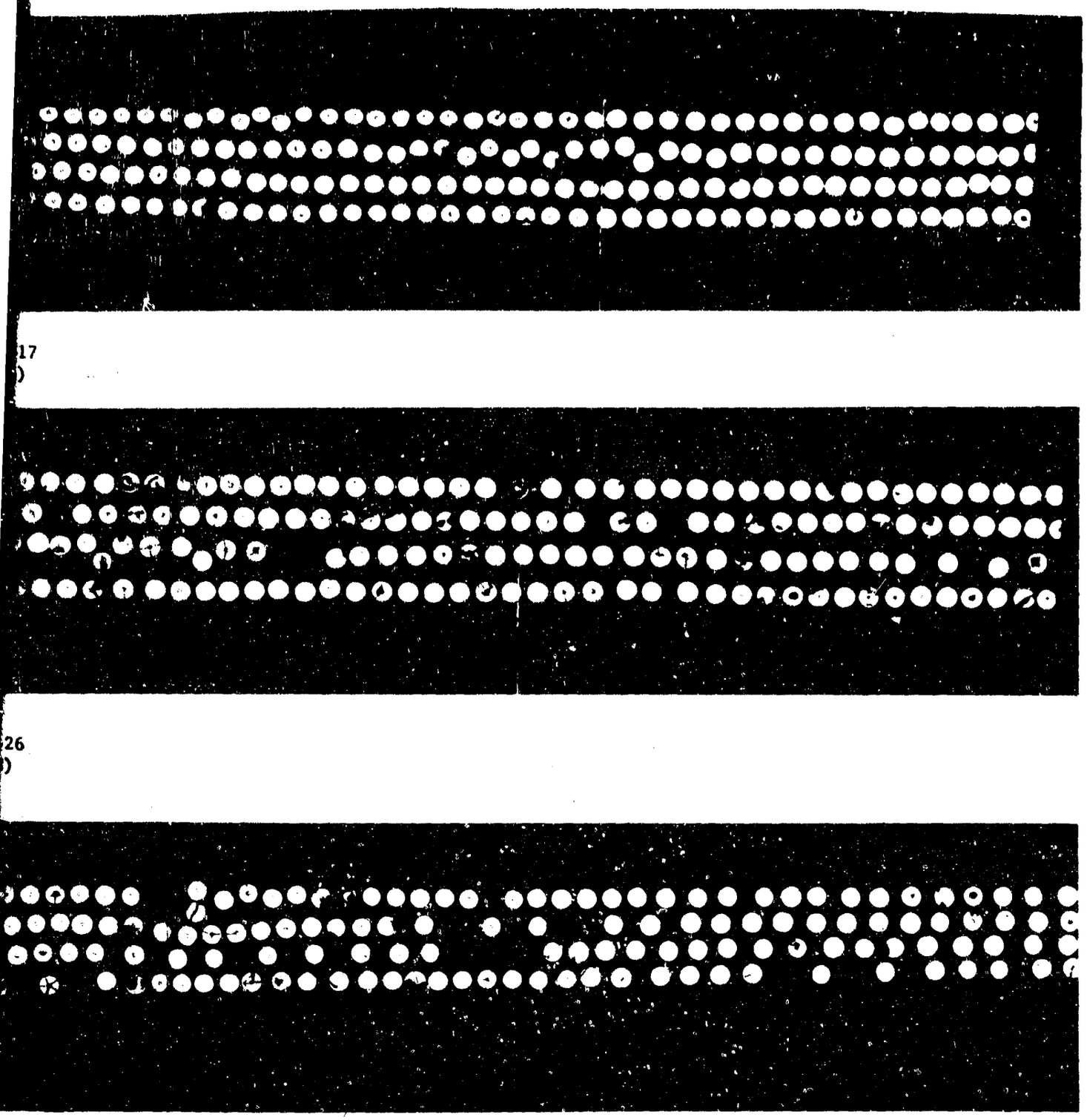

FIGURE 2-47. POLISHED TRANSVERSE VIEW OVER ENTIRE 1/2" WIDTH OF BORON/EPOXY TENSILE SPECIMENS AFTER ELECTRICAL CURRENT INJECTION.

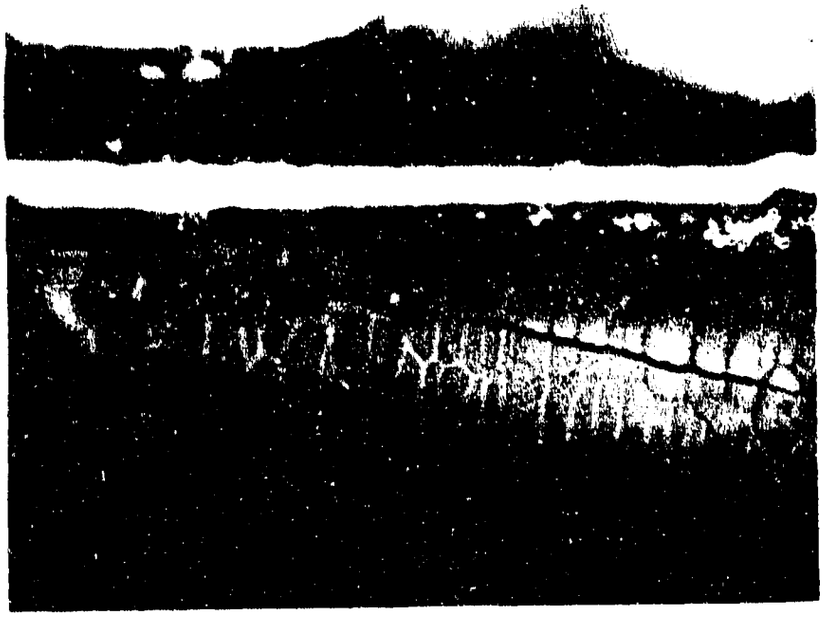

FIGURE 2-48. (800X) VIEW OF DAMAGED BORON FILAMENT IN BU #26 COMPOSITE--AT POINT OF CONTACT WITH NICKEL PLATING.

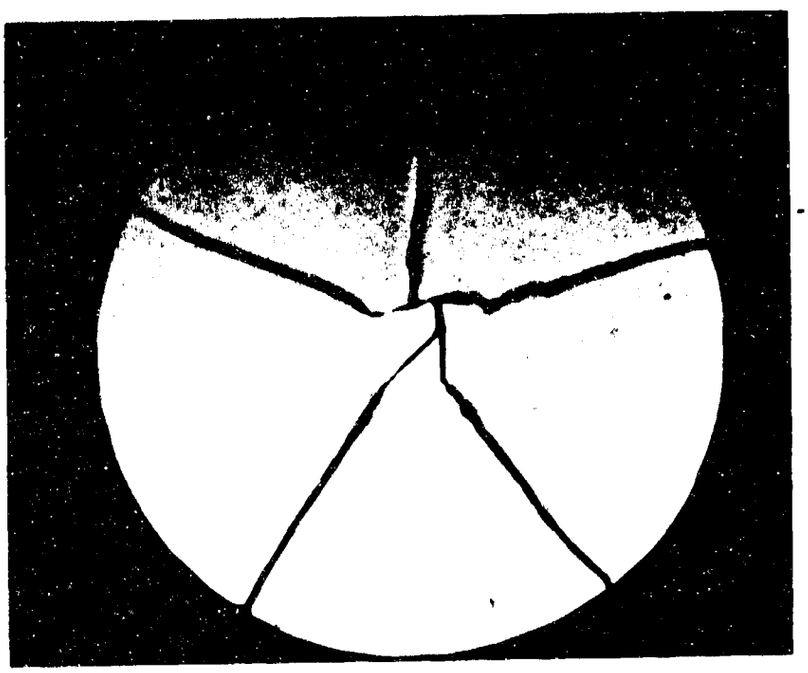

FIGURE 2-49. (800X) VIEW OF ELECTRICALLY DAMAGED BORON FILAMENT IN COMPOSITE SPECIMEN BU #26.

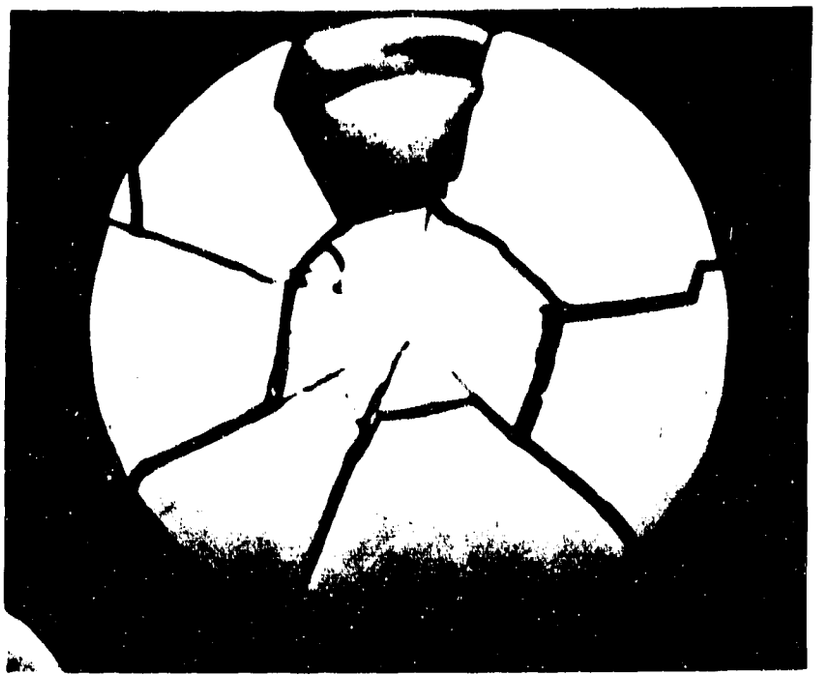

FIGURE 2-50. (800X) VIEW OF ELECTRICALLY DAMAGED BORON FILAMENT IN COMPOSITE SPECIMEN BU #26.

FIGURE 2-51. (2000X) VIEW OF CORE OF DAMAGED BORON FILAMENT (BU #26) THAT HAS BEEN ETCHED TO SHOW EVIDENCE OF MELTING.

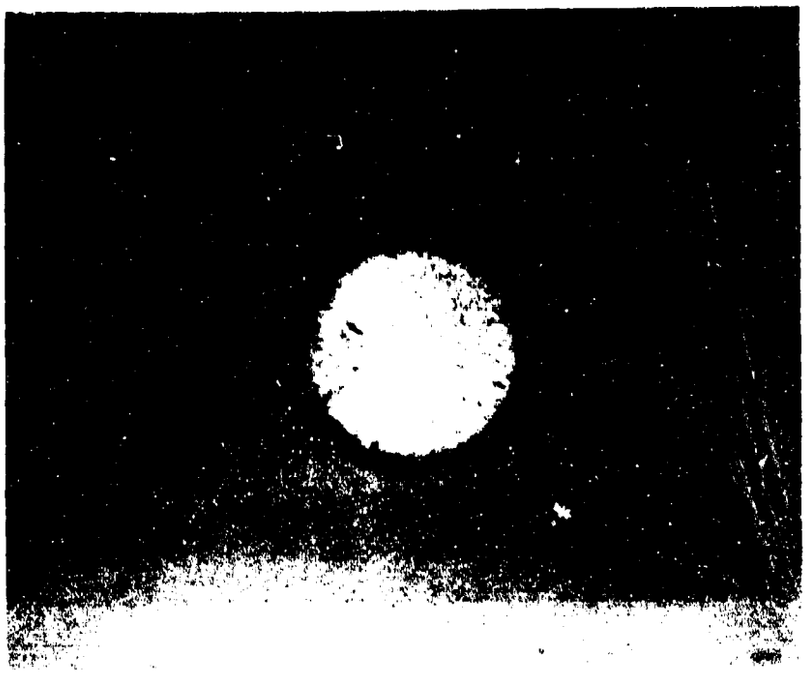

FIGURE 2-52 . (2000X) VIEW OF DAMAGED BORON FILAMENT (BU #26) THAT HAS BEEN ETCHED BUT DOES NOT SHOW EVIDENCE OF MELTING

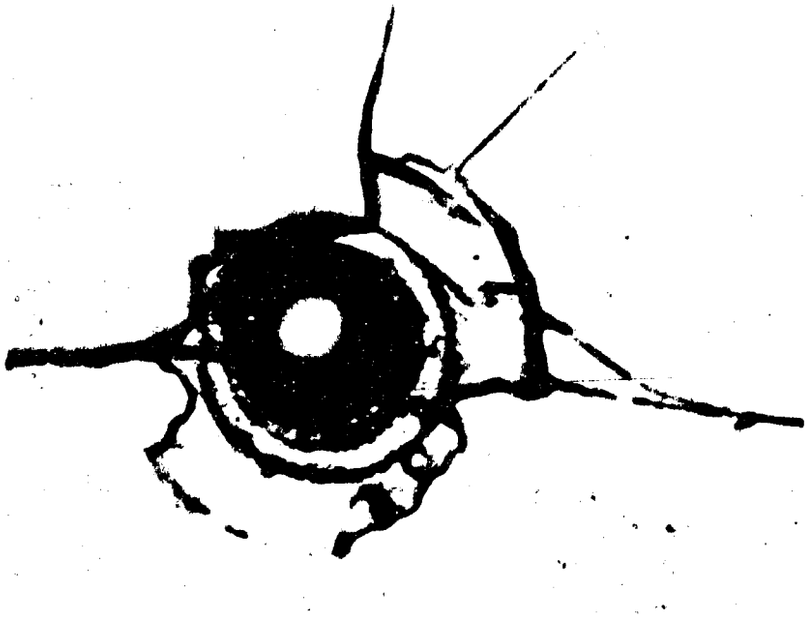

FIGURE 2-53. (2000X) VIEW OF BORON FILAMENT IN BU #26 COMPOSITE WHERE MAJOR PORTION OF THE CORE HAS BEEN LOST DUE TO MELTING OR VAPORIZATION.

Figures 2-54 and 2-55 show 800X views of the cross sections of electrically damaged boron filaments in composite specimen BU #13. Figure 2-55 is of special interest because it shows evidence of diffusion of some of the core material into the surrounding boron.

Figures 2-56 and 2-57 are of electrically damaged boron filaments in composite BU #17. Figure 2-57 has been etched to show that the portion of the 1/2 mil core remaining was melted and has resolidified. As can be seen, the remainder of the core ran into the radial cracks where it resolidified.

For one set of unidirectional boron epoxy composites, current was purposely injected into the outer plies only, in order to determine whether damage would be restricted to the filaments in those plies. Instead of nickel plating the specimen ends, aluminum foil tabs were bonded to 1/2 inch of the ends of each specimen to the surface plies only. Conductive silver filled epoxy paint was used for bonding the tabs to the specimen. The electrical contacts for current injection were made to the tabs. One specimen each then was injected with the standard waveform at crest current amplitudes of 2500, 3220 and 4370 amperes as tabulated in Appendix A. In the previous tests of specimens with nickel plated ends, it had been demonstrated that the 2500 amp crest was at the threshold above which degradation initiated. In this case it had been speculated that if current were restricted to the outer plies that the much higher current load per filament would result in severe degradation in those plies. Instead, however, the 2500 ampere test resulted in no apparent filament degradation thereby indicating that the current must have been distributed throughout the filaments in the specimen and not restricted to the surface plies. Photomicrographs of the specimens injected with the 3220 and 4370 ampere waveforms are shown in Figures 2-58 and 2-59. As can be seen, the specimen injected at the 4370 ampere crest perhaps has a higher incidence of filament degradation in the outer plies, however, both specimens have filament damage in the interior two plies. This migration of current, as evidenced by the damage, from the exterior plies to the interior plies is probably because of close proximity and random contact points of filaments. In other words, the dielectric resin barrier between plies of filaments does not appear to be uniform to a degree that will result in current being restricted to the plies in which it was injected.

c. Scanning Electron Microscope Inspection of Degraded Boron Filament. Boron filament B-13 was selected for scanning electron microscope (SEM) inspection because it was one of a group of filaments that exhibited 50-75 percent degradation as the result of current injection. The filaments had not segmented or split even though their strengths had been reduced. It was thought that the SEM might show some micro-crack or fault initiation that at higher current levels results in splitting and segmentation of the filaments. In a similar manner, the replica technique

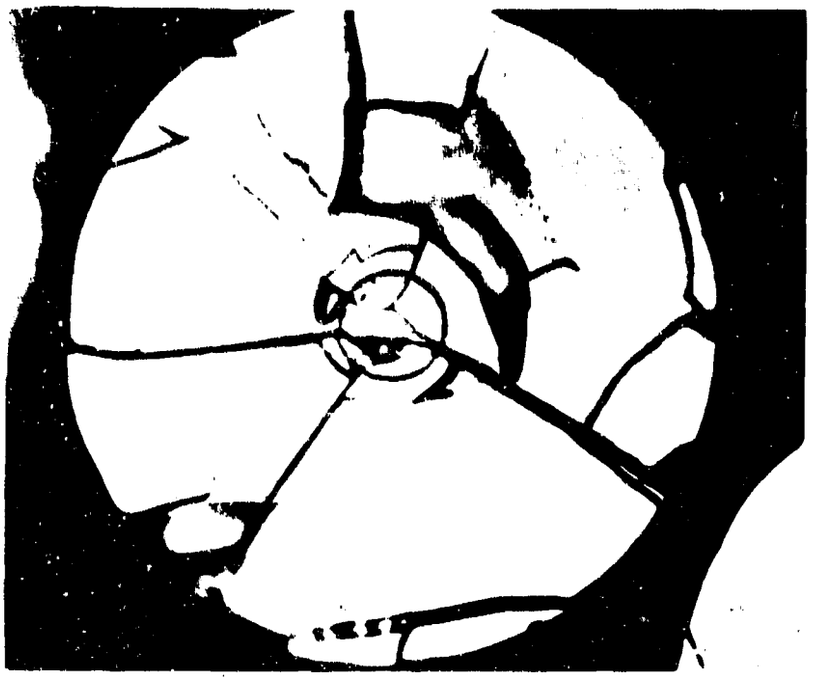

FIGURE 2-54. (800X) VIEW OF ELECTRICALLY DAMAGED BORON FILAMENT IN COMPOSITE SPECIMEN BU #13

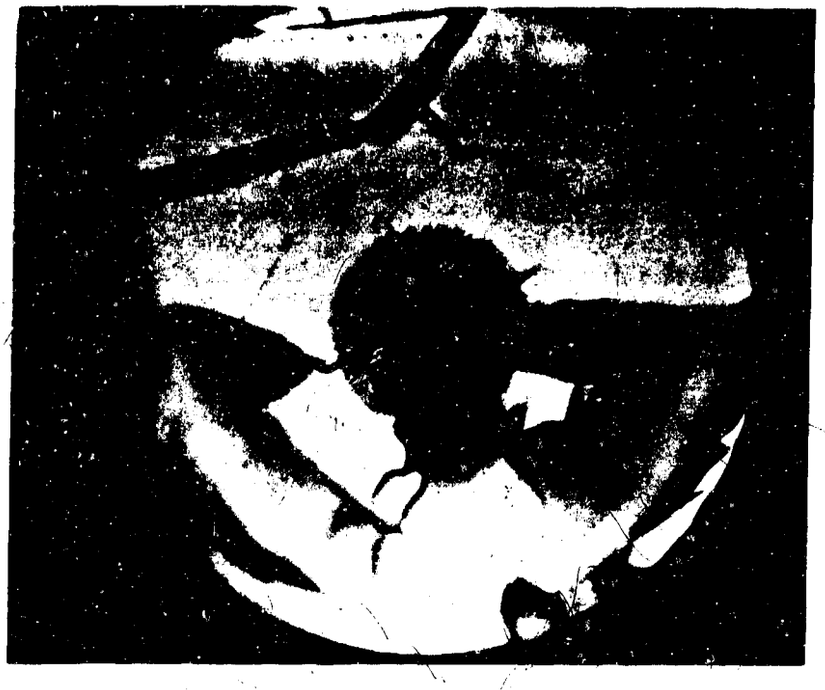

FIGURE 2-55. (800X) VIEW OF ELECTRICALLY DAMAGED BORON FILAMENT IN COMPOSITE SPECIMEN BU #13.

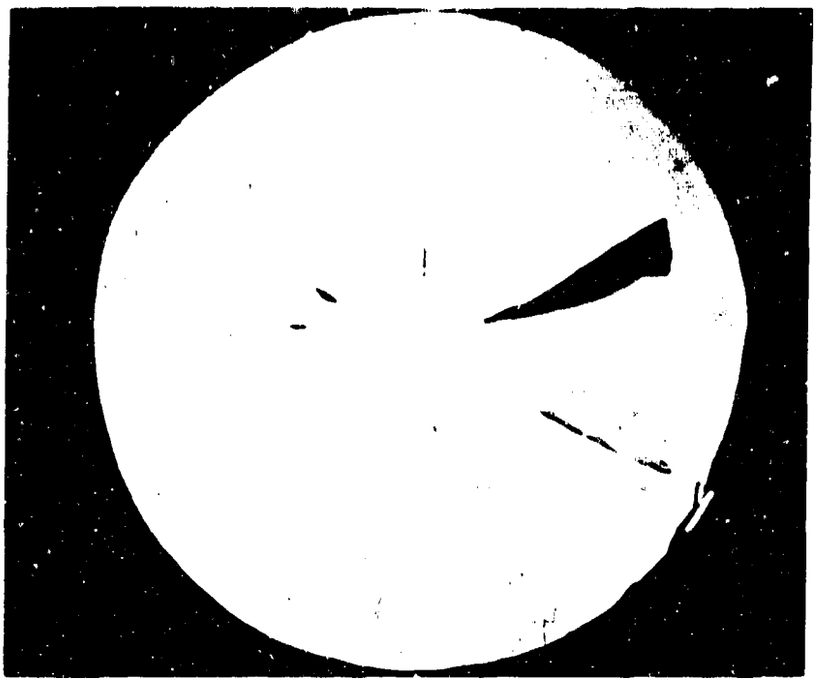

FIGURE 2-56. (800X) VIEW OF ELECTRICALLY DAMAGED BORON FILAMENT IN COMPOSITE SPECIMEN BU #17.

FIGURE 2-57 (2000X) VIEW OF BORON FILAMENT IN BU #17 COMPOSITE WHERE THE CORE HAS MELTED AND RESOLIDIFIED.

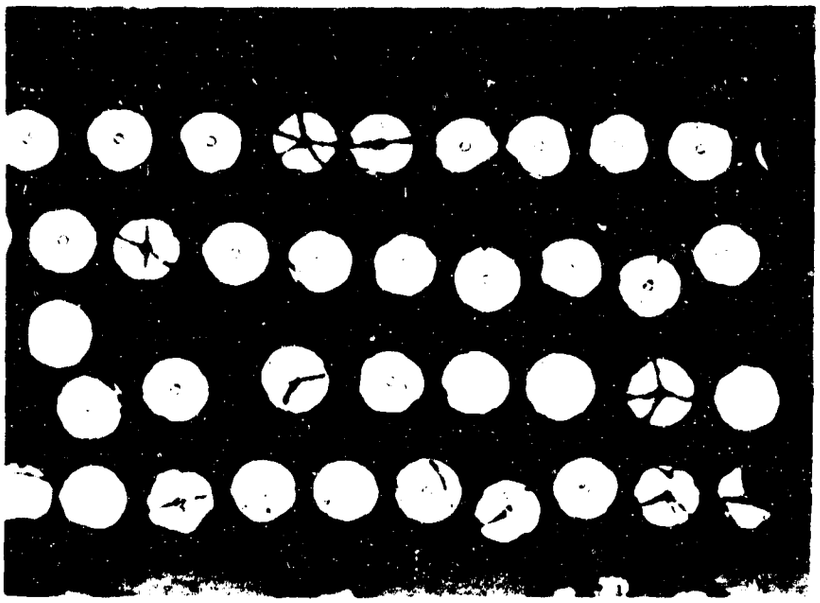

FIGURE 2-58 (100X) BORON/EPOXY BUN-2 SPECIMEN IN WHICH A 3220 AMPERE CREST IMPULSE WAS INJECTED INTO OUTER PLIES.

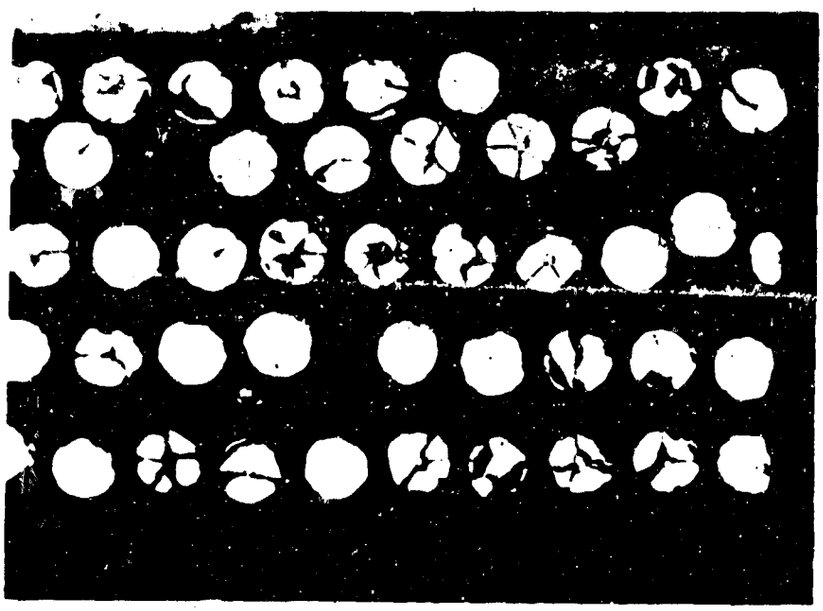

FIGURE 2-59. (100X) BORON/EPOXY BUN-1 SPECIMEN IN WHICH A 4370 AMPERE CREST IMPULSE WAS INJECTED INTO OUTER PLIES.

photomicrographs of totally degraded filaments, Figures 2-41 and 2-42, had shown surface cracks. Figure 2-60 shows a non-degraded non-injected boron filament surface at 1700X by the SEM. Figure 2-61 is a boron filament that has been exposed to a 6.1 ampere crest waveform. Four other identically exposed specimens from the same group exhibited a 50-75% degradation in tensile strength. If this strength decrease is caused by the initiation of faults they are apparently not in the form of surface cracks. The identity of the protrusions (white spots) is not known, however, they are in evidence in both the non-injected and injected filaments. Further SEM scans of filaments exposed to higher current injection levels should be performed.

d. Electron Microprobe X-ray Analysis of Degraded Boron Filament. An electron microprobe X-ray analysis was performed on two boron filaments from unidirectional boron composite specimen BU-26. Both of these filaments exhibited evidence of having had a molten phase in their core as the result of current injection. This was manifest in photomicrographs of cross sections of the filaments where the presence of the substrate core material in adjoining cracks in the boron phase was suspected. Electron beam traverses were performed across the 0.0005 inch diameter substrate cores and permeated cracks of two filaments to confirm location and concentration of boron and tungsten. The core composition and profile were compared with similar traverses on a control--unexposed boron filament. Electron microprobe X-ray images were also made of the respective cross sections to give a visual presentation of the location of boron and tungsten in the filament cross section.

Electron beam traverses were performed with an electron beam energy of 15 KV and 250 nano-amps. Beam diameter was 1 micron with a stepping interval of 1 micron. That is, the beam was stepped across the sample in intervals of 1 micron steps. At each step the relative intensity of $W_{M\alpha}$ and $B_{K\alpha}$ radiation were simultaneously integrated and printed out on a chart recorder. Through the use of standards of tungsten and boron and radiation absorption corrections, the recorded intensity data were reduced and calculated as concentrations of the respective elements. They traverse across a sample then making a concentration profile of the desired elements.

Electron microprobe X-ray images were made by scanning an electron beam across an area of the filament and displaying the relative intensity of the $W_{M\alpha}$ and $B_{K\alpha}$ radiation on an oscilloscope. Pictures of the oscilloscope display, then depict, in a qualitative manner, the location of W and B in the filament cross section. These X-ray images were made using a 1 micron diameter beam operating at 15 KV and 500 na. A beam sweep rate of 25 sec/cm was used to generate a picture approximately 1000X magnification.

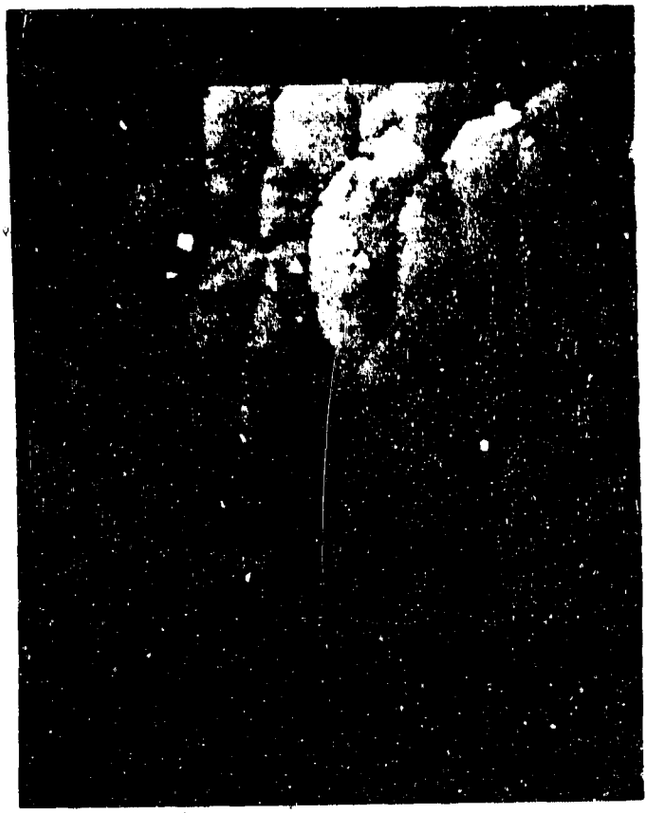

FIGURE 2-60. (1700X) ELECTRON MICROSCOPE SCAN OF UNEXPOSED BORON FILAMENT SURFACE (40 second scan)

FIGURE 2-61. (1700X) ELECTRON MICROSCOPE SCAN OF BORON FILAMENT #13 SURFACE (7.52×10^4 CREST AMPS PER CM^2 OF FILAMENT) (40 second scan)

Shown in Figures 2-62, 2-63 and 2-64 are photomicrographs and X-ray images of the control and the two degraded filaments from BU-26, respectively. The photomicrograph in Figure 2-63 clearly shows the core material in a boron crack adjacent to the core. A similar condition, although not as clear, was seen in Figure 2-64 in the crack designated by the arrow.

The sample current images shown in Figures 2-63 and 2-64 confirm the filament orientation in relation to the cracks. The respective $W_{M\alpha}$ X-ray images in Figure 2-63 d and e and Figure 2-64 d and e indicate the presence of tungsten in the cracks shown in photomicrographs.

The path and direction of the electron beam traverses are also shown in Figures 2-62, 2-63 and 2-64 on photomicrographs taken after the electron microprobe study. In both traverses across the crack, sharp spikes of tungsten were recorded with corresponding decreases in boron concentration. The tungsten in the crack had a composition similar to that of the core near the boron interface, e.g., WB_{12} or WB_{12} + B. No differences in concentration gradients or composition were detected in traverses across the three cores. or 72-45. The diffusion zone associated with the tungsten core was 18 to 20 microns in diameter. The outer 2 to 3 microns of the core having a high boron composition in excess of WB_{12}. A narrow region of composition corresponding to WB_{12} adjoins this outer area. The major composition of the cores was confined to a diameter of 10 to 12 microns and corresponded to W_2B_5. No pure tungsten nor compositions corresponding to WB or W_2B were detected in or near the center of the core. A schematic of the core analysis is shown in Figure 2-65.

Shown in Figure 2-66 is the phase diagram for W-B recently reported by Rudy and co-workers (Ref. 3). In this diagram the boron filament core composition is designated to exist from W_2B_5 to WB_{12} + B. The melting point range of this compositional zone lies between 2150° and 1970°C.

The tungsten boride composition of substrate core material located in adjoining cracks of boron was found to be equivalent to WB_{12} or WB_{12} + B. This composition closely corresponds to the outer composition of the core adjacent to the boron phase. The major composition of the core corresponds to W_2B_5. The melting point of the core compositions are between 2150° and 1970°C.

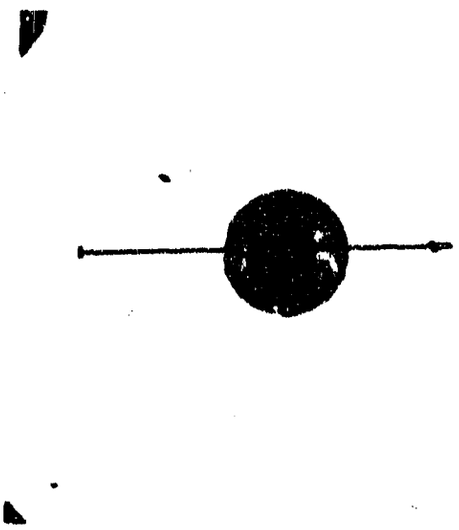

a. PHOTOMICROGRAPH OF ELECTRON BEAM PATH

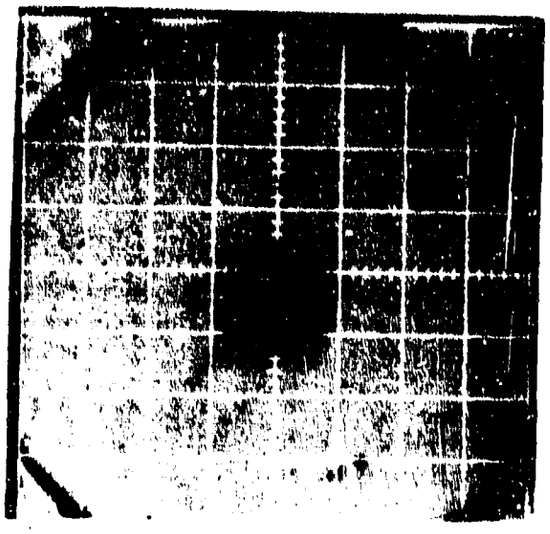

b. SAMPLE CURRENT IMAGE

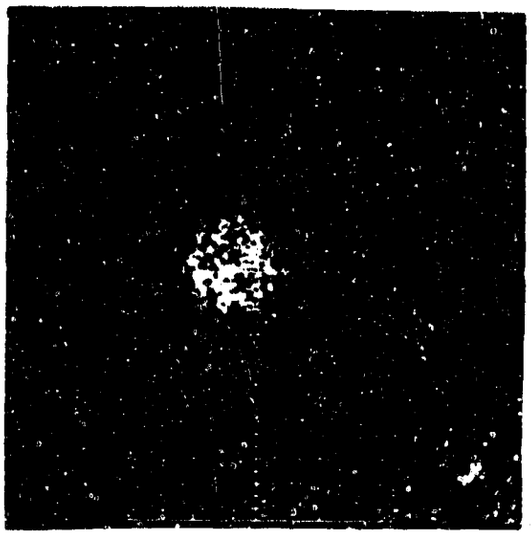

c. TUNGSTEN M_{α} X-RAY IMAGE

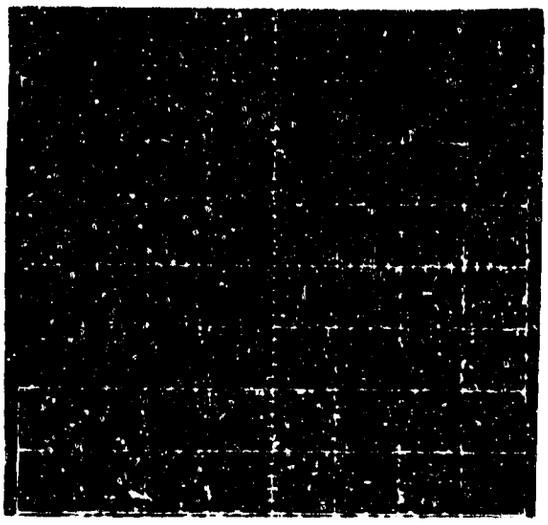

d. BORON K_{α} X-RAY IMAGE SEC-1

FIGURE 2-62. (100X) PHOTOMICROGRAPHS AND X-RAY IMAGES OF CONTROL SAMPLE OF NON-EXPOSED BORON FILAMENT.

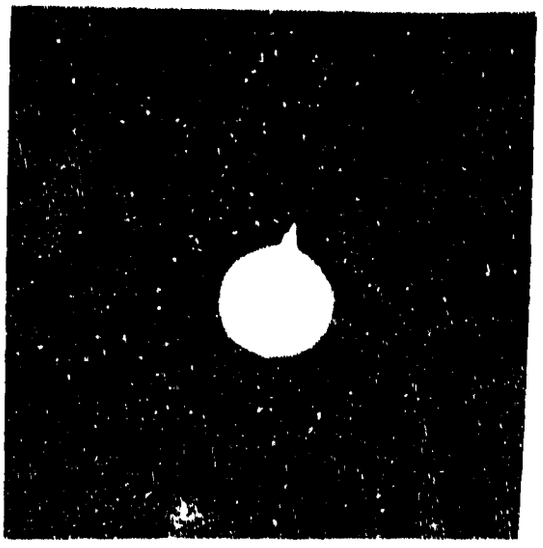

a. PHOTOMICROGRAPH, 1000X

b. PHOTOMICROGRAPH OF TRAVERSE

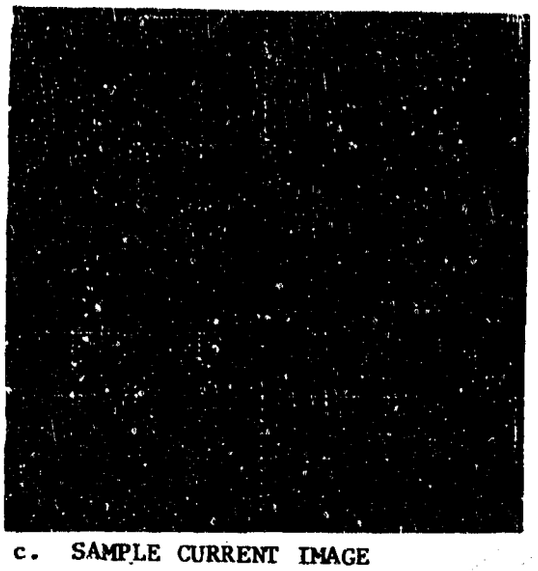

c. SAMPLE CURRENT IMAGE

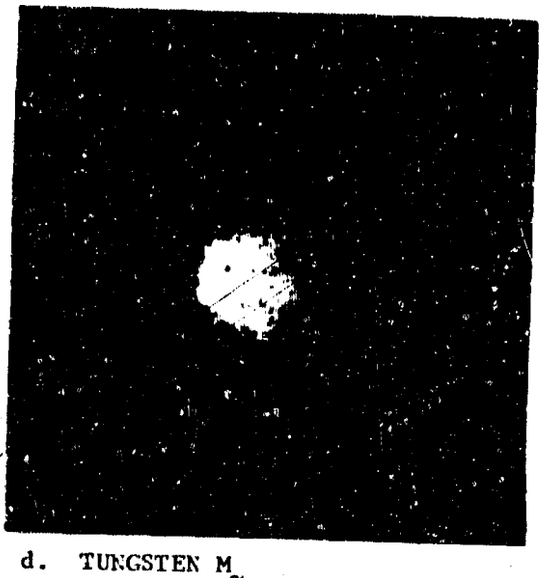

d. TUNGSTEN M_{α}

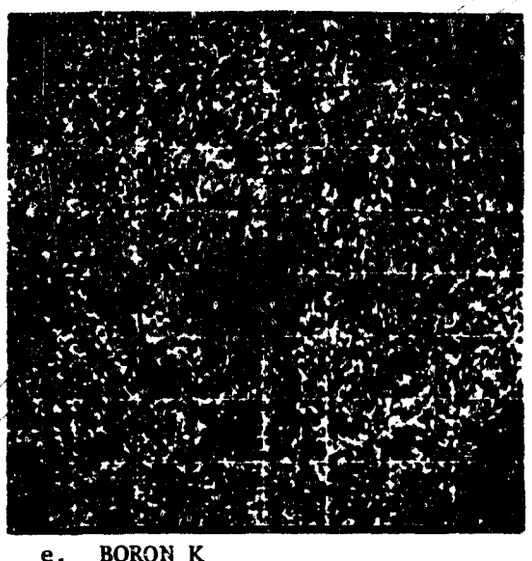

e. BORON K_{α}

FIGURE 2-63. (1000X) PHOTOMICROGRAPHS AND MICROPROBE X-RAY IMAGES OF BORON FILAMENT FROM SPECIMEN BU-26 (9.18×10^4 CREST AMPS PER CM^2 OF FILAMENTS)

a. PHOTOMICROGRAPH , 1000X

b. PHOTOMICROGRAPH OF TRAVERSE

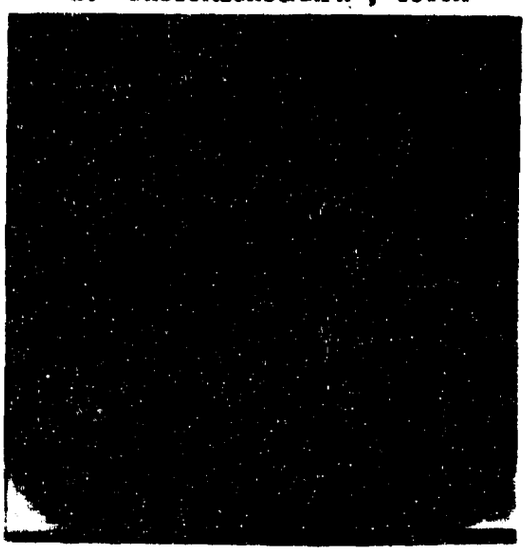

c. SAMPLE CURRENT IMAGE

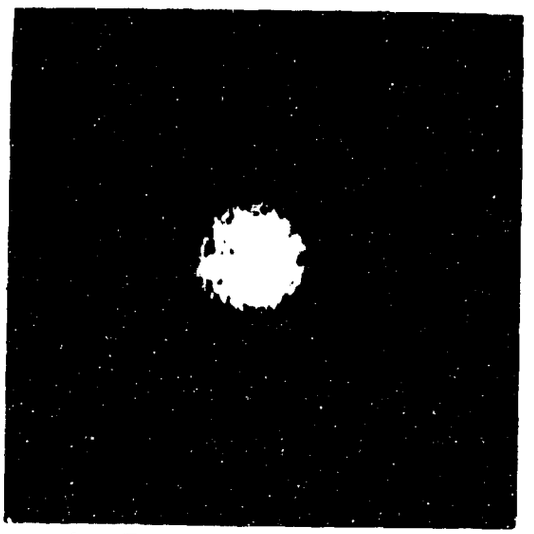

d. TUNGSTEN M_{α} IMAGE

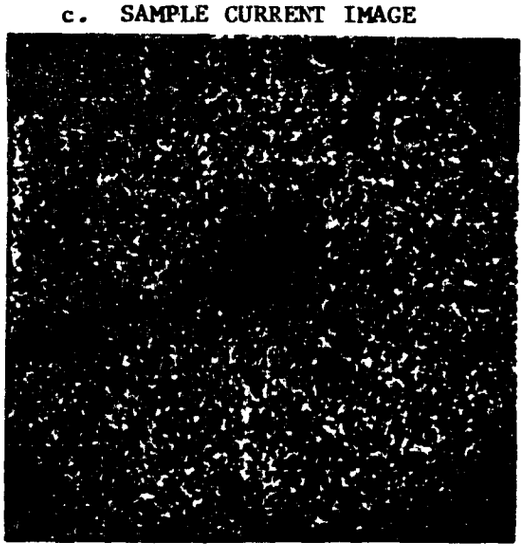

e. BORON K_{α} IMAGE

FIGURE 2-64. (1000X) PHOTOMICROGRAPHS AND MICROPROBE X-RAY IMAGES OF BORON FILAMENT FROM SPECIMEN BU-26 (9.18×10^4 CREST AMPS PER CM^2 OF FILAMENTS)

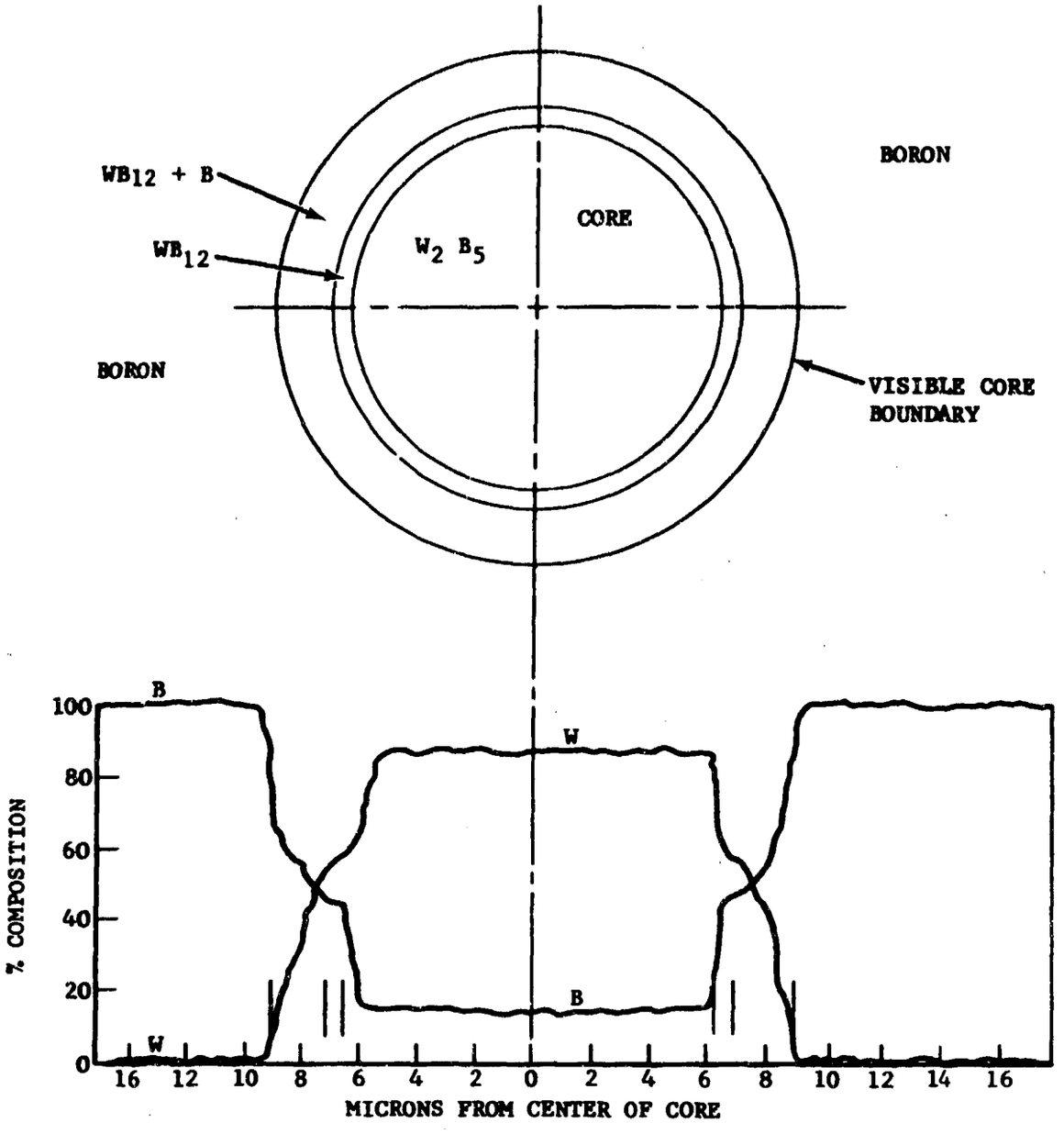

FIGURE 2-65. MICROPROBE ANALYSIS OF BORON FILAMENT CORES

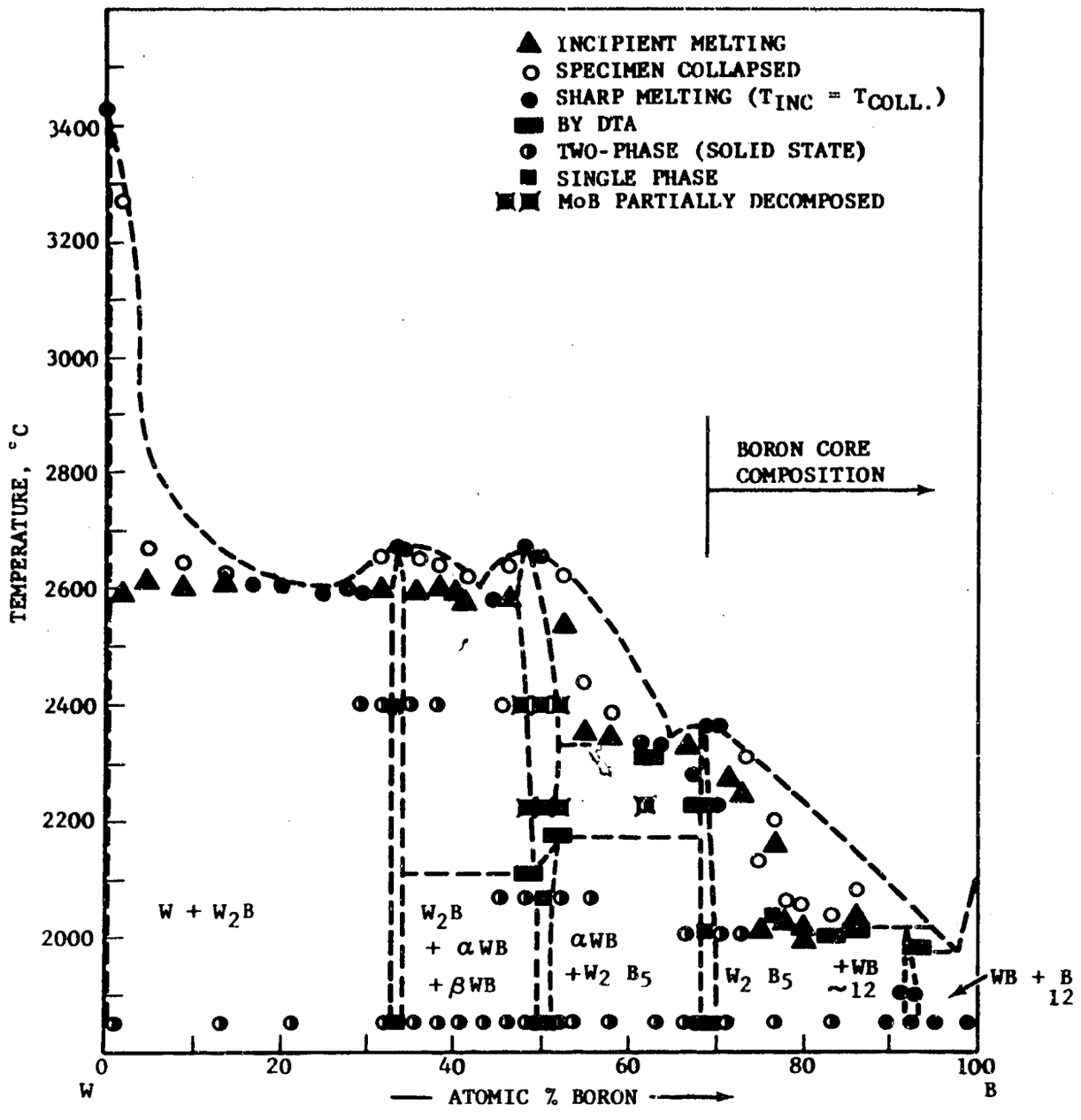

FIGURE 2-66. W-B: MELTING TEMPERATURES, DTA-RESULTS AND QUALITATIVE EVALUATION OF SOLID STATE SAMPLES. QUENCHED ALLOYS

e. Degradation Model for Electric Current Impulsed Boron Filament Epoxy Composites. The degradation of the boron filament epoxy composite due to electric current impulses is controlled by the response of the boron filaments to current flow. It now appears that the concept involved in the initial boron filament degradation model is correct. That model, as discussed in Reference 2, is based on the fact that the core of the filament (tungsten boride) has a much lower resistivity than does the boron surrounding it. The electric current then flows predominately through the core. Some electric energy then is dissipated within the core as heat. The heat build-up causes a thermal expansion of the core both radially and axially. The outer boron sheath then acts to restrain the expansion of the core, which results in a build-up in hoop and axial tensile stresses within the boron. These tensile stresses are additive to the residual stresses that are, in all probability, present as the result of the manufacture of the filament. At such a point when the internal stresses exceed the strength of the boron, the boron sheath cracks either radially or transversely, whichever the case may be. Efforts have been made to improve mathematical interpretation of the degradation model. The evidence of melting, vaporization, and diffusion in the core region appears to be in support of the probability of intense thermal energy build-up within the core.

Assuming this failure model, the degree of correlation with failures noted in experimental tests can be determined by calculating failure stresses at different current levels. In calculating the relationships of current flow and failure stress in the boron using this analytical model, the following assumptions were made:

(1) That virtually all of the current flows through the core,

(2) That the time duration is sufficiently short to preclude heat transfer between the core and the boron,

(3) That all energy dissipated in the core is in the form of heat,

(4) That both the boron and the core are homogeneous.

As the current passes through the core, resistance heating causes the core to expand against the sheath material creating excessive radial, tangential and axial stresses. (There are already present in the filament residual stresses that formed upon cooling the filament to room temperature after its growth at elevated temperature. These stresses are discussed in the Appendix.

The following is an estimate of the maximum temperature rise which can be expected in the core when subjected to current input in the form of a pulse with a front time, $t_f = 3.12\mu$ sec. and a tail time $t_t = 22\mu$ sec.

An expression for the rate of development of heat in conductor requires an expression for the power input to the circuit. The energy given by the charge is:[4]

$dw = dq \text{ (voltage drop)} = i\,dt\Delta V$

and the rate at which energh is given up, or the power input P, is

$$P = \frac{dw}{dt} = i\Delta V.$$

If the current is in amperes and the potential difference is in volts then the power is in joules/sec or watts.

In the special case in which the conductor under consideration is a pure resistance R, all of the energy supplied is converted to heat, and then

$\Delta V = iR$, and

$$P = i\Delta V = i^2R \qquad (1)$$

For most materials including tungsten and tungsten boride, (Ref. 5) the value of electrical resistance, and therefore the rate of heat production increases with increasing temperature. For some materials, notably boron,[6] carbon and fused silica,[9] it is negative. The temperature dependency of the various constituents of the boron filament are presented in Figure 2-67. As an initial approximation we shall assume R is constant for the core and equal to

$\rho\ell/A$ where $\rho = 21.0 \times 10^{-6}$ ohm-cm.

Equation (1) is derived for a constant current level. For a varying current, such as a pulse, the heat dH developed in time dt is

$dH = Ri^2dt$

and in a finite time interval from 0 to t the heat is

$$H = \int_0^t Ri^2dt$$

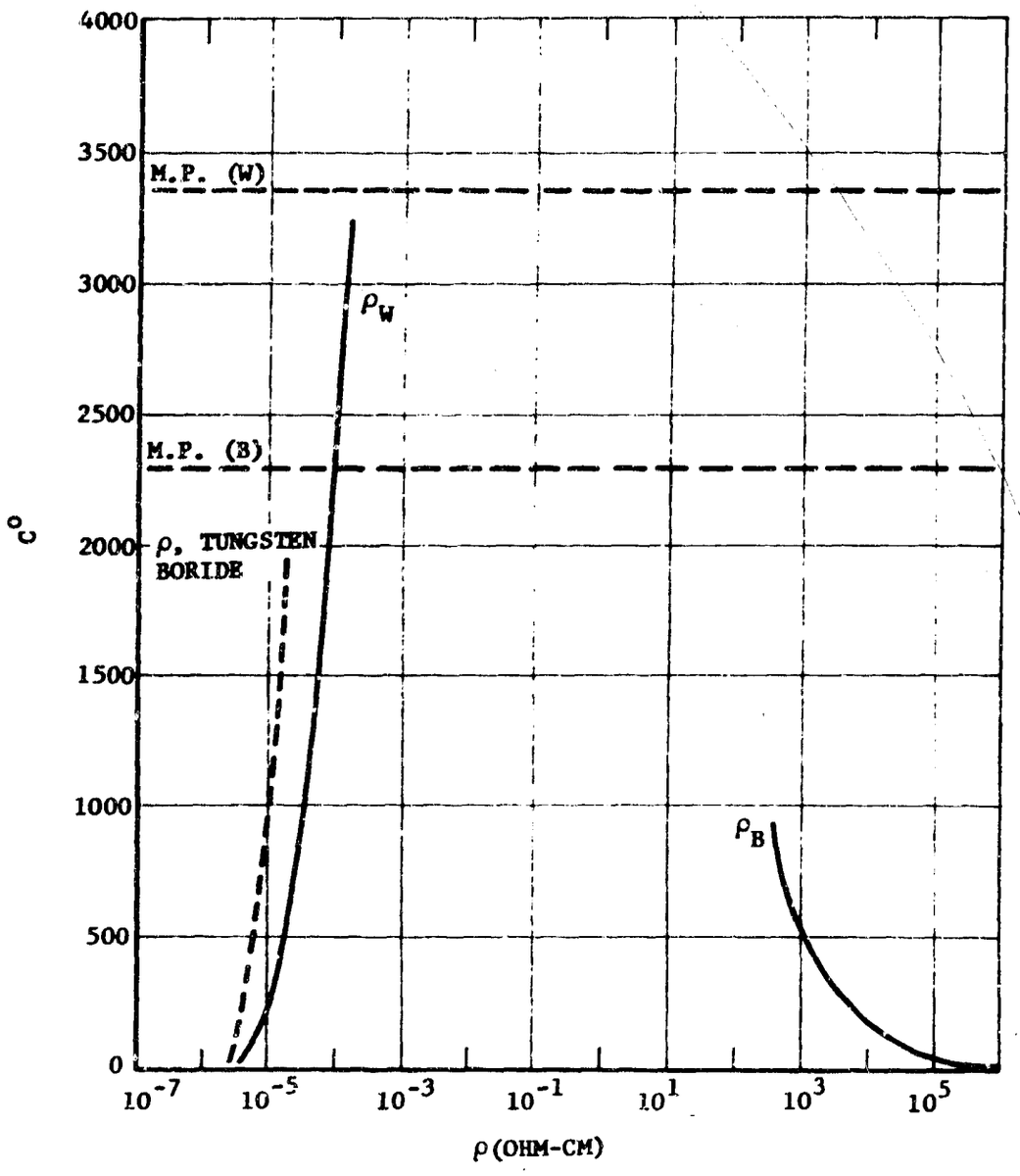

FIGURE 2-67. RESISTIVITIES OF TUNGSTEN, TUNGSTEN BORIDE AND BORON VERSUS TEMPERATURE

or since R is assumed constant $H = R \int_0^t i^2 dt$.

This integration was performed graphically for a unit peak ampere current pulse of Table 1, Reference 6 with the result:

$$\frac{H}{R} = \int_0^{45\mu} i^2 dt = 14.8 \ (I_{max})^2 \ amp^2\text{-}\mu sec$$

Consider a single filament specimen 15 in. in length (38.1 cm) as used in degradation testing, then R = 632 ohms.

The specific heat of the tungsten-boride is given in Reference 2 as 0.06-0.09 cal/gm/^oC and so using a value of 0.075 the maximum temperature rise of the core material weighing 6.27×10^{-4} grams can be calculated from

$$H = R \ (14.8) \ (I_{max})^2 = 9359 \ (I_{max})^2$$

and from

$$\Delta T = \frac{H}{\text{weight x specific heat}} = \frac{9539 \ (I_{max})^2 \times 10^{-6}}{(6.27 \times 10^{-4}) \ (0.075)}$$

$$\Delta T = 198.9 \ (I_{max})^2 \ ^oC = 358 \ (I_{max})^2 \ ^oF$$

This temperature change in the core alone will give rise to axial stress in the boron sheath of

$$\sigma_B = (A_{core}/A_{sheath}) \ E_{core} \ \alpha_{core} \ \Delta T_{core}$$

or

$$\sigma_B = (19.6 \times 10^{-8}/1256.6 \times 10^{-8}) \ 60.0 \times 10^6 \ (4.1 \times 10^{-6}) \ (358) \ I_{max}^2$$

$$\sigma_B = 1376 \ (I_{max})^2$$

This temperature induced axial stress is additive to the residual axial stress of 1686 psi (calculated in the Appendix). Therefore,

$$\sigma_{B(axial)} = 1374\ (I_{max})^2 + 1686 \qquad (2)$$

Similarly, the radial and tangential stresses at the filament-core interface which result from the electrical current may be calculated from:

$$\sigma_r = 55{,}900 + \frac{\delta R_{core}}{\frac{R_{core}}{E_{core}}(1 - \upsilon_{core})}$$

and

$$\delta R_{core} = R_{core}\alpha_{core}\Delta T_{core}$$

giving

$$\sigma_r = 55{,}900 + 125{,}800\ (I_{max})^2 \qquad (3)$$

while the tangential stress at the filament-core interface is expressed by

$$\sigma_t = 57{,}670 + 129{,}800\ (I_{max})^2 \qquad (4)$$

The stresses expressed by equations 2, 3 and 4 are plotted in Figure 2-68 for values of maximum current.

In summary then, from Figure 2-68, it is predicted that for the standard waveshape, boron filaments would crack radially due to the high tangential stresses at a current flow of 1.5 to 2 amperes. Also, the predicted current flow where axial stresses would cause segmentation is 15-20 amperes crest. In other words, radial cracking should occur at lower levels of current flow than would axial segmentation due to transverse cracks. The predicted current levels where these cracks will occur does not correspond directly to the experimental evidence reported for single boron filament tests; however, this is probably due to the following:

(1) Uncertainty in the values of resistivity used, particularly under conditons of high current loading rates.

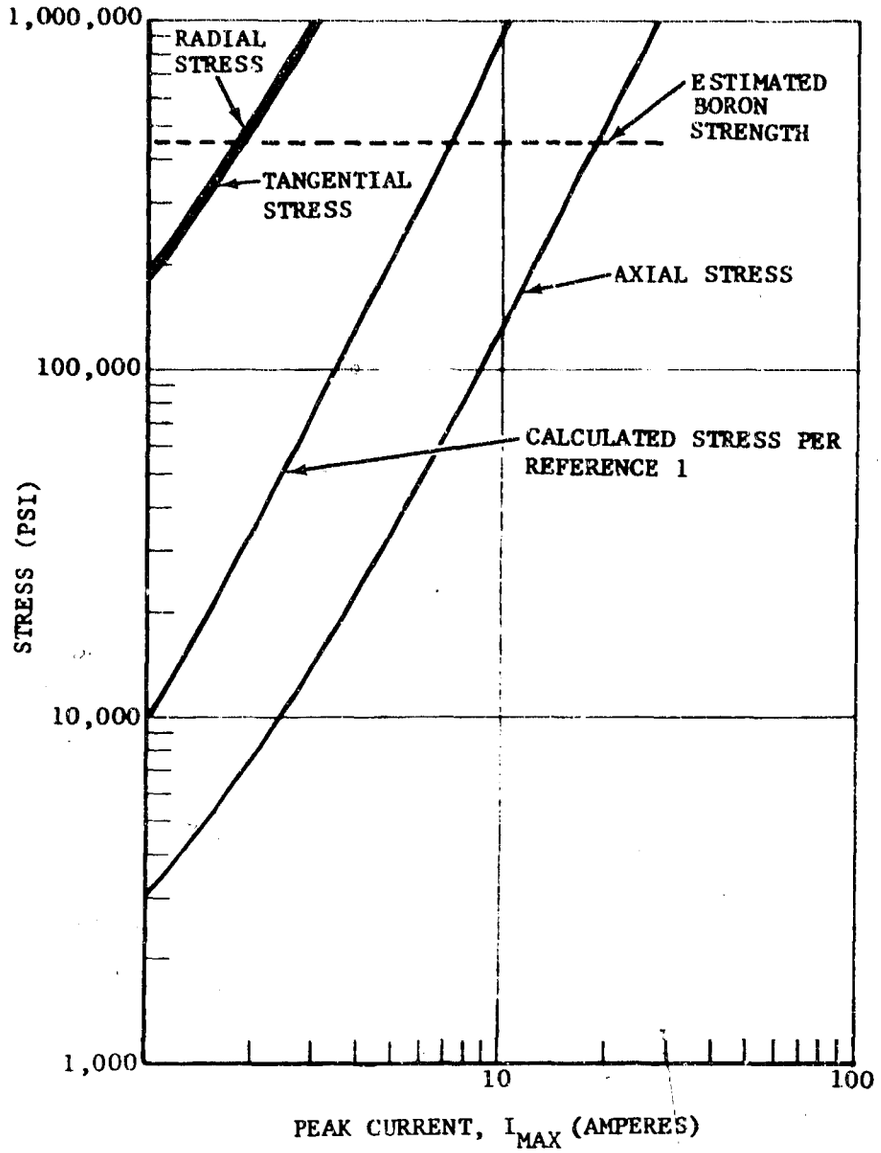

FIGURE 2-68. CALCULATED BORON FILAMENT STRESS

(2) Uncertainty as to the strengths of the boron and core, under the conditions of heat rise noted.

(3) Thermal shock effects not accounted for in mathematical model.

It has been reported previously that filament splitting (due to axial cracks) and filament segmentation both began to occur at approximately the same crest current amplitudes. It has been observed though that segmented filaments always also have radial cracks, but there have been some instances of radially cracked or split boron filaments that are not segmented or otherwise cracked transversely. This then is a probable indication that radial cracks occur at lower impulse levels than do transverse cracks. The differences in the impulse levels, however, is probably not as significant as calculated and reported in Figure 2-68.

Further details of the mathematics of the boron failure model development are given in Appendix B.

2.3.2 GRAPHITE FILAMENT AND COMPOSITES DEGRADATION

In the same manner as for the boron filaments and composites and according to the previously discussed test procedures, specimens of HMG-50 graphite yarn, HM-S graphite tow and epoxy matrix unidirectional composites of each reinforcement were injected with different levels of crest current amplitude using the standard waveform. These current injection tests are tabulated in the appendix. Following are discussions of the respective tests and analyses performed to determine degree of degradation and mechanisms involved.

a. Strength Degradation of Graphite Filaments and Composites. As the result of current injection it was found that the breaking strength of HMG-50 yarns and HM-S tow bundles was reduced at crest current amplitudes of 19 x 10^4 amps per cm^2 of HMG-50 and 86 x 10^4 amps per cm^2 of HM-S. Two factors are believed to contribute to this strength reduction. The first, and probably the most important is the considerable excitation and movement that occurred at the higher current injection levels. This excitation and movement is believed to have caused physical abrasion and damage to the filaments. In the case of the HMG-50 yarn, the excitation and movement was obvious at the 19 x 10^4 amp per cm^2 level, which also corresponded to the point at which strength degradation occurred. The excitation became more violent at higher current injection levels. At crest current injection levels of 45 - 56 x 10^4 amps per cm^2 the breaking strength was reduced by approximately 40%. In the case of the HM-S tow bundles excitation and movement was obvious at crest current injection levels of 29 x 10^4 amps per cm^2 of filament and higher; however, a reduction in breaking strength did not occur until crest current injection levels of 86 x 10^4 amps per cm^2 were used. This is thought to be due to the loosely bound nature of the tow bundles within which the filaments are free to move. The filaments

in the HMG-50 yarn are, however, twisted and plied together tightly. As such, then, very little movement could cause filament damage in the yarn. The filament damage in the HMG-50 yarn as the result of current injection is obvious in Figure 2-69.

The other contributing factor to the HMG-50 yarn and HM-S tow degradation could be filament oxidation and heat build-up within the filaments due to the dissipation of electric current. Example of weight loss in the HMG-50 yarn tests are shown in Table 2-2. Since graphite yarns often have a plastic sizing (and such sizings can burn off to create a weight loss), the thermogravimetric analysis (TGA) curve of Figure 2-70 was measured. A weight loss of only 0.8 - 0.9% was noted at temperatures to 1000°C. Under such inert atmosphere heating, plastic coatings would have reduced to a residual carbon coating on the filaments with typically a 50% weight loss in the form of effluent H_2, H_2O, and CO. The 7.5% weight loss of the yarn specimens then exceeds the amount that could result from loss of sizing, thereby indicating a true loss in weight of the graphite filaments.

TABLE 2-2

WEIGHT LOSS OF GRAPHITE YARN AFTER ELECTRICAL CURRENT INJECTION

SPECIMEN NO.	CREST CURRENT INJECTED, 10^4 AMPS/CM^2	WEIGHT OF 8" SECTION, GRAMS	WEIGHT LOSS, %
HMG-1	Control (none)	0.0146	
-2	Control (none)	0.0145	
-3	Control (none)	0.0146	
-4	Control (none)	0.0149	
-5	Control (none)	0.0146	
-6	Control (none)	0.0146	
-7	Control (none)	0.0146	
-8	Control (none)	0.0145	
-9	Control (none)	0.0148	
-10	Control (none)	0.0146	
		0.0146 AVG	0
HMG-80	45	0.0136	
-83	46.7	0.0134	
		0.0135 AVG	7.5
HMG-70	59.9	0.0134	
-78	54.2	0.0136	
		0.0135 AVG	7.5

FIGURE 2-69. FRAYING OF GRAPHITE FIBERS AS A RESULT OF WHIPPING ACTION DURING CURRENT INJECTION.

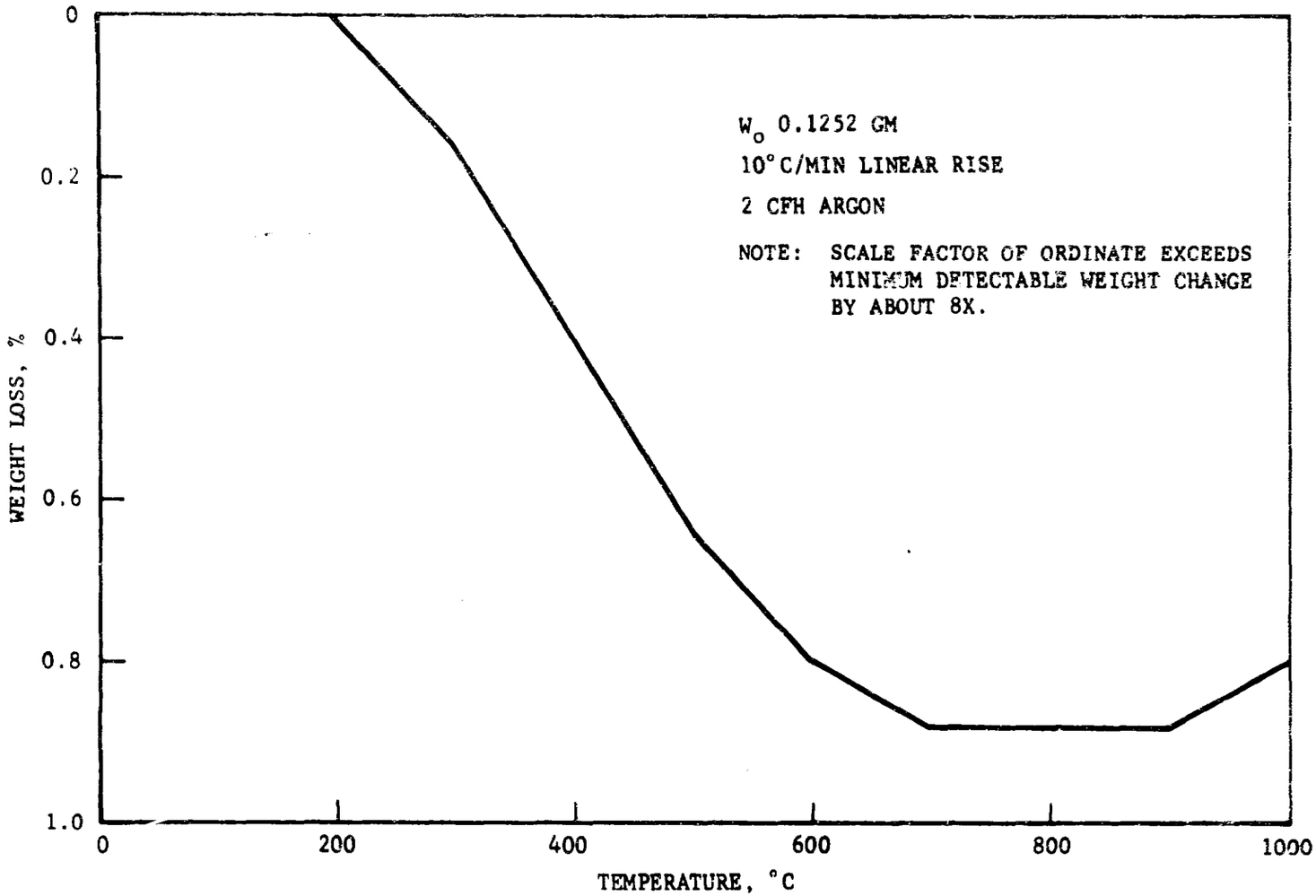

FIGURE 2-70. HMG-50 YARN THERMOGRAVIMETRIC ANALYSIS.

In the same manner as for the boron composites, unidirectional HMG-50/epoxy and HM-S/epoxy graphite filament composites were exposed to series of electric current injection at increasing crest amplitudes, but with the standard waveform shape. In the case of the HMG-50 composite specimens, no strength degradation was observed at crest current density levels as high as 13 x 10^4 amperes per cm^2 of filament cross-section. At an injected crest current density level of 20.4 x 10^4 amperes per cm^2 of filament the specimens burst into flames. The resulting specimens exhibited a 43% reduction in tensile strength. The specimens immediately after exposure are shown in Figure 2-71. The HMG-50/epoxy unidirectional composite specimens exposed to 24.2 x 10^4 amperes per cm^2 of filament delaminated in addition to burning, as shown in Figure 2-72. The HMG-50 epoxy specimen exposed to 55.8 x 10^4 amperes per cm^2 of filament crest current burned even more violently and delaminated more extensively, as shown in Figure 2-73.

Graphite HM-S tow/epoxy unidirectional composite specimens exposed at crest current densities as high as 21 x 10^4 amperes per cm^2 were not degraded. However, identical specimens exposed at 25 x 10^4 amperes per cm^2 burned and charred, as shown in Figure 2-74. The specimens exhibited a 46% reduction in tensile strength. The HM-S epoxy specimens exposed to 52 x 10^4 amperes per cm^2 burned and exfoliated severely, as shown in Figure 2-75.

b. Photomicrographic Inspection of Degraded Filament Composites. The Figure 2-76 photomicrograph shows an HMG-50 specimen after 13 x 10^4 ampere per cm^2 of filament injection. No damage occurred. Figures 2-77, 2-78 and 2-79 are, respectively, photomicrographs of cross-sections of specimens shown in Figures 2-71, 2-72 and 2-73. The increasing severity of damage for current injection levels of 20.4 x 10^4, 24.2 x 10^4 and 55.8 x 10^4 amperes per cm^2 of filament cross-section is obvious.

Figure 2-80 shows a non-damaged HM-S/epoxy specimen cross-section that has been exposed to 21 x 10^4 amperes per cm^2 of filament crest current. Figures 2-81 and 2-82, respectively, show the damaged cross-section of specimens from Figure 2-74 and 2-75.

c. Scanning Electron Microscope Inspection of Degraded Graphite Filaments. In an attempt to determine if the surface of graphite filaments was changed in any way due to current injection, some scanning election microscope scans were made. Figure 2-83 and 2-84 are scans of the surface of an unexposed HM-S filament and a filament from an HM-S tow that had been injected with 98.71 crest amps per cm^2 of filament. Considerable decrease in breaking strength had been measured for tow specimens from the same group as the filament in Figure 2-84. As can be seen, it appears that the surface of the filament in Figure 2-84 has been altered. The two scans, which were taken under identical conditions, show much less

FIGURE 2-71. HMG-50/EPOXY SPECIMENS AFTER 20.4 x 10^4 AMPERES PER CM^2 OF FILAMENT CREST CURRENT INJECTION--showing charring.

FIGURE 2-72. HMG-50/EPOXY SPECIMENS AFTER 24.4 x 10^4 AMPERES PER CM^2 OF FILAMENT CREST CURRENT INJECTION--charred and delaminated.

FIGURE 2-73. HMG-50/EPOXY SPECIMENS AFTER 55.8 x 10^4 AMPERES PER CM^2 OF FILAMENT CREST CURRENT INJECTION--extensively charred and delaminated.

FIGURE 2-74. HM-S/EPOXY SPECIMENS AFTER 25 x 10^4 AMPERES PER CM^2 OF FILAMENT CREST CURRENT INJECTION--showing charring.

FIGURE 2-75 HM-S/EPOXY SPECIMENS AFTER 52 x 10^4 AMPERES PER CM^2 CREST CURRENT INJECTION--charred and exfoliated.

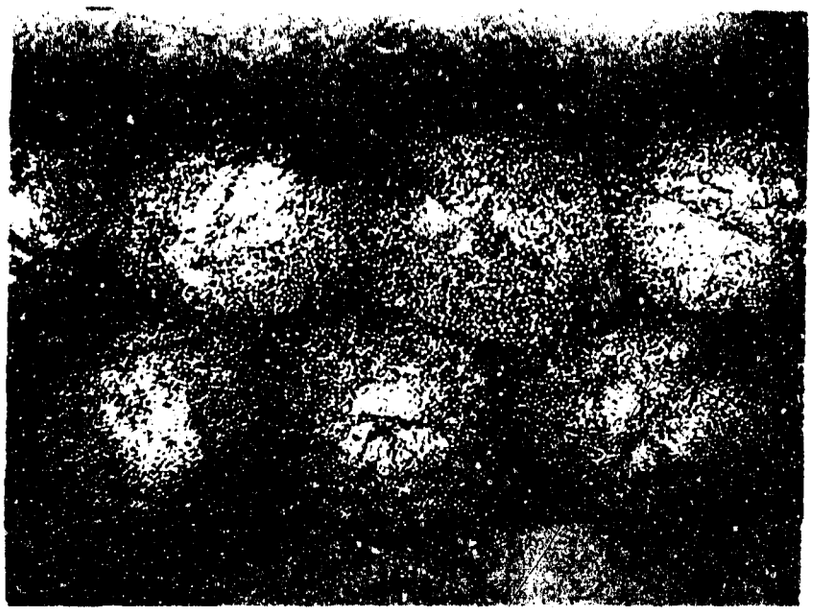

FIGURE 2-76. (100X) HMG-50/EPOXY SPECIMEN AFTER 13.04×10^4 AMPERES PER CM^2 OF FILAMENT CREST CURRENT INJECTION--NO DAMAGE.

FIGURE 2-77. (100X) HMG-50/EPOXY SPECIMEN AFTER 20.4×10^4 AMPERES PER CM^2 OF FILAMENT CREST CURRENT INJECTION--BURNED AND DELAMINATED.

FIGURE 2-78. (100X) HMG-50/EPOXY SPECIMEN AFTER 24.2×10^4 AMPERES PER CM^2 OF FILAMENT CREST CURRENT INJECTION--SEVERELY BURNED AND DELAMINATED.

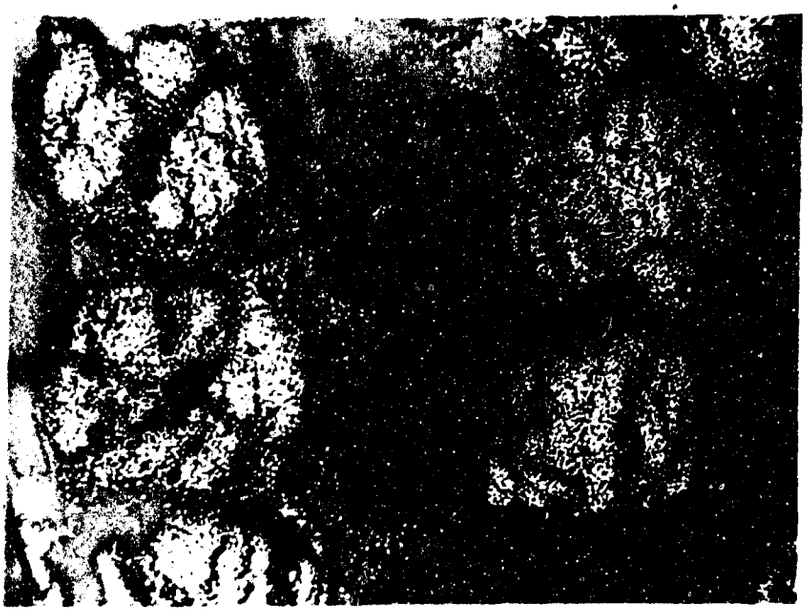

FIGURE 2-79. (100X) HMG-50/EPOXY SPECIMEN AFTER 55.8×10^4 AMPERES PER CM^2 OF FILAMENT CREST CURRENT INJECTION--SEVERELY BURNED AND DELAMINATED.

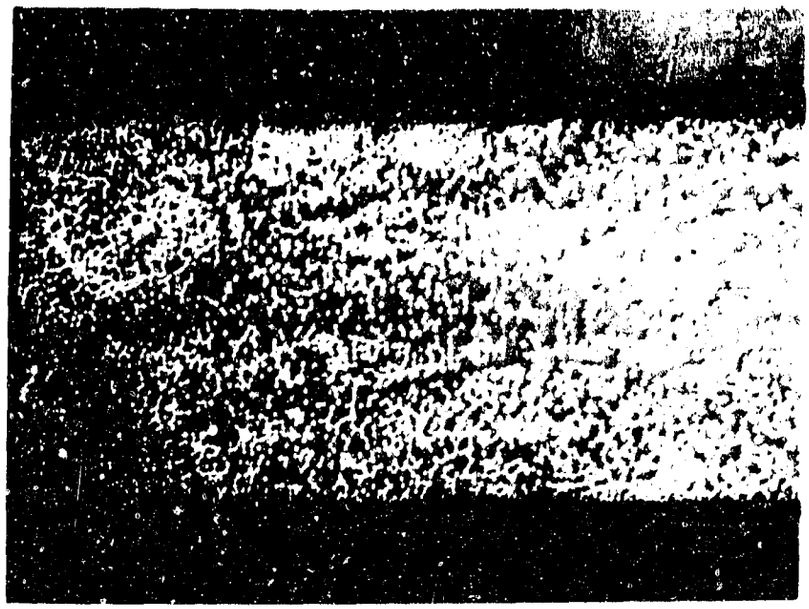

FIGURE 2-80. (100X) HM-S/EPOXY SPECIMEN AFTER 21 x 10^4 AMPERES PER CM^2 OF FILAMENT CREST CURRENT INJECTION --NO DAMAGE.

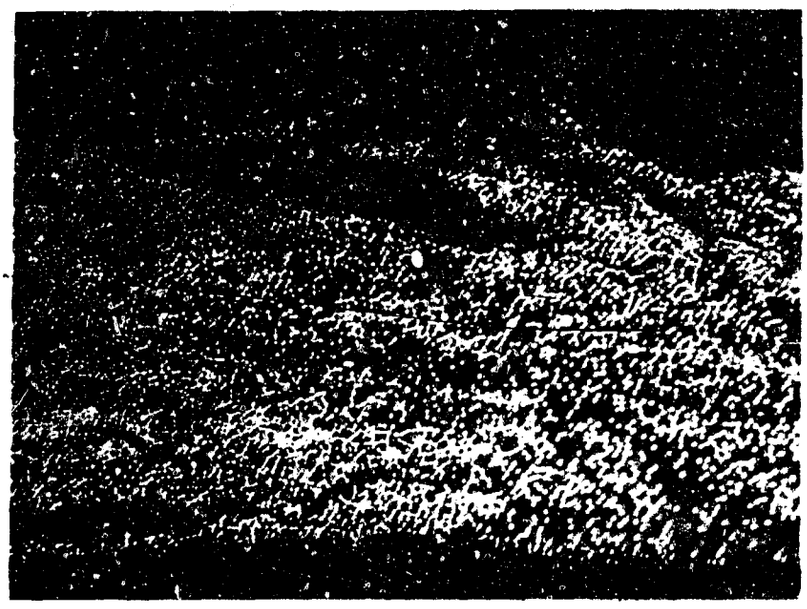

FIGURE 2-81. (100X) HM-S/EPOXY SPECIMEN AFTER 25 x 10^4 AMPERES PER CM^2 OF FILAMENT CREST CURRENT INJECTION-- SOME BURNING AND DELAMINATION.

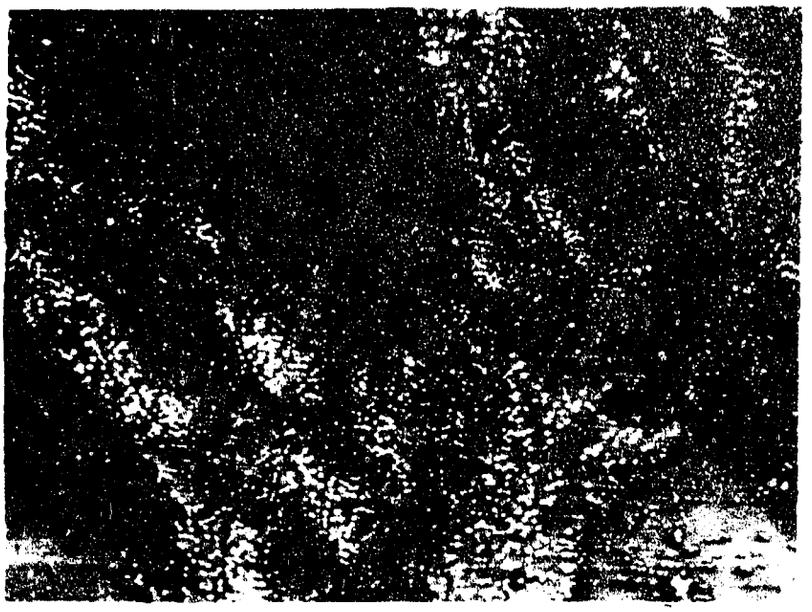

FIGURE 2-82. (100X) HM-S/EPOXY SPECIMEN AFTER 52 x 10^4 AMPERES PER CM^2 OF FILAMENT CREST CURRENT INJECTION--SEVERELY BURNED AND EXFOLIATED.

FIGURE 2-83. (16,000X) ELECTRON MICROSCOPE SCAN OF UNEXPOSED HM-S GRAPHITE FILAMENT SURFACE (40 sec scan)

FIGURE 2-84. (16,000X) ELECTRON MICROSCOPE SCAN OF SURFACE OF GRAPHITE FILAMENT FROM HM-S TOW #74 (98.71×10^4 CREST CURRENT AMPS PER CM^2 OF FILAMENT) (40 sec. scan)

ridging in the case of the exposed filament. This could possibly be due to loss of material from the surface of the filament as the result of oxidation. Further work with the scanning electron microscope would be required before these observations could be taken as conclusive. Also, scans of filaments from different exposure levels should add further evidence if, in fact, surface loss due to oxidation has occurred.

d. Degradation Model for Electric Current Impulsed Graphite Filament Epoxy Composites. The degradation mechanisms of electrically impulsed HMG-50 graphite yarn or HM-S graphite tow reinforced composites appears to be quite simple in comparison to the failure model of boron filament reinforced composites. In the case of the graphite fiber reinforced composites the degradation is not due to a breakdown of the filaments. Instead, the degradation of the composites, when impulsed at damaging levels, is due to pyrolyzation of the resin and mechanical separation or delamination of the fibers one from another. The sequence for this is presently believed to be as follows:

(1) Electric energy flows through the filaments and energy is dissipated in the form of an almost instantaneous heat build-up within the graphite filaments.

(2) At damaging current levels the almost instantaneous build-up of heat causes thermal decomposition (pyrolysis) of the epoxy resin that is in intimate contact with the filaments. This decomposition forms gaseous species.

(3) The rapid decomposition of the resin surrounding the filaments into gaseous species causes a very rapid increase in pressure within the composite.

(4) At a point where the internal pressure exceeds the dynamic tensile strength of the remaining resin matrix, the composite exfoliates or delaminates.

(5) As air then comes in contact with the very hot filaments and decomposing resin, the whole mass bursts into flames. The flames continue until the temperature of the mass is reduced to below the point where the epoxy resin stops burning.

An estimate of the temperature rise which can be expected in a graphite yarn and a graphite tow material subjected to an electrical current pulse is shown in Figure 2-85. A current pulse shape with a front time of t_f = 3.12μsec and a tail time, t_t = 22μsec was used. An analytical expression for the current as a function of time was derived for this pulse shape. This expression was squared and integrated to provide an expression for the integral of i^2dt. Assuming the yarn and tow resistance remained

	YARN	TOW
CROSS SECTION	534.2×10^{-6}	5064.5×10^{-6} CM^2
DENSITY	1.68	1.84 GM/CM^3
ℓ	35.6	35.6 CM
RESISTIVITY	1.35×10^{-3}	0.83×10^{-3} OHM-CM
SPECIFIC HEAT	0.3	0.3 CAL/GM/°C

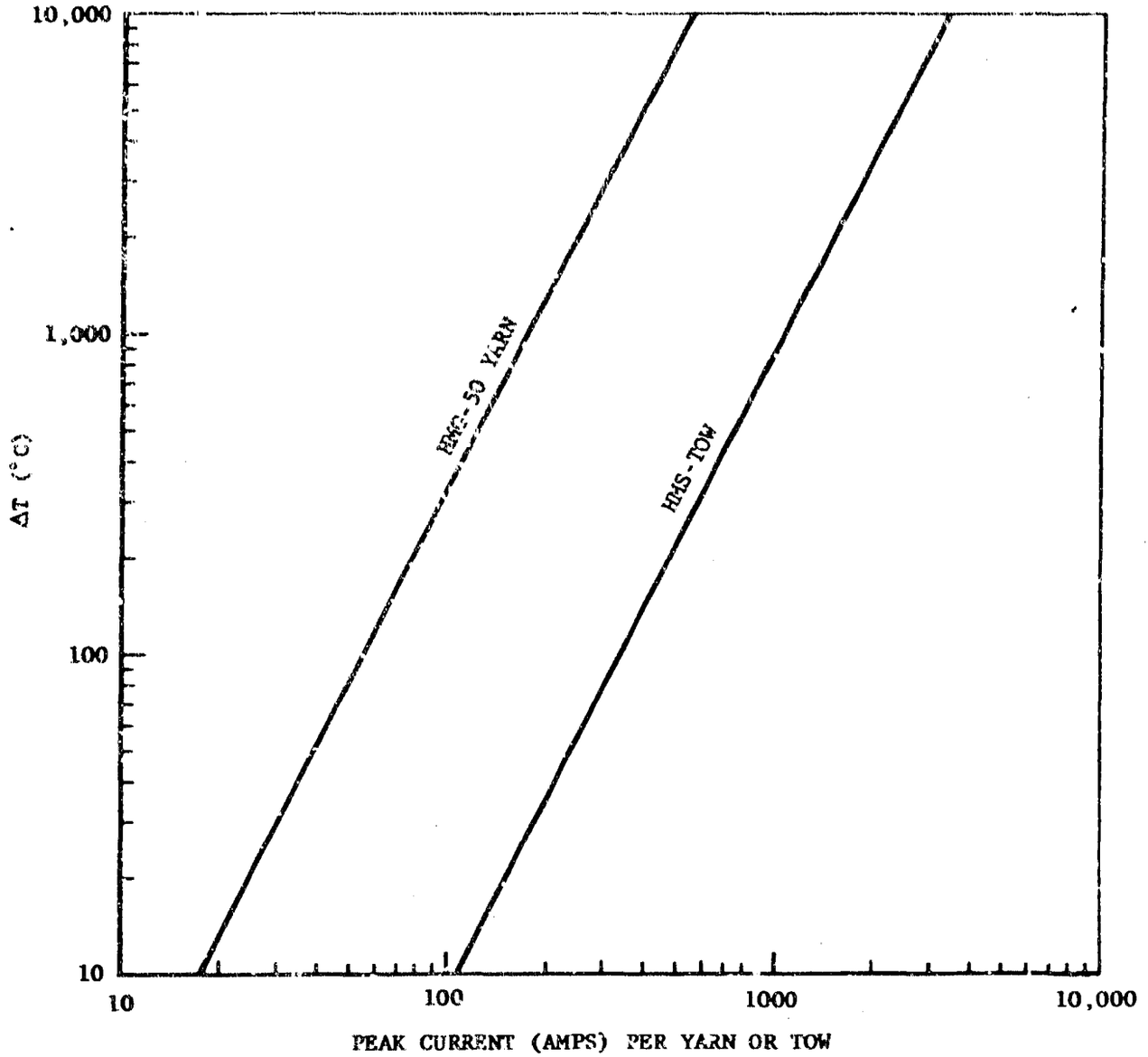

FIGURE 2-85. PREDICTED TEMPERATURE INCREASE IN HMG-50 YARN AND HMS-TOW AS A FUNCTION OF PEAK APPLIED CURRENT

constant and that all energy was converted to heat, the temperature increase was calculated from

$$\Delta T = \frac{R\int_0^t i^2 dt}{WC} \qquad (5)$$

where R = test sample resistance
W = test sample weight
C = material specific heat

An actual current-time pulse from an oscillograph record was plotted and integrated graphically as a check of the analytical expression. This analysis also assumes no heat energy is lost by radiation or conduction to the surroundings and assumes the entire energy of the pulse is deposited within 45μsec.

From Figure 2-85 it can be seen that the HMG-50 yarn calculated temperature rise at 300 amperes injection was 3000°C. For the HM-S tow at a 3000 amp current injection, the calculated temperature rise was 8000°C. Because of heat losses that would have occurred, these temperature rises would not have been realized.

From Figure 2-85 it can be seen that the build-up in heat within the graphite filaments is rapid with increasing levels of current injection. Also, the rate of heat loss or dissipation is expected to be low because of the highly thermal insulative characteristics of the epoxy resin matrices. The Whittaker 2387 resin and the DEN 438/MNA resin were tested and exhibited thermal conductivities of 1.99 and 1.66 Btu-in/hr-ft^2-°F. Because of the low thermal conductivity of the epoxy resin, heat is dissipated into the resin slowly and the resin in immediate contact with the graphite filaments is exposed to a temperature that causes pyrolysis.

As previously discussed, burning of HMG-50 graphite unidirectional composites initiated at a crest current level of 19-20 x 10^4 amps per cm^2 of HMG-50 yarn. That current level corresponds to a crest amplitude of approximately 100 amps per HMG-50 yarn. From Figure 2-85 it can be seen that the resulting peak temperature would be 330°C for HMG-50 filaments. This is typical of the temperature where epoxy resins begin to pyrolyze.

2.4 DEVELOPMENT OF INTERNAL PROTECTION TECHNIQUES FOR ADVANCED COMPOSITES

A direct approach to improving the resistance of boron epoxy and graphite epoxy composites to damage from electric currents would be to improve the electrical conductivity of the composites. This then would result in less energy dissipation and heat build-up. In the case of the boron epoxy composites the heat build-up within the filaments causes filament degradation and in the case of graphite epoxy composites the heat build-up causes resin pyrolysis. Since the basic electric conductivity of the filaments cannot be improved without altering this make-up, and probably their structural properties, a viable approach would involve establishing alternate and more conductive paths within the composites. Obviously, these alternate paths must occupy a minimum volume so that the filament volume content and structural properties of the composite are not compromised. Two such approaches have been investigated and are discussed as follows:

a. Hybrid Boron-Graphite Filament Epoxy Composites. As previously discussed, the impulsive electric current degradation threshold for unidirectional graphite epoxy composites is apparently 4-5 times greater than for unidirectional boron epoxy composites. Therefore, it was conceived that dispersions of graphite filaments between the plies of boron filaments could well serve to improve the resistance of the boron composite to damage. Furthermore, the resistivity of the HM-S tow graphite filaments is typically 0.825×10^{-3} ohm-cm, whereas the resistivity of the boron filaments is typically $4\text{-}8 \times 10^{-3}$ ohm-cm. The order of magnitude lower resistivity of the graphite filaments should result in primary current flow in the interply graphite filaments instead of in the boron filaments. Also, the diameter of the graphite filaments is typically 0.0003 inches or less as compared to 0.004 inches for the boron filaments. This should make possible the incorporation of very thin layers of graphite filaments without significantly decreasing the boron filament volume.

The specimens described in Table 2-3 were provided to this program from an internal development project in progress. As noted in Table A-6 of the Appendix, no severe strength degradations were measured for either Hybrid-1 or Hybrid-2 specimens at injected crest current densities of 9.84 or 10.40×10^4 amperes per cm^2 of filament cross-section, respectively. One each of the two Hybrid-1 and Hybrid-2 specimens showed a somewhat lower tensile strength than did their respective unexposed control specimens (114:143 and 140:176, respectively); however, the other specimens of each Hybrid had virtually the same strength as the control. Apparently, this approach toward improving the electrical current damage resistance of boron composites has some merit because the crest current density (based on total filament cross-sectional area) was approximately twice the level that would have produced significant strength reduction in boron epoxy composites.

TABLE 2-3

COMPOSITION OF HYBRID #1 AND HYBRID #2 BORON-GRAPHITE FILAMENT UNIDIRECTIONAL COMPOSITE SPECIMENS

COMPOSITION	VOLUME %
Hybrid-1:	
Boron filaments	34
HM-S Tow Graphite Filaments	15
Epoxy resin	51
Hybrid-2:	
Boron Filaments	49
HM-S Graphite Tow	11
Epoxy Resin	40

Photomicrographs of one each of the exposed hybrid specimens are shown in Figures 2-86 and 2-87. The incorporation of graphite filaments between layers of boron filaments is shown. There is no evidence of any of the star shaped boron filament cracks that are produced by current injection. The few cracks shown are of the type sometimes produced when the specimens are polished in order to take the photomicrographs.

b. Boron Composites With Imbedded Conductive Wires. This approach was conceived based on a concept of imbedding an array of fine conductive wires within a composite to direct electric current flow away from the filaments. To be a practical approach to improving the resistance of composites to damage from high intensity electric currents, certain objectives must be met:

(1) The wires must be of a metal with good electric conductance and, as such, be of superior conductance to the boron and graphite filaments.

(2) The wires must be of fine diameter so that they can be incorporated to a sufficient degree as to direct current flow without displacing a significant volume of filaments or adding severe weight penalties. If either happened the advantage of using a composite material could be reduced or eliminated.

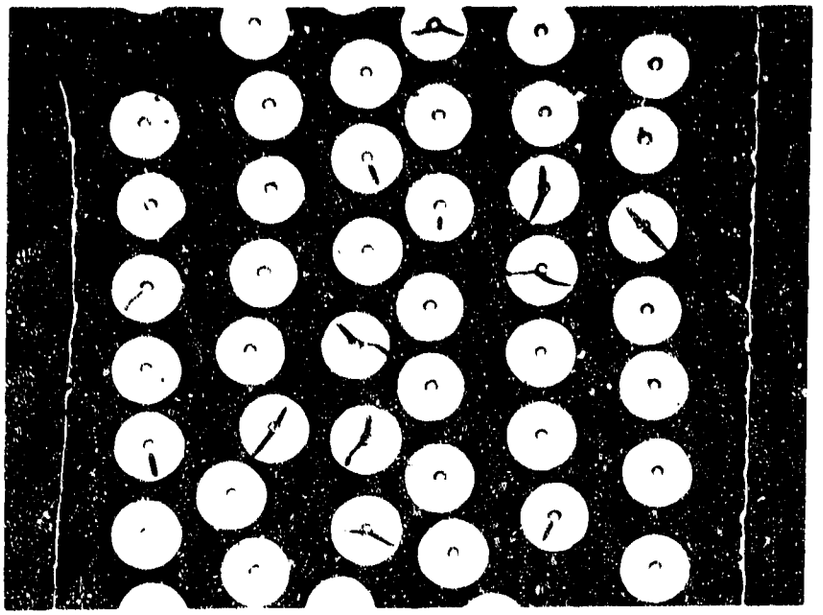

FIGURE 2-86. (100X) HYBRID-2 SPECIMEN AFTER 10.4×10^4 AMPERES PER CM^2 OF FILAMENT AVERAGE CREST CURRENT INJECTION--NO DAMAGE.

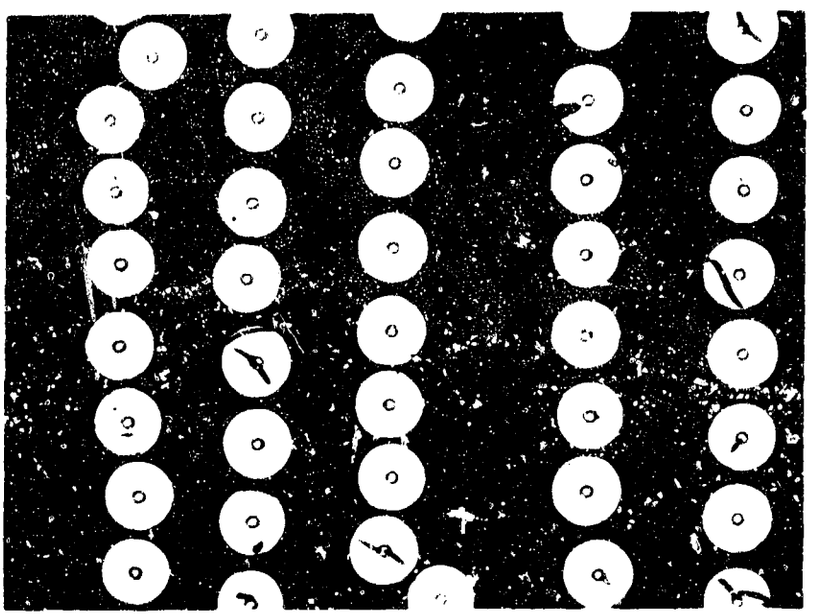

FIGURE 2-87. (100X) HYBRID-1 SPECIMEN AFTER 9.84×10^4 AMPERES PER CM^2 OF FILAMENT AVERAGE CREST CURRENT INJECTION--NO DAMAGE.

(3) The conductive wires must not cause any adverse effects on the composite, either thermally or mechanically.

A survey was made of the availability of fine wires or thin woven fabrics of conductive metals. The finest wire and thinnest fabric available was of tungsten. The material chosen was as supplied by the Newark Wire Cloth Company of Newark, New Jersey. It is a 140 x 140 mesh cloth that is woven from 0.0012-0.0013 inch diameter tungsten wire. Tungsten has a resistivity at room temperature of 5.5×10^{-6} ohm-cm, considerably lower than for either the boron or graphite filaments.

Two unidirectional laminates were fabricated of boron filaments and 2387 epoxy resin with the tungsten cloth incorporated. The fabrication process was identical to that used for all other boron epoxy laminates. In one laminate (BUTCM), one layer of the tungsten cloth was incorporated between the center two plies of the four ply laminate. In the other laminate (BUTC), one layer of the tungsten cloth was laminated onto both faces of the four ply laminate. In both laminates one of the two wire directions in the tungsten cloth was parallel to the boron filament direction. In exactly the same manner as for the boron test specimens, 1/2 inch wide specimens of both the BUTC and BUTCM laminates were prepared for current injection by nickel plating of the specimen ends.

The electric exposure test data and mechanical property data for the BUTC and BUTC specimens is in Table A-7 of the Appendix. As can be seen, the non-exposed BUTC and BUTCM specimens, respectively, had tensile strengths of 144,000 psi and 155,860 psi. Both were as strong or stronger than unexposed boron control specimens tested in the program, which indicated that the addition of the tungsten cloth did not significantly reduce the boron filament content or otherwise decrease the strength of the boron composite. As also noted in Table A-7, the BUTC specimens that were exposed to an average crest current injection of 7.88×10^4 amps per cm^2 of filament had no decrease in strength. At a current injection level of 13.5×10^4 amps per cm^2 only a 24% strength reduction occurred. For boron epoxy composites with no tungsten cloth incorporated, a 50% strength reduction resulted from a 7.85×10^4 amps per cm^2 injection.

The BUTCM specimens exposed to 8.5×10^4 crest amps per cm^2 injection exhibited $< 8\%$ average decrease in strength. The BUTCM specimens exposed to 13.5×10^4 amps per cm^2 of current injection delaminated down the center adjacent to the layer of tungsten cloth. This resulted in a 46% decrease in tensile strength.

The bulk densities of the BUTC and BUTCM laminates were 1.93 and 1.82 gm/cm^3, respectively. The typical densities of boron-epoxy composites range from 1.83 - 1.915 gm/cm^3. Therefore, the incorporation of the tungsten wire on both sides of a four ply boron laminate (BUTC) resulted

in a >100% increase in resistance to gradation with only 0.8% increase in bulk density (weight penalty). The incorporation of the tungsten wire between the center two plies of a four ply boron epoxy laminate resulted in > 50% in resistance to degradation with no measurable weight penalty.

Figure 2-88 is a photomicrograph of one of the BUTCM specimen that was exposed to cross current injection of 13.08×10^4 amps per cm^2 of filament. The fact that the tungsten wire, between the two center boron plies, carried a high current load is evidenced by the fact that some of the wires have melted. Also, none of the typical star shaped cracks in boron filaments, as typically caused by current flow in the boron filaments, are present, except for the one filament in contact with tungsten that has been melted. This further indicates that the tungsten wire carried sufficient current to keep current flow in the boron filaments to below a damaging level. All specimens but BUTCM #1 in this group delaminated. The delamination was probably the result of the hot tungsten wire causing resin pyrolysis and gaseous blowing.

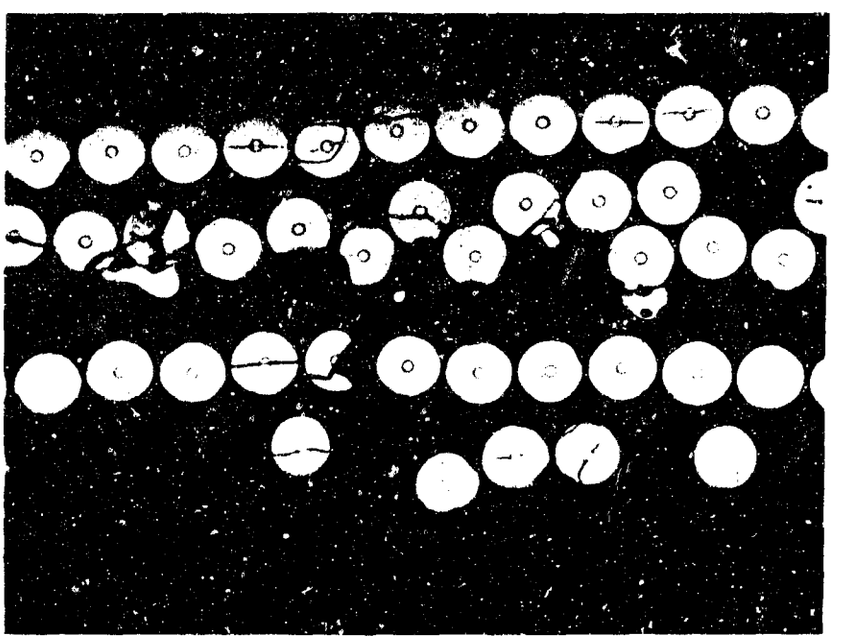

FIGURE 2-88. BUTCM #1 SPECIMEN SUBJECTED WITH 13.08×10^4 CREST AMPS PER CM^2 OF BORON FILAMENTS.

Figure 2-89 and 2-90 are, respectively, BUTC specimens which have been injected with current levels of 7.64×10^4 and 13.96×10^4 crest amps per cm^2 of boron filament cross-section. Specimens of the same group as BUTC #2, Figure 2-89, showed no loss in tensile strength. Specimens of the same group as BUTC #3, Figure 2-90, showed an average loss in tensile strength of 24%. There are indications of the star shaped boron filament crack , as typically caused by current injection, in specimen BUTC #3. In both BUTC #2 and #3 it appears that some of the surface tungsten wires have shattered. This type of tungsten wire damage probably occurs at lower current levels than would cause the tungsten melting evidenced in Figure 2-89.

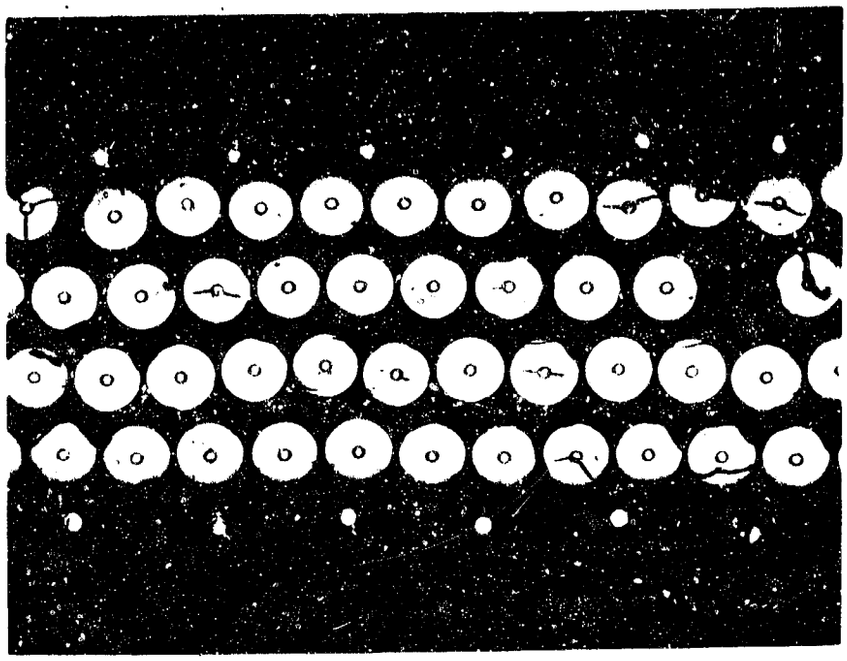

FIGURE 2-89 BUTC #2 SPECIMENS INJECTED WITH 7.64 x 10^4 CREST AMPS PER CM^2 OF BORON FILAMENTS.

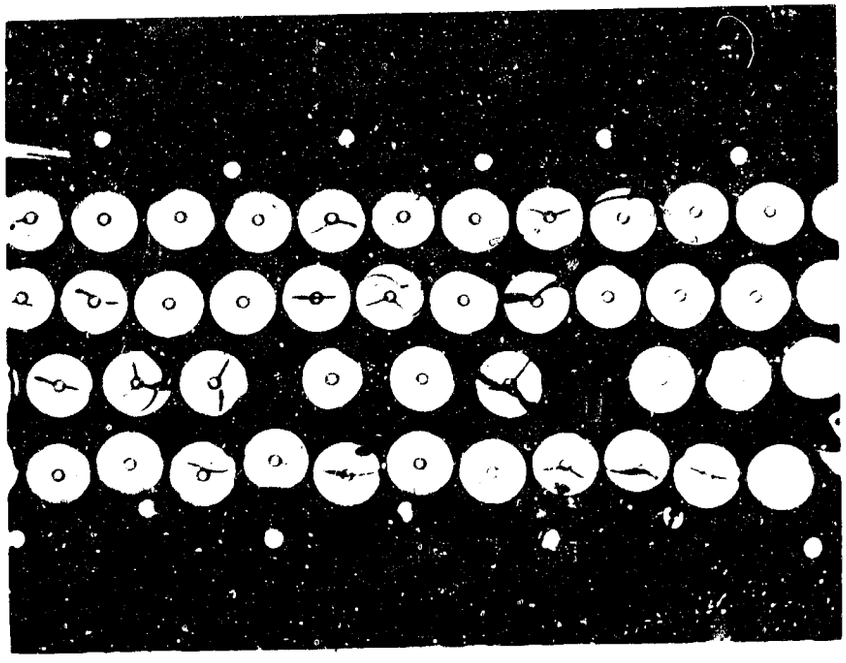

FIGURE 2-90. BUTC #3 SPECIMEN INJECTED WITH 13.96 x 10^4 CREST AMPS PER CM^2 OF BORON FILAMENTS.

SECTION 3

CONCLUSIONS

(1) Electric current flow processes within epoxy resin composites of both boron and graphite filaments is analogous to a complex array of resistors (filaments) with the epoxy resin serving as a dielectric barrier between filaments. The processes, however, that determine the proportions of current flowing in each filament or layers of filaments are very complicated and difficult to mathematically model. Many factors such as why current flow tends to concentrate at random in a fraction of the total boron filaments in a composite are not fully understood at present.

(2) The limiting factors in the degradation of boron/epoxy composites are the boron filaments themselves. The filaments begin to crack and break up at crest current densities of $3.7\text{-}5.7 \times 10^4$ amperes per cm^2 for the standard waveform used in the tests reported. Above that point, loss in strength is rapid with increasing current levels.

(3) The limiting factor in the degradation of graphite/epoxy filaments is the resin matrix. For the HMG-50/epoxy and HM-S/epoxy composites tested with the standard waveform, degradation by burning of the resin was initiated at crest current densities of $20\text{-}25 \times 10^4$ amperes per cm^2 of filament cross-section, for the standard waveform used. At that point the temperature of the filaments was sufficiently high (600-800°F) to cause pyrolyzation of the epoxy resin. At increasing current levels the build-up of pyrolysis gases within the composite is so rapid as to cause delamination.

(4) The controlling factors in the degree of degradation of the filaments and composites tested are the total electric energy input and the fraction thereof dissipated in the form of heat. To demonstrate this crest current amplitude as well as waveform duration was varied. As such, crest current amplitude is less important then the waveform or or total energy.

(5) It appears feasible that the resistance of boron-epoxy composites to degradation by electric currents can be improved through the incorporation of alternate and more conductive paths. Fine wires of conductive metals can be used to provide >50-100% improvement without decreasing the strength of the composite.

REFERENCES

1. USA Standard 062.1, 1967, (IEEE Standard No. 28).

2. "Lightning and Static Electricity Conference, 3-5 Dec. 1968, Part II," AFAL-TR-68-290 Part II, May 1969.

3. E. Rudy and St. Windisch, "Related Binary Systems Mo-B and W-B," Ternary Phase Equilibria In Transition Metal-Boron-Carbon-Silicon Systems, Part I, Vol. III, AFML-TR-65-2, July 1965.

4. F. W. Sears, "Electricity and Magnetism, "Addison-Wesley Publishing Co., Inc., Cambridge, Mass., 1953.

5. J. T. Milet and S. J. Welles, "Boron" Electronic Properties Information Center Data Sheet, DS-151, Feb. 1967.

6. H. S. Carslaw and J. C. Jaeger, "Conduction of Heat in Solids," 2nd Ed., Oxford at the Clarendon Press, 1959.

7. F. E. Wawner, Jr., "Boron Filaments," Chapter 10 of Modern Composite Materials, edited by L. J. Broutman and R. H. Krock, Addison-Wesley Publishing Co., Reading, Mass., 1967.

8. R. J. Roark, "Formulas for Stress and Strain," 3rd Ed., McGraw-Hill Book Co., Inc., New York, 1954.

9. J. Selsing, "Internal Stresses in Ceramics," Journa, of the American Ceramic Society, Vol. 44, Aug. 1961, p. 419.

APPENDIX A

TABLE A-1

INITIAL FIBER AND FILAMENT ELECTRICAL EXPOSURE RESULTS

Specimen	Current Crest		Resistivity, ohm-cm Before-After Exposure	Tensile Strength lbs
	Actual Current Applied, Amps	Current Applied Per Unit Cross-Sectional Area, $Amps/cm^2$		
Boron (Control Specimens)	0	0	not exposed	3.6 4.1 4.1 3.9 AVG
Boron (1)	2.30 2.19 2.09 2.09	2.84×10^4 2.70 " 2.58 " 2.58 "	$6.84 - 6.92 \times 10^{-3}$ 5.38 - 5.64 " 4.83 - 4.68 " 5.77 - 3.75 "	3.6 4.3 4.5 4.8 4.3 AVG
Boron (1)	5.17 5.02 5.00 5.00	6.38×10^4 6.19 " 6.17 " 6.17 "	$4.87 - 4.68 \times 10^{-3}$ 7.54 - 6.82 " 6.46 - 4.48 " 6.20 - 5.96 "	3.8 4.1 5.1 4.2 4.3 AVG
Boron (1)	6.55 6.85 6.85 6.85 6.65 7.00	8.08×10^4 8.45 " 8.45 " 8.45 " 8.20 " 8.63 "	6.02 - ∞ 9.57 - ∞ 5.56 - ∞ 3.80 - ∞ 11.85 - ∞ 9.25 - ∞	Totally disintegrated Totally disintegrated Totally disintegrated Totally disintegrated Broken but not disintegrated Broken but not disintegrated
Graphite HMS Tow (Control Specimen)	0	0	not exposed	73.4 83.5 66.0 74.3 AVG

TABLE A-1 (Continued)

Specimen	Current Crest: Actual Current Applied, Amps	Current Crest: Current Applied Per Unit Cross-Sectional Area, Amps/cm^2	Resistivity, ohm-cm Before-After Exposure	Tensile Strength lbs	Approximate Peak Temperature of Specimens During Exposure
Graphite Tow (3)	127	2.51×10^4	$8.29 - 8.25 \times 10^{-4}$	63.0	$< 140^\circ F$
Graphite Tow (3)	287	$.67 \times 10^4$	$8.11 - 8.09 \times 10^{-4}$	78.0	
	312	6.16 "	8.09 - 8.09 "	60.5	
	312	6.16 "	8.35 - 8.35 "	67.0	$< 140^\circ F$
	304	6.00 "	8.53 - 8.45 "	74.5	
				70.0 AVG	
Graphite Tow (3)	1230	24.28×10^4	$8.09 - 8.09 \times 10^{-4}$	66.5	$350\text{-}400^\circ F$
	985	19.45 "	8.19 - 8.11 "	73.5	$350\text{-}400^\circ F$
	1230	24.28 "	8.87 - 8.82 "	66.0	$350\text{-}400^\circ F$
				68.7 AVG	
Graphite Yarn (Control Specimens)	0	0	not exposed	9.2	
				9.9	
				8.3	
				9.1 AVG	
Graphite Yarn (2)	13.2	2.47×10^4	$1.25 - 1.25 \times 10^{-3}$	10.0	
	13.7	2.57 "	1.28 - 1.28 "	9.7	
				9.9 AVG	
Graphite Yarn (2)	31.5	5.90×10^4	$1.28 - 1.28 \times 10^{-3}$	10.0	
	36.5	6.83 "	1.63 - 1.61 "	8.0	
	31.7	5.93 "	1.23 - 1.23 "	9.8	
	30.4	5.69	1.31 - 1.30 "	9.9	
				9.0 AVG	
Graphite Yarn (2)	157	29.39×10^4	$1.35 - \infty \times 10^{-3}$	5.0	Yarn burned through at terminal $400^\circ F - 490^\circ F$
	147	27.52 "	$1.36 - \infty \times$ "	5.1	
	131	24.52 "	1.28 - 1.29 "	3.0	
	131	24.52 "	1.34 - 1.31 "	7.5	
				5.2 AVG	

(1) $t_f = 4.3\mu$ sec and $t_t = 22\mu$ sec

(2) $t_f = 3.12\mu$ sec and $t_t = 22\mu$ sec

(3) $t_f = 2.5\mu$ sec and $t_t = 24\mu$ sec

TABLE A-2

SECOND SERIES FIBER AND FILAMENT EXPOSURE RESULTS

Specimen	Current Crest: Actual Current Applied, Amps	Current Crest: Current Applied per Unit Cross Sectional Area, Amps/cm^2	Resistivity, ohm-cm Before-After Exposure	Tensile Strength, Lbs	Approximate Peak Temperature During Exposure
Boron (Control Specimens) 1 2 3 4	0	0	not exposed	3.65 4.90 5.70 4.40 4.66 AVG	NT
Boron (1) 44 26 28 6 43	2.92 2.83 3.02 3.13 3.03	3.60×10^4 3.49×10^4 3.72×10^4 3.86×10^4 3.74×10^4	$6.67 - 6.50 \times 10^{-3}$ $6.62 - 6.45 \times 10^{-3}$ $5.39 - 5.24 \times 10^{-3}$ $5.11 - 5.54 \times 10^{-3}$ $4.39 - 4.28 \times 10^{-3}$	4.10 5.15 4.22 4.49 AVG	NT
Boron (1) 22 24 45 23 25 21	3.60 3.62 3.45 3.60 3.60 3.60	4.44×10^4 4.46×10^4 4.25×10^4 4.44×10^4 4.44×10^4 4.44×10^4	$3.96 - 7.16 \times 10^{-3}$ $4.31 - 4.01 \times 10^{-3}$ $3.94 - 2.98 \times 10^{-3}$ $4.29 - 2.19 \times 10^{-3}$ $8.88 - 6.15 \times 10^{-3}$ $9.70 - 6.33 \times 10^{-3}$	2.30 2.95 3.95 5.20 3.60 AVG	NT
Boron (1) 34 20 46 31 18 19	4.00 4.00 4.30 4.00 4.35 4.20	4.93×10^4 4.93×10^4 5.30×10^4 4.93×10^4 5.36×10^4 5.18×10^4	$5.10 - 3.42 \times 10^{-3}$ $5.66 - 2.05 \times 10^{-3}$ $6.18 \times 10^{-3} - \infty$ $4.92 \times 10^{-3} - \infty$ $8.04 - 6.04 \times 10^{-3}$ $4.67 \times 10^{-3} - \infty$	0.40 8.00 4.90 1.25 2.14 AVG	NT
Boron (1) 17	5.00	6.17×10^4	$8.53 - \infty \times 10^{-3}$	1.35 AVG	NT

NT = No Test

TABLE A-2 (Continued)

SECOND SERIES FIBER AND FILAMENT EXPOSURE RESULTS

Specimen	Current Crest: Actual Current Applied, Amps	Current Crest: Current Applied per Unit Cross Sectional Area, Amps/cm^2	Resistivity, ohm-cm Before-After Exposure	Tensile Strength, Lbs	Approximate Peak Temperature During Exposure
Boron (1)					
13	6.10	7.52×10^4	$8.97 - 16.20 \times 10^{-3}$		
15	6.00	7.40×10^4	$7.07 - 2.17 \times 10^{-3}$		
14*	6.00	7.40×10^4	$5.43 \times 10^{-3} - \infty$	2.65	
11*	6.50	8.01×10^4	$9.40 \times 10^{-3} - \infty$	1.45	NT
12	6.10	7.52×10^4	$5.28 - 4.77 \times 10^{-3}$	2.75	
16	6.00	7.40×10^4	$7.50 - 3.05 \times 10^{-3}$	2.65	
				2.38 AVG	
Boron (1)					
37**	6.85	8.45×10^4	$3.80 \times 10^{-3} - \infty$		
39**	6.65	8.20×10^4	$11.84 \times 10^{-3} - \infty$		
8	6.85	8.45×10^4	$9.57 \times 10^{-3} - \infty$		
10*	6.85	8.45×10^4	$5.56 \times 10^{-3} - \infty$	0.30	
7*	6.55	8.08×10^4	$6.02 - 5.44 \times 10^{-3}$	0.35	220 - 240°F
40**	7.20	8.88×10^4	$9.25 \times 10^{-3} - \infty$	0.33 AVG	
Boron					
(2) 50*	7.20	8.88×10^4	$7.18 - 4.59 \times 10^{-3}$	1.40	
(8) 51**	5.75	7.09×10^4	$7.25 \times 10^{-3} - \infty$		
(8) 52**	6.00	7.40×10^4	$3.83 \times 10^{-3} - \infty$		NT
(8) 53**	6.40	7.89×10^4	$8.22 \times 10^{-3} - \infty$		
(8) 54**	6.55	8.08×10^4	$4.60 \times 10^{-3} - \infty$		
(8) 55**	6.50	8.01×10^4	$5.98 \times 10^{-3} - \infty$		
				1.40 AVG	
Graphite HMS-Tow (Control Specimen)					
1				72	
2	0	0	not exposed	77	NT
3				84	
				78 AVG	

*Partially disintegrated - longest piece tested in tension

**Completely disintegrated

NT = No Test

TABLE A-2 (Continued)

SECOND SERIES FIBER AND FILAMENT EXPOSURE RESULTS

Specimen	Current Crest		Resistivity, ohm-cm Before-After Exposure	Tensile Strength, Lbs	Approximate Peak Temperature During Exposure
	Actual Current Applied, Amps	Current Applied per Unit Cross Sectional Area, Amps/cm^2			
Graphite Tow (3)					
62	213	4.21×10^4	$10.00 - 9.35 \times 10^{-4}$		
25	221	4.36×10^4	$8.14 - 8.10 \times 10^{-4}$		
24	218	4.30×10^4	$8.14 - 8.14 \times 10^{-4}$		
20	230	4.54×10^4	$8.31 - 8.28 \times 10^{-4}$		
19	230	4.54×10^4	$8.67 - 8.55 \times 10^{-4}$		NT
21	226	4.47×10^4	$8.19 - 8.12 \times 10^{-4}$	79	
23	222	4.39×10^4	$8.65 - 8.51 \times 10^{-4}$	85	
				82 AVG	
Graphite Tow (3)					
18	246	4.86×10^4	$8.04 - 8.04 \times 10^{-4}$		
17	254	5.01×10^4	$8.04 - 8.04 \times 10^{-4}$	NT	NT
16	250	4.94×10^4	$7.99 - 7.98 \times 10^{-4}$		
15	238	4.70×10^4	$8.03 - 8.03 \times 10^{-4}$		
45	262	5.17×10^4	$8.57 - 8.72 \times 10^{-4}$		
14	>230	$>4.54 \times 10^4$	$8.73 - 8.64 \times 10^{-4}$		
Graphite Tow (3)					
13	362	7.15×10^4	$8.15 - 8.12 \times 10^{-4}$		
12	390	7.70×10^4	$8.83 - 8.61 \times 10^{-4}$	NT	NT
11	374	7.38×10^4	$8.11 - 8.08 \times 10^{-4}$		
55	374	7.38×10^4	$8.25 - 8.24 \times 10^{-4}$		
54	364	7.19×10^4	$8.20 - 8.15 \times 10^{-4}$		
53	361	7.13×10^4	$8.02 - 8.02 \times 10^{-4}$		
Graphite Tow (3)					
51	426	8.41×10^4	$8.23 - 8.19 \times 10^{-4}$		
49	410	8.09×10^4	$8.28 - 8.18 \times 10^{-4}$		
47	483	9.54×10^4	$8.19 - 8.11 \times 10^{-4}$		$<130^{\circ}F$
52	430	8.50×10^4	$8.34 - 8.30 \times 10^{-4}$	67	
50	430	8.50×10^4	$8.31 - 8.29 \times 10^{-4}$	84	
48	452	8.93×10^4	$8.80 - 8.49 \times 10^{-4}$	67	
				73 AVG	

TABLE A-2 (Continued)

SECOND SERIES FIBER AND FILAMENT EXPOSURE RESULTS

Specimen	Current Crest		Resistivity, ohm-cm Before-After Exposure	Tensile Strength, Lbs	Approximate Peak Temperature During Exposure
	Actual Current Applied, Amps	Current Applied per Unit Cross Sectional Area, Amps/cm^2			
Graphite Tow (3)					
43	642	12.68×10^4	$8.11 - 8.04 \times 10^{-4}$		
41	647	12.77×10^4	$8.25 - 8.18 \times 10^{-4}$		
46	635	12.50×10^4	$8.25 - 8.19 \times 10^{-4}$	65	
42	615	12.20×10^4	$8.01 - 7.45 \times 10^{-4}$	83	140 - 160°F
1	615	12.20×10^4	$8.11 - 8.11 \times 10^{-4}$	89	
44	655	12.90×10^4	$8.71 - 8.59 \times 10^{-4}$	84	
				80 AVG	
Graphite Tow (3)					
4	941	18.58×10^4	$8.22 - 8.16 \times 10^{-4}$		
6	860	16.98×10^4	$7.83 - 9.83 \times 10^{-4}$		
2	942	18.60×10^4	$8.15 - 8.11 \times 10^{-4}$	89	
3	942	18.60×10^4	$7.38 - 8.01 \times 10^{-4}$	82	180 - 200°F
5	942	18.60×10^4	$8.21 - 8.21 \times 10^{-4}$	89	
7	902	17.80×10^4	$8.21 - 8.11 \times 10^{-4}$	82	
				86 AVG	
Graphite Tow (3)					
66	1600	31.59×10^4	$8.16 - 8.08 \times 10^{-4}$		
59	1450	28.63×10^4	Broken terminal		
65	1760	37.18×10^4	$8.31 - 8.27 \times 10^{-4}$	86	300 - 350°F
57	1515	29.94×10^4	$8.23 - 8.17 \times 10^{-4}$	62	
22	1540	30.43×10^4	$8.07 - 8.05 \times 10^{-4}$	84	
				77 AVG	

TABLE A-2 (Continued)

SECOND SERIES FIBER AND FILAMENT EXPOSURE RESULTS

Specimen	Current Crest: Actual Current Applied, Amps	Current Crest: Current Applied per Unit Cross Sectional Area, Amps/cm^2	Resistivity, ohm-cm Before-After Exposure	Tensile Strength, Lbs	Approximate Peak Temperature During Exposure
Graphite Tow (6)					
83	2500	49.36×10^4	$8.25 - 8.77 \times 10^{-4}$*		
86	2500	49.36×10^4	$8.42 - 8.60 \times 10^{-4}$		
82	2500	49.5×10^4	$8.25 - 8.47 \times 10^{-4}$	60	
84	2500	49.5×10^4	$8.04 - 8.32 \times 10^{-4}$	76	
85	2500	49.5×10^4	$8.23 - 8.35 \times 10^{-4}$	83	>490°F
87	2500	49.5×10^4	$8.11 - 8.25 \times 10^{-4}$	84	
				76 AVG	
Graphite Tow (6)					
89	3080	60.81×10^4	$8.30 - 8.72 \times 10^{-4}$	*	
68	3000	59.23×10^4	$8.27 - 8.35 \times 10^{-4}$	*	
88	2960	58.6×10^4	$8.20 - 8.45 \times 10^{-4}$	80*	
90	3000	59.5×10^4	$8.15 - 8.44 \times 10^{-4}$	63*	>490°F
69	3000	59.5×10^4	$8.05 - 8.15 \times 10^{-4}$	84*	
67	3000	59.5×10^4	$9.15 - 9.48 \times 10^{-4}$	*	
				76 AVG	
Graphite Yarn (Control Specimen)	0	0	not exposed	10.00 10.00 9.80 9.90 AVG	NT
Graphite Yarn (4)					
11	39	7.30×10^4	$1.29 - 1.29 \times 10^{-3}$		
13	39.5	7.39×10^4	$1.30 - 1.29 \times 10^{-3}$		
8	38	7.12×10^4	$1.34 - 1.32 \times 10^{-3}$	9.40	
10	38	7.12×10^4	$1.53 - 1.54 \times 10^{-3}$	9.85	180 - 200°F
12	40	7.49×10^4	$1.25 - 1.25 \times 10^{-3}$	10.20	
14	37	6.93×10^4	$1.33 - 1.33 \times 10^{-3}$	8.35	
				9.45 AVG	

*Frayed appearance after current injection.

TABLE A-2 (Continued)

SECOND SERIES FIBER AND FILAMENT EXPOSURE RESULTS

Specimen	Current Crest		Resistivity, ohm-cm Before-After Exposure	Tensile Strength, Lbs	Approximate Peak Temperature During Exposure
	Actual Current Applied, Amps	Current Applied per Unit Cross Sectional Area, Amps/cm^2			
Graphite Yarn (4)					
16	46	8.61×10^4	$1.32 - 1.31 \times 10^{-3}$		
60	45	8.43×10^4	$1.27 - 1.26 \times 10^{-3}$		
15	46	8.61×10^4	$1.30 - 1.29 \times 10^{-3}$	8.20	
45	43.5	8.15×10^4	$1.45 - 1.55 \times 10^{-3}$	9.15	220 - 240°F
61	45	8.43×10^4	$1.28 - 1.27 \times 10^{-3}$	10.30	
59	47	8.80×10^4	$1.25 - 1.24 \times 10^{-3}$	10.20	
				9.46 AVG	
Graphite Yarn (4)					
56	65.5	12.26×10^4	$1.31 - 1.30 \times 10^{-3}$		
51	65.5	12.26×10^4	$1.70 \times 10^{-3} - \infty$		
58	69.5	13.02×10^4	$1.26 - 1.26 \times 10^{-3}$	9.70	
57	65.5	12.27×10^4	$1.32 - 1.30 \times 10^{-3}$	9.20	300 - 350°F
55	69.5	13.02×10^4	$1.28 - 1.28 \times 10^{-3}$	10.00	
				9.60 AVG	
Graphite Yarn (4)					
50	102	19.10×10^4	$1.27 - 1.27 \times 10^{-3}$		
48	90	16.85×10^4	$1.32 - 1.33 \times 10^{-3}$		
54	66	12.36×10^4	$1.27 - 1.27 \times 10^{-3}$	9.80	
53	99	18.54×10^4	$1.31 - 1.30 \times 10^{-3}$	7.90	
52	99	18.54×10^4	$1.28 - 1.28 \times 10^{-3}$	6.25	
49	99	18.54×10^4	$1.31 - 1.31 \times 10^{-3}$	9.15	400 - 490°F
47	115	21.54×10^4	$1.28 \times 10^{-3} - \infty$	7.60	
				8.14 AVG	

TABLE A-2 (Continued)

SECOND SERIES FIBER AND FILAMENT EXPOSURE RESULTS

Specimen	Current Crest: Actual Current Applied, Amps	Current Crest: Current Applied per Unit Cross Sectional Area, Amps/cm^2	Resistivity, ohm-cm Before-After Exposure	Tensile Strength, Lbs	Approximate Peak Temperature During Exposure
Graphite Yarn (4)					
24	143	26.78×10^4	$1.36 - 2.66 \times 10^{-3}$	*	
22	140	26.22×10^4	$1.31 - 1.35 \times 10^{-3}$	*	
26	139	26.03×10^4	$1.36 - 1.54 \times 10^{-3}$	7.80*	
25	143	26.78×10^4	$1.27 - 1.33 \times 10^{-3}$	7.60*	
23	143	26.78×10^4	$1.29 - 1.33 \times 10^{-3}$	6.55*	NT
65	140	26.22×10^4	$1.27 - 1.29 \times 10^{-3}$	8.50*	
				7.61 AVG	
Graphite Yarn (4)					
29	150	28.07×10^4	$1.27 - 1.32 \times 10^{-3}$	*	
63	156	29.21×10^4	$1.29 - \infty \times 10^{-3}$	*	
31	152	28.46×10^4	$1.28 - 1.36 \times 10^{-3}$	5.95*	
30	156	29.21×10^4	$1.27 - 1.37 \times 10^{-3}$	6.75*	>490°F
27	152	28.46×10^4	$1.27 - 1.31 \times 10^{-3}$	6.55*	
66	156	29.21×10^4	$1.29 - 1.35 \times 10^{-3}$	5.95*	
				6.30 AVG	
Graphite Y Yarn (4)					
18	162	30.34×10^4	$1.30 - 1.54 \times 10^{-3}$	*	
64	163	30.52×10^4	$1.35 - 0.32 \times 10^{-3}$	*	
20	162	30.34×10^4	$1.26 - 1.31 \times 10^{-3}$	6.95*	
19	162	30.34×10^4	$1.24 - 1.38 \times 10^{-3}$	7.45*	
17	163	30.52×10^4	$1.28 - 1.32 \times 10^{-3}$	7.70*	>490°F
62	172	32.21×10^4	$1.30 - 1.36 \times 10^{-3}$	6.10*	
				7.05 AVG	
Graphite Yarn (5)					
80	240	45.00×10^4	$1.29 - 1.49 \times 10^{-3}$	*	
83	250	46.70×10^4	$1.41 - \infty \times 10^{-3}$	*	
79	240	45.0×10^4	$1.27 - 1.38 \times 10^{-3}$	4.2*	
81	240	45.0×10^4	$1.25 - 1.40 \times 10^{-3}$	5.1*	>490°F
82	240	45.0×10^4	$1.25 - 1.40 \times 10^{-3}$	5.6*	
73	250	46.7×10^4	$1.28 - 1.46 \times 10^{-3}$	5.8*	
				5.2 AVG	

*Frayed appearance after current injection.

TABLE A-2 (Continued)

SECOND SERIES FIBER AND FILAMENT EXPOSURE RESULTS

Specimen	Current Crest: Actual Current Applied, Amps	Current Crest: Current Applied per Unit Cross Sectional Area, Amps/cm^2	Resistivity, ohm-cm Before-After Exposure	Tensile Strength, Lbs	Approximate Peak Temperature During Exposure
Graphite Yarn (5)					
70	320	59.90×10^4	$1.23 - 1.53 \times 10^{-3}$	*	
78	290	54.20×10^4	$1.26 - 1.42 \times 10^{-3}$	*	
71	290	54.20×10^4	$1.25 - 1.41 \times 10^{-3}$	5.0*	
72	300	56.0×10^4	$1.25 - 1.41 \times 10^{-3}$	5.2*	>490°F
74	280	52.3×10^4	$1.25 - 1.42 \times 10^{-3}$	6.3*	
77	300	56.0×10^4	$1.28 - 1.46 \times 10^{-3}$	5.9*	
				5.6 AVG	
	(1) t_f = 4.3μsec and t_t = 22μsec (2) t_f = 1.2μsec and t_t = 13.5μsec (3) t_f = 2.5μsec and t_t = 24μsec (4) t_f = 3.12μsec and t_t = 22μsec (5) t_f = 3.5μsec and t_t = 33μsec (6) t_f = 3.5μsec and t_t = 25μsec (7) t_f = 3.7μsec and t_t = 24μsec (8) t_f = 4.0μsec and t_t = 24μsec				

*Frayed appearance after current injection.

TABLE A-3

THIRD SERIES FIBER AND FILAMENT EXPOSURE RESULTS

Specimen	Current Crest: Actual Current Applied, Amps	Current Crest: Current Applied Per Unit Cross Sectional Area, Amps/cm^2	Resistivity, Ohm-cm Before-After Exposure	Tensile Strength, Lbs	Approximate Peak Temperature During Exposure
Boron (Control Specimens) 1 2 3 4 5	0	0	Not exposed	3.5 3.9 3.9 4.2 4.9 4.1 AVG	NT
Boron (9) 63	6.0	7.39×10^4	$3.01 - 2.99 \times 10^{-3}$		
64	6.0	7.39×10^4	$3.61 - 2.97 \times 10^{-3}$		
56	4.5	5.54×10^4	$10.98 - 10.34 \times 10^{-3}$	4.3	
59	7.0	8.63×10^4	$4.86 - 2.27 \times 10^{-3}$	3.9	NT
60	6.5	8.01×10^4	$12.58 \times 10^{-3} - \infty$	2.8	
62	6.0	7.39×10^4	$3.50 - 2.86 \times 10^{-3}$	5.2	
76	6.0	7.39×10^4	$4.61 - 3.64 \times 10^{-3}$	4.5 4.1 AVG	
Graphite HMS-Tow (Control Specimen 1				81	
2	0	0	Not exposed	85	NT
3				86	
4				68	
5				67 77 AVG	

TABLE A-3 (Continued)

Specimen	Current Crest: Actual Current Applied, Amps	Current Crest: Current Applied Per Unit Cross Sectional Area, Amps/cm^2	Resistivity, Ohm-cm Before-After Exposure	Tensile Strength, Lbs	Approximate Peak Temperature During Exposure
Graphite Tow (1)					
71	5000	98.71×10^4	$10.25 - 30.70 \times 10^{-4}$	*	
74	5000	98.71×10^4	$8.31 - 9.77 \times 10^{-4}$	*	
70	5000	98.71×10^4	$8.39 - 13.35 \times 10^{-4}$	27*	T >490°F
72	4350	85.88×10^4	$10.53 - 45.81 \times 10^{-4}$	23*	Motion Restricted
73	5000	98.71×10^4	$8.39 - 12.14 \times 10^{-4}$	17*	" "
75	5000	98.71×10^4	$8.22 - 10.44 \times 10^{-4}$	20*	" "
				22 AVG	
Graphite Yarn (Control Specimen)					
1				10.4	
2	0	0	Not exposed	10.3	NT
3				10.0	
4				9.4	
5				10.5	
				10.1 AVG	
Graphite Yarns (3)					
88	500	93.59×10^4	$1.36 - 2.96 \times 10^{-3}$	*	Motion was restricted for all six specimens
85	500	93.59×10^4	$1.32 - 1.43 \times 10^{-3}$	5.3*	
86	500	93.59×10^4	$1.35 - 1.56 \times 10^{-3}$	2.5*	
87	500	93.59×10^4	$1.29 - 1.48 \times 10^{-3}$	6.1*	
89	514	96.21×10^4	$1.27 - 1.45 \times 10^{-3}$	5.9*	
90	488	91.35×10^4	$1.28 - 1.47 \times 10^{-3}$	5.5*	
				5.1 AVG	

(1) t_f = 4.3μsec and t_t = 22μsec

(3) t_f = 2.5μsec and t_t = 24μsec

(9) t_f = 4μsec and t_t = 12μsec

*Specimens fuzzy and fluffed after current injection.

TABLE A-4

FOURTH SERIES FILER AND FILAMENT EXPOSURE RESULTS

Specimen	Current Crest: Actual Current Applied, Amps	Current Crest: Current Applied Per Unit Cross Sectional Area, Amps/cm^2	Resistivity, ohm-cm Before-After Exposure	Tensile Strength, Lbs	Approximate Peak Temperature During Exposure
Boron (Control Specimens)					
1				6.0	
2				4.2	
3	0	0	not exposed	5.9	NT
4				6.4	
				5.6 AVG	
Boron (10)					
65	3.2	3.94×10^4	$4.53 - 4.48 \times 10^{-3}$		
66	3.2	3.94×10^4	$4.35 - 3.52 \times 10^{-3}$		
67	3.2	3.94×10^4	$4.75 - 2.16 \times 10^{-3}$	4.4	
68	3.2	3.94×10^4	$5.43 - 3.72 \times 10^{-3}$	4.4	
69	3.2	3.94×10^4	$4.51 - 3.52 \times 10^{-3}$	4.3	
70	3.2	3.94×10^4	$3.75 - 2.56 \times 10^{-3}$	4.6	
				4.4 AVG	

(10) $t_f = 4.3\mu$ sec and $t_t = 50\mu$sec

TABLE A-5

INITIAL UNIDIRECTIONAL LAMINATE
EXPOSURE RESULTS

Specimen	Filament Volume Content, %	Current Crest		Current Applied per Filament	Resistivity, ohm-cm Before-After Exposure	Tensile Strength, psi modulus, psi x 10^{-6}	Approximate Peak Temperature During Exp
		Actual Current Applied, Amps	Current Applied per Unit Cross Sectional Area of Filament, Amps/cm^2				
Boron unidirectional Laminate (Control Specimen)							
49	40.27	0	0	0	not exposed	108,850-21.8	NT
51						102,650	
Boron unidirectional Laminate (7)							
1		3760			$15.35\text{-}7.2\times10^{-3}$		130 - 140°F
4		3980			$11.0\text{-}16.55\times10^{-3}$		160 - 180°F
13		3980			$9.07\text{-}44.4\times10^{-3}$	34,050	180 - 200°F
17	50.11	3700	8.64×10^4	7.00	$8.64\text{-}7.8\times10^{-3}$	94,170-25.0	140 - 160°F
20		3980			$13.75\text{-}10.15\times10^{-3}$	67.783	140 - 160°F
26	41.36	3930	9.18×10^4	7.44	$10.62\text{-}76.8\times10^{-3}$	25,581-14.3	180 - 200°F

NT = No Test

(7) $t_f = 3.7\mu$ sec and $t_t = 24\mu$ sec.

TABLE A-5

SECOND SERIES UNIDIRECTIONAL LAMINATE EXPOSURE RESULTS

Specimen	Filament Volume Content, %	Current Crest: Actual Current Applied, Amps	Current Crest: Current Applied Per unit Cross Sectional Area of Filament, Amps/cm^2	Current Crest: Current Applied Per Cross Sectional Area of Specimen, Amps/cm^2	Current Applied Per Filament, Amps	Resistivity, Ohm-cm Before-After Exposure	Tensile* Strength, PSI	Approx. Peak Temperature During Exposure
Boron Unidirectional Laminate (Control Specimens)								
55	50	0	0	0	0	Not exposed	81,422	NT
56							139,670	
							110,546 AVG	
Boron Unidirectional Laminate (1)								
3		2400	5.56×10^4	2.77×10^4	4.51	$14.96\text{-}11.90 \times 10^{-3}$		$140 < T < 150^\circ F$
29		2600	6.39×10^4	3.19×10^4	5.18	$8.06\text{-}6.88 \times 10^{-3}$		$130 < T < 140^\circ F$
8	50	2300	5.53×10^4	2.76×10^4	4.48	$12.48\text{-}8.09 \times 10^{-3}$	113,798	$T < 180^\circ F$
6		2500	5.92×10^4	2.96×10^4	4.80	$8.72\text{-}6\ 89 \times 10^{-3}$	110,047	$130 < T < 140^\circ F$
68		2600	6.29×10^4	3.14×10^4	5.10	$10.73\text{-}14.41 \times 10^{-3}$	67,461	$160 < T < 190^\circ F$
58		2600	6.40×10^4	3.19×10^4	5.19	$8.05\text{-}6.87 \times 10^{-3}$	65,855	$130 < T < 140^\circ F$
							89,290 AVG	
Boron Unidirectional Laminate (1)								
19		3160	7.50×10^4	3.75×10^4	6.08	$8.95\text{-}1100 \times 10^{-3}$		$170 < T < 180^\circ F$
14		3250	7.68×10^4	3.84×10^4	6.23	$15.87\text{-}9.95 \times 10^{-3}$		$T < 130^\circ F$
21	50	3400	8.02×10^4	4.01×10^4	6.50	$7.86\text{-}6.41 \times 10^{-3}$	69,445	$150 < T < 160^\circ F$
18		3290	7.74×10^4	3.87×10^4	6.28	$15.72\text{-}18.65 \times 10^{-3}$	70,424	$160 < T < 170^\circ F$
15		3250	7.70×10^4	3.85×10^4	6.24	$11.45\text{-}48.87 \times 10^{-3}$	35,154	$180 < T < 200^\circ F$
11		3250	7.66×10^4	3.83×10^4	6.21	$12.59\text{-}16.65 \times 10^{-3}$	46,599	$160 < T < 170^\circ F$
							55,406 AVG	

*Based on original cross-sectional area

TABLE A-6 (Continued)

SECOND SERIES UNIDIRECTIONAL LAMINATE EXPOSURE RESULTS

Specimen	Filament Volume Content %	Current Crest: Actual Current Applied Amps	Current Crest: Current Applied Per unit Cross Sectional Area of Filament Amps/cm^2	Current Crest: Current Applied Per Cross Sectional Area of Specimen Amps/cm^2	Current Applied Per Filament	Resistivity Ohm-cm Before-After Exposure	Tensile Strength PSI Modulus PSI x 10^{-6}	Approx. Peak Temperature During Exposure
Boron Unidirectional Laminate (1)								
40		4550	10.76×10^4	5.38×10^4	8.73	$8.66\text{-}7.52 \times 10^{-3}$		T< 130°F
22		4600	10.92×10^4	5.46×10^4	8.86	$14.24\text{-}8.48 \times 10^{-3}$		130<T< 140°F
44	50	4550	10.74×10^4	5.37×10^4	8.71	$10.37\text{-}13.98 \times 10^{-3}$	35,599	140<T< 150°F
38		4550	10.74×10^4	5.37×10^4	8.71	$10.18\text{-}13.03 \times 10^{-3}$	45,690	150<T< 160°F
33		4550	10.88×10^4	5.44×10^4	8.82	$9.96\text{-}7.79 \times 10^{-3}$	78,635	130<T< 140°F
30		4550	10.70×10^4	5.35×10^4	8.68	$9.90\text{-}16.44 \times 10^{-3}$	49,387	160<T< 170°F
							53,328 AVG	
60		5200	12.26×10^4	6.13×10^4	9.94	$9.49\text{-}13.00 \times 10^{-3}$		140<T< 150°F
46		5200	12.30×10^4	6.15×10^4	9.98	$8.68\text{-}7.17 \times 10^{-3}$		" "
61	50	5260	12.44×10^4	6.22×10^4	10.09	$12.29\text{-}11.44 \times 10^{-3}$	46,562	" "
48		5200	12.30×10^4	6.15×10^4	9.98	$10.11\text{-}8.44 \times 10^{-3}$	56,639	130<T< 140°F
52		5200	12.32×10^4	6.16×10^4	9.99	$10.76\text{-}8.66 \times 10^{-3}$	56,552	" "
50		5200	12.32×10^4	6.16×10^4	9.99	$7.73\text{-}36.39 \times 10^{-3}$	13,909	160<T< 170°F
							43,416 AVG	
65		10,800	25.70×10^4	12.85×10^4	20.84	$13.30\text{-}52.43 \times 10^{-3}$		130<T< 140°F
64		10,800	25.64×10^4	12.82×10^4	20.79	$22.75\text{-}29.96 \times 10^{-3}$	29,100	---
67	50	10,800	25.64×10^4	12.82×10^4	20.79	$11.66\text{-}20.41 \times 10^{-3}$	25,285	160<T< 170°F
5		10,800	24.46×10^4	12.23×10^4	19.87	$104.56\text{-}52.75 \times 10^{-3}$	38,714	140<T< 150°F
66		10,800	24.70×10^4	12.85×10^4	20.03	$21.43\text{-}21.83 \times 10^{-3}$	45,304	150<T< 160°F
							34,600 AVG	
72	50	21,800	49.28×10^4	24.64×10^4	39.97	$9.99\text{-}81.94 \times 10^{-3}$	10,318	

TABLE A-6 (Continued)

SECOND SERIES UNIDIRECTIONAL LAMINATE EXPOSURE RESULTS

Specimen	Filament Volume Content, %	Current Crest			Current Applied Per Filament, Amps	Resistivity, Ohm-cm Before-After Exposure	Tensile* Strength, PSI	Approx. Peak Temperature During Exposure
		Actual Current Applied, Amps	Current Applied Per unit Cross Sectional Area of Filament, Amps/cm^2	Current Applied Per Cross Sectional Area of Specimen, Amps/cm^2				
Graphite Unidirectional Laminate Tow (Control Specimen)								
74							62,223	
75	55	0	0	0	0	Not exposed	71,594	NT
76							90,338	
							74,718 AVG	
Graphite Unidirectional Laminate Tow (7)								
2		5540	12.95×10^4	7.12×10^4	656	$2.44\text{-}2.42 \times 10^{-3}$		200 <T< 220
66		5540	13.55×10^4	7.45×10^4	686	$2.34\text{-}2.32 \times 10^{-3}$		220 <T< 240
4	55	5540	12.96×10^4	7.13×10^4	656	$2.44\text{-}2.47 \times 10^{-3}$	79,381	200 <T< 220
3		5540	12.95×10^4	7.12×10^4	656	$2.33\text{-}2.32 \times 10^{-3}$	86,744	" "
69		5540	13.49×10^4	7.42×10^4	683	$2.45\text{-}2.43 \times 10^{-3}$	83,003	" "
62		5540	13.55×10^4	7.45×10^4	686	$2.26\text{-}2.23 \times 10^{-3}$	88,546	" "
							84,419 AVG	

* Based on original cross-sectional area

TABLE A-6 (Continued)

SECOND SERIES UNIDIRECTIONAL LAMINATE EXPOSURE RESULTS

Specimen	Filament Volume Content %	Current Crest: Actual Current Applied, Amps	Current Crest: Current Applied Per Unit Cross Sectional Area of Filament, Amps/cm^2	Current Crest: Current Applied Per Cross Sectional Area of Specimen, Amps/cm^2	Current Applied Per Filament, Amps	Resistivity, Ohm-cm Before-After Exposure	Tensile Strength PSI	Approx. Peak Temp. During Exposure
Graphite Unidirect. Laminate Tow (Control Specimen)								
72	55	0	0	0	0	Not exposed	80,667	NT
73							76,638	
							78,652AVG	
Graphite Unidirect. Laminate Tow (7)								
46		8,250	20.11×10^4	11.06×10^4	1019	$2.63\text{-}2.64 \times 10^{-3}$		350<T<400°F
49		8,250	20.19×10^4	11.10×10^4	1023	$2.87\text{-}2.85 \times 10^{-3}$		350<T<400°F
55	55	8,250	20.19×10^4	11.10×10^4	1023	$2.81\text{-}2.81 \times 10^{-3}$	86,810	400<T<490°F
24		8,250	20.13×10^4	11.07×10^4	1020	$2.72\text{-}2.77 \times 10^{-3}$	89,181	350<T<400°F
27		8,250	20.13×10^4	11.07×10^4	1020	$2.84\text{-}3.37 \times 10^{-3}$	72,725	350<T<400°F
18		8,250	20.11×10^4	11.06×10^4	1019	$2.83\text{-}2.98 \times 10^{-3}$	83,874	350<T<400°F
							83,148AVG	
Graphite Unidirect. Laminate Tow (7)								
19		9,000	21.00×10^4	11.55×10^4	1064	$2.70\text{-}2.85 \times 10^{-3}$		300<T<350°F
23		9,000	21.00×10^4	11.55×10^4	1064	$2.61 + \times 10^{-3}$		400<T<490°F
9		9,000	21.03×10^4	11.55×10^4	1065	$2.59\text{-}2.56 \times 10^{-3}$	106,198	300<T<350°F
10	55	8,850	20.73×10^4	11.39×10^4	1050	$2.62\text{-}2.62 \times 10^{-3}$	80,000	300<T<350°F
13		9,000	21.08×10^4	11.60×10^4	1068	$2.69\text{-}2.74 \times 10^{-3}$	83,000	300<T<350°F
22		9,000	21.03×10^4	11.56×10^4	1065	$2.62\text{-}2.97 \times 10^{-3}$	92,083	300<T<350°F
							90,507	

+ = No reading made after test

TABLE A-6 (Continued)

SECOND SERIES UNIDIRECTIONAL LAMINATE EXPOSURE RESULTS

Specimen	Filament Volume Content, %	Current Crest: Actual Current Applied, Amps	Current Crest: Current Applied Per unit Cross Sectional Area of Filament, Amps/cm^2	Current Crest: Current Applied Per Cross Sectional Area of Specimen, Amps/cm^2	Current Applied Per Filaments, Amps	Resistivity, Ohm-cm Before-After Exposure	Tensile* Strength, PSI	Approx. Peak Temperature During Exposure
Graphite Unidirectional Laminate Tow (4)								
11		10,200	24.89×10^4	13.69×10^4	1260	$2.28\text{-}2.52 \times 10^{-3}$	**	Flames-30 sec
59		10,200	26.07×10^4	14.34×10^4	1320	$2.20\text{-}2.30 \times 10^{-3}$	**	" "
17	55	10,200	24.85×10^4	13.67×10^4	1259	$2.23\text{-}2.44 \times 10^{-3}$	36,394**	" "
7		10,200	25.51×10^4	14.03×10^4	1282	$2.24\text{-}2.26 \times 10^{-3}$	51,733**	" "
60		10,800	27.49×10^4	15.12×10^4	1392	$2.27\text{-}2.39 \times 10^{-3}$	42,366**	" "
45		10,800	27.49×10^4	15.12×10^4	1392	$2.20\text{-}2.32 \times 10^{-3}$	40,014**	" "
							42,627 AVG	
Graphite Unidirectional Laminate Tow (4)								
30		20,500	52.20×10^4	28.71×10^4	2544	$2.23\text{-}2.65 \times 10^{-3}$	***	1 FT High
21		21,800	55.51×10^4	30.53×10^4	2816	$1.98\text{-}36.82 \times 10^{-3}$	***	Flames-15 sec
41	55	21,800	56.05×10^4	30.83×10^4	2839	$2.26\text{-}2.98 \times 10^{-3}$	5,474***	" "
29		20,500	52.35×10^4	28.79×10^4	2652	$2.38\text{-}1.36 \times 10^{-3}$	2,265***	" "
12		21,800	55.65×10^4	30.61×10^4	2819	$2.12\text{-}2.52 \times 10^{-3}$	11,233***	" "
34		21,800	55.65×10^4	30.61×10^4	2819	$2.11\text{-}12.25 \times 10^{-3}$	1,631***	" "
							5,151 AVG	
Graphite Unidirectional Laminate Yarn (Control Specimen)								
47							87,492	
48	55	0	0	0	0	Not exposed	88,665	NT
49							64,689	
							80,282 AVG	

*Based on original cross-sectional area
**Burned and charred on surface
***Charred with loose fiber

TABLE A-6 (Continued)

SECOND SERIES UNIDIRECTIONAL LAMINATE EXPOSURE RESULTS

Specimen	Filament Volume Content, %	Actual Current Applied, Amps	Current Crest: Current Applied Per unit Cross Sectional Area of Filament, Amps/cm^2	Current Crest: Current Applied Per Cross Sectional Area of Specimen, Amps/cm^2	Current Applied Per Filament, Amps	Resistivity, Ohm-cm Before-After Exposure	Tensile* Strength, PSI	Approx. Peak Temperature During Exposure
Graphite Unidirectional Laminate Yarn (7)								For all six specimens:
21		5540	13.04×10^4	7.17×10^4	69.66	$2.82\text{-}2.79 \times 10^{-3}$		220< T <240°C
7		5540	13.04×10^4	7.17×10^4	69.66	$2.94\text{-}2.91 \times 10^{-3}$		
34	55	5540	13.04×10^4	7.17×10^4	69.66	$2.91\text{-}2.87 \times 10^{-3}$	96,088	
27		5540	13.05×10^4	7.18×10^4	69.71	$2.80\text{-}2.78 \times 10^{-3}$	102,905	
16		5540	13.04×10^4	7.17×10^4	69.66	$2.98\text{-}3.04 \times 10^{-3}$	89,819	
10		5540	13.00×10^4	7.15×10^4	69.45	$2.95\text{-}2.97 \times 10^{-3}$	52,080	
							65,223 AVG	
Graphite Unidirectional Laminate Yarn (7)								For all six specimens:
25		8250	20.36×10^4	11.20×10^4	108.8	$2.96\text{-}2.76 \times 10^{-3}$	**	Flames
39		8250	20.29×10^4	11.16×10^4	108.4	$2.88\text{-}2.81 \times 10^{-3}$	**	
1	55	8250	19.29×10^4	10.61×10^4	103.0	$2.75\text{-}2.76 \times 10^{-3}$	45,495 **	
46		8250	20.20×10^4	11.11×10^4	107.9	$2.74\text{-}2.76 \times 10^{-3}$	52,156 **	
26		8250	20.29×10^4	11.16×10^4	108.4	$2.71\text{-}2.68 \times 10^{-3}$	54,993 **	
44		8250	20.09×10^4	11.05×10^4	107.3	$2.76\text{-}2.76 \times 10^{-3}$	46,689 **	
							49,833 AVG	
Graphite Unidirectional Laminate Yarn (4)								For all six specimens:
63	55	10,200	24.24×10^4	13.33×10^4	129.5	$2.43\text{-}3.25 \times 10^{-3}$	**	Flames ~30sec
55		10,200	25.05×10^4	13.78×10^4	133.8	$2.35\text{-}2.38 \times 10^{-3}$	**	
64		10,200	23.89×10^4	13.14×10^4	127.6	$2.60\text{-}2.86 \times 10^{-3}$	22,770 **	
61		10,200	23.95×10^4	13.17×10^4	127.9	$2.41\text{-}2.43 \times 10^{-3}$	42,493 **	
59		10,200	24.98×10^4	13.74×10^4	133.4	$2.41\text{-}2.75 \times 10^{-3}$	23,288 **	
52		10,200	24.98×10^4	13.74×10^4	133.4	$2.52\text{-}\infty \times 10^{-3}$	6,085 **	
							23,659 AVG	

*Based on original cross-sectional area

**Charred with loose fiber

TABLE A-6 (Continued)

SECOND SERIES UNIDIRECTIONAL LAMINATE EXPOSURE RESULTS

Specimen	Filament Volume Content, %	Current Crest: Actual Current Applied, Amps	Current Crest: Current Applied Per Unit Cross Sectional Area of Filament, Amps/cm^2	Current Crest: Current Applied Per Cross Sectional Area of Specimen, Amps/cm^2	Current Applied Per Filament, Amps	Resistivity, Ohm-cm Before-After Exposure	Tensile* Strength PSI	Approx. Peak Temp. During Exposure
Graphite Unidirect. Laminate Yarn (4)								For all 6 specimens: Flames - 15 sec
57		21,800	55.82×10^4	30.70×10^4	298.2	$2.66\text{-}2.86 \times 10^{-3}$	**	
54		21,800	58.55×10^4	32.20×10^4	312.8	$2.34\text{-}3.54 \times 10^{-3}$	**	
65	55	21,800	55.75×10^4	30.66×10^4	297.8	$2.60\text{-}2.69 \times 10^{-3}$	23,136**	
56		21,800	55.82×10^4	30.70×10^4	298.2	$2.44\text{-}4.96 \times 10^{-3}$	6,723**	
51		21,800	$55,82 \times 10^4$	30.70×10^4	298.2	$2.67\text{-}2.97 \times 10^{-3}$	8,721**	
60		21,800	$55,98 \times 10^4$	30.79×10^4	299.0	$2.38\text{-}8.76 \times 10^{-3}$	8,195**	
							11,693AVG	
Graphite Unidirect. Laminate Yarn (Control Specimen)								
53							72,640	
58	55	0	0	0	0	not exposed	83,200	N.T.
62							90,076	
							81,972	
Graphite Unidirect. Laminate								
Yarn 17		6,900	15.98×10^4	8.79×10^4	85	$3.28\text{-}3.44 \times 10^{-3}$		$260 < T < 300^{\circ}F$
35		6,900	16.33×10^4	8.98×10^4	87	$3.19\text{-}3.30 \times 10^{-3}$		"
18		7,350	16.48×10^4	9.06×10^4	88	$3.32\text{-}3.31 \times 10^{-3}$	82,142	"
38	55	6,900	16.25×10^4	8.94×10^4	87	$3.14\text{-}3.17 \times 10^{-3}$	92,063	"
40		6,900	16.31×10^4	8.97×10^4	87	$3.12\text{-}3.18 \times 10^{-3}$	88,235	"
41		6,900	16.16×10^4	8.89×10^4	86	$3.20\text{-}3.21 \times 10^{-3}$	65,000	"
							81,865	

*Based on original cross-sectional area

**Charred with loose fibers

TABLE A-6 (Continued)

SECOND SERIES UNIDIRECTIONAL LAMINATE EXPOSURE RESULTS

Specimen	Filament Volume Content, %	Current Crest: Actual Current Applied, Amps	Current Crest: Current Applied Per Unit Cross Sectional Area of Filament, $Amps/cm^2$	Current Crest: Current Applied Per Cross Sectional Area of Specimen $Amps/cm^2$	Current Applied Per Filament, Amps	Resistivity, Ohm-cm Before-After Exposure	Tensile* Strength PSI	Approx. Peak Temp. During Exposure
Hybrid-1 (Control Specimen) 1-8	49	0	0	0	0	Not exposed	143,181	NT
Hybrid-1 (1) 1-16	49	6850	9.84×10^4	4.82×10^4		$3.388\text{-}31.48 \times 10^{-3}$	137,272	$140<T<150^{\circ}F$
1-17		6850	9.84×10^4	4.82×10^4		$3.951\text{-}7.61 \times 10^{-3}$	113,636	$150<T<160^{\circ}F$
							125,454AVG	
Hybrid-2 (Control Specimen) 19	60	0	0	0	0	Not exposed	176,000	NT
Hybrid-2 (1) 16	60	6850	10.40×10^4	6.24×10^4		$4.90\text{-}4.94 \times 10^{-3}$	140,000	$180<T<190^{\circ}F$
17		5260	7.97×10^4	4.78×10^4		$3.99\text{-}3.75 \times 10^{-3}$	179,411	$140<T<150^{\circ}F$
							159,706AVG	
Boron Unidirectional Laminate Aluminum Foil Tabs Init. Injection(7)								
1	50	4370	10.22×10^4	5.11×10^4	8.29	$1\text{-}0.78 \times 10^{-3}$		$<180^{\circ}F$
2	50	3220	7.54×10^4	3.77×10^4	6.11	$2\text{-}1.45 \times 10^{-3}$		$180<T<200^{\circ}F$
3	50	2500	5.84×10^4	2.92×10^4	2.37	$0.55\text{-}0.425 \times 10^{-3}$		$<180^{\circ}F$

(1) $t_f = 4.3\mu$ sec and $t_t = 22\mu$ sec

(4) $t_f = 3.12\mu$ sec and $t_t = 22\mu$ sec

(7) $t_f = 3.7\mu$ sec and $t_t = 24\mu$ sec

*Based on original cross-sectional area.

TABLE A-7

THIRD SERIES UNIDIRECTIONAL LAMINATE EXPOSURE RESULTS

Specimen	Filament Volume Content %	Current Crest: Actual Current Applied, Amps	Current Crest: Current Applied Per Unit Cross Sectional Area of Filament, Amps/cm^2	Current Crest: Current Applied Per Cross Sectional Area of Specimen, Amps/cm^2	Current Applied Per Filament	Resistivity, ohm-cm Before-After Exposure	Tensile Strength, psi	Approximate Peak Temperature During Exposure
Boron Unidirectional Lam. Tungsten Cloth Outside (Cont. Spec.)								
BUTC-1	50						164,100	
BUTC-12	50	0	0	0	0	not exposed	134,000	NT
BUTC-11	50						134,100	
							144,000AVG	
Boron Unidirectional Lam. Tungsten Cloth Outside (1)								
BUTC-4	50	3700	7.86×10^4	3.93×10^4	6.37	$0.55\text{-}0.62 \times 10^{-3}$	165,800	T<130°F
BUTC-7	50	3700	7.90×10^4	3.95×10^4	6.41	$0.50\text{-}0.77 \times 10^{-3}$	158,900	
BUTC-6	50	3700	7.88×10^4	3.94×10^4	6.39	$0.73\text{-}0.67 \times 10^{-3}$	157,600	
BUTC-9	50	3700	7.88×10^4	3.94×10^4	6.39	$2.31\text{-}1.24 \times 10^{-3}$	156,500	
BUTC-10	50	3700	7.86×10^4	3.93×10^4	6.37	$0.56\text{-}0.53 \times 10^{-3}$	147,300	
BUTC-2	50	3700	7.64×10^4	3.82×10^4	6.20	$0.75\text{-}0.50 \times 10^{-3}$	145,700	
							155,300AV	
Boron Unidirectional Laminate Tungsten Cloth Outside (11)								Smoke: 130<T<140
BUTC-16		6100	13.04×10^4	6.52×10^4	10.58	$0.60\text{-}0.91 \times 10^{-3}$		
BUTC-17		6100	13.52×10^4	6.76×10^4	10.86	$0.54\text{-}0.60 \times 10^{-3}$		
BUTC-5		6100	13.52×10^4	6.76×10^4	10.96	$0.57\text{-}0.53 \times 10^{-3}$	145,700	
BUTC-3		6100	13.96×10^4	6.98×10^4	11.32	$0.52\text{-}0.54 \times 10^{-3}$	129,500	
BUTC-8	50	6100	13.48×10^4	6.74×10^4	10.93	$0.59\text{-}0.69 \times 10^{-3}$	99,000	
BUTC-14		6100	13.04×10^4	6.52×10^4	10.58	$0.71\text{-}0.54 \times 10^{-3}$	97,200	
							117,800AV	

TABLE A-7 (Continued)

THIRD SERIES UNIDIRECTIONAL LAMINATE EXPOSURE RESULTS

Specimen	Filament Volume Content %	Current Crest: Actual Current Applied Amps	Current Crest: Current Applied Per Unit Cross Sectional Area of Filament Amps/cm^2	Current Crest: Current Applied per Cross Sectional Area of Specimen Amps/cm^2	Current Applied Per Filament	Resistivity, ohm-cm Before-After Exposure	Tensile Strength PSI	Approx. Peak Temperature During Exposure
Boron Unidirectional Laminate-Tungsten Cloth (Middle) Control								
BUTCM-12	50						150,200	
BUTCM-13	50	0	0	0	0	not exposed	162,200	NT
BUTCM-14	50						155,200	
							155,860AV	
Boron Unidirectional Lam. Tungsten Cloth (middle)								
(11) BUTCM-5	50	3700	8.52×10^4	4.26×10^4	6.91	$0.99 - 0.92 \times 10^{-3}$	124,100	T<130°F
BUTCM-7	50	3700	8.50×10^4	4.25×10^4	6.89	$0.88 - 0.84 \times 10^{-3}$	155,500	
BUTCM-9	50	3700	8.52×10^4	4.26×10^4	6.91	$0.89 - 0.82 \times 10^{-3}$	137,300	
BUTCM-8	50	3700	8.88×10^4	4.44×10^4	7.20	$0.90 - 0.86 \times 10^{-3}$	156,700	
BUTCM-17	50	3700	8.86×10^4	4.43×10^4	7.18	$0.91 - 0.89 \times 10^{-3}$		
BUTCM-18	50	3700	8.52×10^4	4.26×10^4	6.91	$0.93 - 0.88 \times 10^{-3}$		
							143,400AV	
Boron Unidirectional Lam. Tungsten Cloth (Middle)								
(11) BUTCM-11	50	6100	13.48×10^4	6.74×10^4	10.93	$0.98 - 9.48 \times 10^{-3}$		Split
BUTCM-10	50	6100	13.08×10^4	6.54×10^4	10.61	$0.56 - 9.18 \times 10^{-3}$		140<T<160°F
BUTCM-3	50	6100	13.64×10^4	6.82×10^4	11.06	$0.93 - 11.15 \times 10^{-3}$		Split*
BUTCM-6	50	6100	13.04×10^4	6.52×10^4	10.58	$0.96 - 15.37 \times 10^{-3}$		Split
BUTCM-4	50	6100	13.56×10^4	6.78×10^4	11.00	$1.40 - 3.03 \times 10^{-3}$		Split*
BUTCM-1	50	6100	13.08×10^4	6.54×10^4	10.61	$0.58 - 9.01 \times 10^{-3}$	77,400	Split*
							88,100	160<T<180°F
							82,700AV	

(11) t_f = 3.7μsec and t_t = 22μsec

* No temp. recorded--thermopapers were

APPENDIX B

RESIDUAL AND INDUCED STRESS PRESET IN BORON FILAMENTS

Boron monofilaments are produced commercially by chemical vapor deposition (CVD) process in which boron forms on a hot (~2000°F) tungsten wire by hydrogen reduction of boron trichloride vapor.[7]*

F. E. Wawner, Jr., on pages 254-256 of Reference 7 states that during the deposition of the boron onto the tungsten substrate the core increases in diameter from its original diameter of 0.0005 in. to 0.00065 in. placing the deposited boron layer in tension. We can calculate an equivalent internal pressure to replace the core that will produce the same expansion of the internal diameter. Using the material properties of Reference 7 and Equation (27) of Reference 8 (uniform internal radial pressure p lb. per sq. in. with longitudinal pressure zero or externally balanced)

$$\Delta R_1 = p \frac{\bar{R}_1}{E_B} \left(\frac{R_2^2 + R_1^2}{R_2^2 - R_1^2} + \nu \right) \qquad (1)$$

where p = internal pressure (psi)

E_B = modulus of elasticity for boron (psi)

R_1 = inner radius (in.)

R_2 = outer radius (in.)

ν_B = Poisson's ratio

*Superscripted numbers in parentheserefer to referenced material listed on page 79.

which for $\Delta R_1 = 0.00015/2 = 0.000075 = 7.5 \times 10^{-5}$ in. becomes

$$p = \frac{7.5 \times 10^{-5}}{\frac{2.5 \times 10^{-4}}{60.0 \times 10^{6}} \left(\frac{4.0 \times 10^{-6} + 6.25 \times 10^{-8}}{4.0 \times 10^{-6} - 6.25 \times 10^{-8}} + .2 \right)} = 1.46 \times 10^{7} \text{ psi}$$

By using Equation 29 of Reference 8 (uniform internal pressure p lb. per sq. in. in all directions) which is probably the most reasonable approximation, we obtain:

$$\Delta P_1 = p \frac{a}{E_B} \left[\frac{R_2^2 + R_1^2}{R_2^2 - R_1^2} - \nu \left(\frac{R_1^2}{R_2^2 - R_1^2} - 1 \right) \right] \qquad (2)$$

or

$$p = \frac{7.5 \times 10^{-5}}{\frac{2.5 \times 10^{-4}}{60.0 \times 10^{6}} \left[\frac{4.0 \times 10^{-6} + 6.25 \times 10^{-8}}{4.0 \times 10^{-6} - 6.25 \times 10^{-8}} - .2 \left(\frac{6.25 \times 10^{-8}}{4.0 \times 10^{-6} - 6.25 \times 10^{-4}} - 1 \right) \right]}$$

and $p = 2.16 \times 10^{-7}$ psi.

An internal pressure of this magnitude would result in a circumferential or tangential stress, σ_t, at the inner surface of the boron core of

$$\sigma_t = p \left[\frac{R_2^2 + R_1^2}{R_2^2 - R_1^2} \right] = 2.16 \times 10^{7} \ (1.0317) = 2.23 \times 10^{7} \text{ psi}$$

Now the boron case is obviously incapable of supporting tensile stresses of this magnitude and therefore core growth must take place at the expense of sheath material. This conclusion is supported by statements on page 254 of Reference 7 which states, "Small voids have been observed along the interface and are tentatively attributed to rapid diffusion of boron into tungsten and subsequent vacancy condensation along the interface between the two materials (Kirkendall effect)."

For the moment assume that the boron sheath deposition and the core transformation from tungsten to tungsten-boride with its accompanying core growth can all be accomplished without the creation of residual stresses existing at the deposition temperature of 2000°F. Residual stresses existing at room temperature will then be the result of cooling the composite filament from the stress free deposition temperature to room temperature.

Using a core diameter of 0.0005 in. (using the larger value of 0.00065 in. changes the final result by only 1000 psi), a filament diameter of 0.004 in., a coefficient of thermal expansion for the boron sheath of 5.0×10^{-6} in./in./°F for the core we can calculate the resultant longitudinal thermal stress. Upon cooling 2000°F the boron sheath by itself would shrink an amount

$$\epsilon_B = \alpha_B \Delta T = (5.0 \times 10^{-6})\ (2000^{\circ}F) = 0.010 \text{ in./in.}$$

while the core would shrink only

$$\epsilon_w = \alpha_w \Delta T = (4.1 \times 10^{-6})(2000^{\circ}F) = 0.0082 \text{ in./in.}$$

a difference of 0.0018 in./in. But since the core and the sheath are intimately bonded together

$$\epsilon_B \text{ must } = \epsilon_w$$

and so the boron sheath must be stretched some amount by the core (resulting in a residual tensile stress in the sheath) and the core must be compressed by the outer boron sheath. From static considerations the total force acting on a unit length of the sheath must be balanced by an equal force acting over the area of the core, or

$$P_B = P_w, \text{ or } \sigma_B A_B = \sigma_w A_w \qquad (3)$$

where σ_B is the stress level in the boron sheath and σ_w is the stress level in the core. A_B and A_w are the respective cross sectional areas where

$$A_B = \frac{\pi}{4} (D_B)^2 = 1256.6 \times 10^{-8} \text{ in.}^2, \text{ and}$$

$$A_w = \frac{\pi}{4} (D_w)^2 = 19.6 \times 10^{-8} \text{ in.}^2$$

Now assuming that the coefficients of thermal expansion and the modulus of elasticity of both the boron sheath and the tungsten core are constant throughout the 2000°F temperature range, then (3) becomes

$$E_B \epsilon_B A_B = E_w \epsilon_w A_w$$

or solving for

$$\epsilon_B, \ \epsilon_B = \frac{E_w}{E_B} \times \frac{A_w}{A_B} \times \epsilon_w \qquad (4)$$

And also since the total amount of strain from a zero stress room temperature condition must be 0.0018 in/in. because the sheath and core are in intimate contact, we can also write,

$$\epsilon_B + \epsilon_w = .0018 \text{ in/in} \qquad (5)$$

Substituting (4) into (5) yields,

$$\frac{E_w A_w}{E_B A_B} \epsilon_w + \epsilon_w = .0018$$

or $\epsilon_w = .001772$ in/in.

and the average compressive stress in the tungsten core is

$$\sigma_w = E_w \epsilon_w = 60.0 \times 10^6 (0.001722) = 106{,}310 \text{ psi}$$

and the average tensile stress in the boron sheath is

$$\sigma_B = E_B \epsilon_B = 60.0 \times 10^6 (0.0018 - 0.001772) = 1686 \text{ psi.}$$

This value for the compressive stress in the core is somewhat lower than the experimentally measured value of 150 to 200 x 10^3 psi and the theoretical value of 211 x 10^3 psi cited on page 254 of Reference 7. However, this

analysis assumes linear material properties over a large temperature range, uses for the coefficient of thermal expansion of the boron sheath the coefficient measured in the Aeronutronic Research Laboratories for a single filament and uses a coefficient of thermal expansion of tungsten-boride for the core. Any, or all, of these assumptions or measurements are subject to some adjustment. In any event, the resultant longitudinal tensile stress in the boron sheath is quite small (1686 psi) while the resultant longitudinal compressive stress in the core (100 to 200 x 10^3 psi) is large. These stresses are oriented along the axis of the filament and are not directly additive to the stresses calculated and reported.
We can now, however, consider the temperature-induced radial stresses.

Again, assuming that the deposition process results in a stress free composite filament formed at 2000°F, residual stresses are developed as the boron sheath shrinks around the slower shrinking core. These stresses can be calculated in a manner similar to that of the Philco-Ford paper in Reference 2. Except here there is a thermal contraction in both the sheath and the core, rather than a thermal expansion of the core alone as assumed by Philco-Ford in Reference 2.

Proceeding as in the longitudinal analysis, the free thermal contraction of the sheath inner radius alone would be:

$$\delta R_B = R_I \alpha_B \Delta T = (.00025)(5.0 \times 10^{-6})(2000) = 2.5 \times 10^{-6} \text{ in.}$$

while that of core alone would be:

$$\delta R_w = R_I \alpha_w \Delta T = (.00025)\ (4.1 \times 10^{-6})\ (2000) = 2.05 \times 10^{-6} \text{ in.}$$

a difference in radial deflection of $.45 \times 10^{-6}$ in. But since the core and the sheath must each shrink the same amount

δR_B must = δR_w (shrinkage from deposition temperature)

or

$$\delta R_B + \delta R_w = .45 \times 10^{-6} \text{ in.} \qquad (6)$$

(deflection from free thermal contraction of zero stress condition.)

and so the boron sheath must be expanded some amount from the free or zero stress condition, resulting in a tensile radial stress and the sheath acting on the core will compress the core. Again from a consideration of a static force balance, the pressure at the interface between the sheath and the core must act equally on the sheath and core. For the core:

$$\delta R_w = p \frac{R_1}{E_w} (1 - \nu_w)$$

or the internal pressure, p, equals

$$\frac{\delta R_w}{\frac{R_1}{E_w} (1 - \nu_w)}$$

and for the sheath

$$\delta R_B = p \frac{R_1}{E_B} \left(\frac{R_2^2 + R_1^2}{R_2^2 - R_1^2} + \nu_B\right)$$

or

$$p = \frac{\delta R_B}{\frac{R_1}{E_B} \left(\frac{R_2^2 + R_1^2}{R_2^2 - R_1^2} + \nu_B \right)}$$

Equating the two pressures gives

$$\frac{\delta R_w}{\frac{R_1}{E_w} (1 - \nu_w)} = \frac{\delta R_B}{\frac{R_1}{E_B} \left(\frac{R_2^2 + R_1^2}{R_2^2 - R_1^2} + \nu_B \right)} \qquad (7)$$

Substituting equation (6) into (7) gives

$$\frac{.45 \times 10^{-6} - \delta R_B}{\frac{R_1}{E_w} (1 - \nu_w)} = \frac{\delta R_B}{\frac{R_1}{E_B} \left(\frac{R_2^2 + R_1^2}{R_2^2 - R_1^2} + \nu_B \right)}$$

and using $\nu_w = .3$ along with the previous constants we get

$$\delta R_B = 2.869 \times 10^{-7} \text{ in.},$$

or the inner radius of the boron sheath is forced by the slower shrinking core to be this amount larger than the stress free condition, resulting in a residual radial stress at the inner surface of the sheath, equivalent to an internal pressure of:

$$p = \frac{2.869 \times 10^{-7}}{\frac{R_1}{E_B}\left(\frac{R_2^2 + R_1^2}{R_2^2 - R_1^2} + \nu_B\right)} = 5.59 \times 10^4 \text{ psi}$$

This internal pressure gives rise to tangential and radial stresses in the boron sheath. The maximum values of σ_r and σ_t occur at the inner surface and are expressed by

$$\sigma_r = P, \quad \sigma_t = P \frac{R_2^2 + R_1^2}{R_2^2 - R_1^2} = 1.0317\ P$$

or

$$\sigma_r = 55{,}900 \text{ psi}, \quad \sigma_t = 57{,}670 \text{ psi}$$

These stresses are in the planeof the filament and are directly additive to the stresses produced by an electrical current passing through the core.

The tensile radial stress σ_r is a maximum at the inner surface of the sheath and decreases to zero at the outer surface, while the tangential stress σ_t is a tensile maximum at the inner surface and decreases, but not to zero, with increasing radius. A plot of the radial and tangential stresses is shown in Figure A-1. Within the core the radial stress is equal to the tangential stress and this stress is a constant compressive stress equal to P or 55,900 psi.

F. E. Wawner, on page 256 of Reference 7 attibutes the often observed radial cracks in the boron sheath to the stresses calculated from the radius of curvature assumed by split and longitudinally polished filaments. These

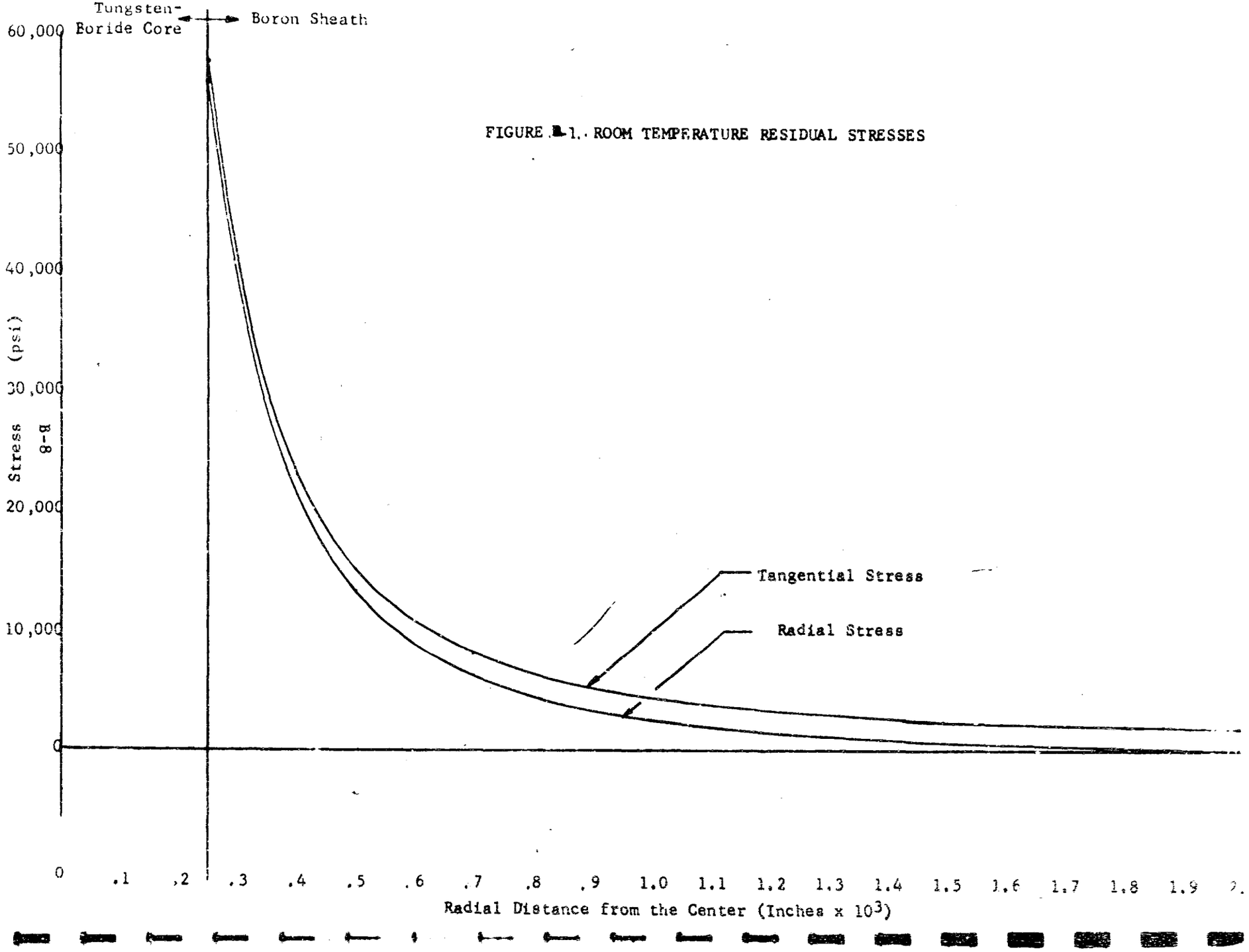

FIGURE B-1. ROOM TEMPERATURE RESIDUAL STRESSES

stresses, however, are the axial or longitudinal stresses and act in the plane of the radial cracks and are not the cause of radial cracking. Radial cracks are the result of the tangential (or hoop) stresses calculated above, and this stress does not go from tension to compression with increasing radial position as does the axial stress, and therefore, the only reason cracks might be observed to terminate at some radial distance is because the tangential stress level drops below the level required to propagate the crack.

The actual amplitude of the stresses calculated in this study are subject to the sheath and core sizes used and the physical property data used. The shape of the stress-location curves, however, is fundamental to the assumption that the boron sheath tends to shrink onto the core material as the composite filament cools from the high temperature of the deposition process.

The equation developed in Reference 9 and referred to in Reference 7 was developed for internal stresses in a spherical thick walled medium and may not be directly applicable to the cylindrical case of the boron filament.